TECHNICAL INFORMATION SERIES

CA
AS AD

THE THEORY OF MAGNETOHYDRODYNAMIC POWER GENERATORS*

SPACE SCIENCES LABORATORY
AEROPHYSICS SECTION

THE THEORY OF MAGNETOHYDRODYNAMIC POWER GENERATORS*

by

G. W. Sutton

*This work was sponsored by the Air Force Office of Scientific Research, Office of Aerospace Research, under Contract AF49(638)-914

R62SD990
December, 1962

MISSILE AND SPACE VEHICLE DEPARTMENT

GENERAL ELECTRIC

THE THEORY OF MAGNETOHYDRODYNAMIC POWER GENERATORS

By

George W. Sutton

ABSTRACT

Magnetohydrodynamic power generation has now been under active development for over four years, but there has not yet appeared any complete description of the theory. This report is intended to close this obvious gap. Most of the theory presented herein was developed by the author and personnel at the General Electric Company. Some of this material has not been published previously; those results which have been published are referenced.

The topics covered are: electrical conductivity in MHD generators, optimum "seed" ratio, local analyses of the continuous and segmented electrode geometries; Hall geometry, helical flow geometry; magnetically induced ionization; polytropic efficiencies; compressible analyses of the constant velocity, temperature, Mach number, pressure and cross-sectional area flows; end losses; AC generation; cycle efficiencies; and a summary of generating experiments at the General Electric Company and other places. Geometries other than linear are not considered herein; the most important of those omitted is the vortex generator.

This report has been written as Chapter 14 for a forthcoming book, Engineering Magnetohydrodynamics. References to other chapters refer to chapters in that book.

TABLE OF CONTENTS

TABLE OF CONTENTS (cont)

TABLE OF CONTENTS (cont)

LIST OF TABLES

14.1 INTRODUCTION

In principle, the magnetohydrodynamic (MHD) generator is a variation of the Faraday generator, in which the solid conductors are replaced by a moving electrically conducting fluid. Historically, Faraday recognized the possibilities of this method; he planned to use the interaction of the motion of the Thames River with the magnetic field of the earth to generate electrical power; however, his experiments yielded only sporadic results.[1]

A more obvious source of electrical power is fuel. The conversion is usually accomplished by combusting a chemical or fossil fuel with an oxidizer, which converts the stored chemical energy of the fuel into thermal energy of the products of combustion. This thermal energy is then usually converted directly into mechanical energy in an internal combustion engine or gas turbine; or the thermal energy may be transferred to a different working fluid from which mechanical power is extracted in a closed cycle, such as a steam or gas cycle.

In the case of nuclear energy, this is normally converted into thermal energy in the fuel rods, which is transferred to a cooling fluid, and then converted into mechanical energy. Finally, the mechanical energy is converted into electrical energy by means of an alternator, in either of these two systems.

Now, in both cases, if the primary working fluid, that is, the combustion gases or nuclear reactor coolant, can be made electrically conducting and can have part of its thermal energy converted into directed kinetic energy, then the working fluid can be passed directly into a magnetic field, and there convert its kinetic energy into electrical energy directly, thus eliminating the "mechanical" intermediary step.

The potential advantage of MHD power generation is based on utilizing higher temperatures of the working fluid than are compatible with turbines. This may lead to either higher overall thermal efficiencies, or in the case of "space power" to a higher reject temperature and thus a reduction of the radiator area.

In comparison to the usually wire-wound generator, the MHD generator is more complex to analyze, because the electrical conductivity and gas velocity are variable properties and the gas is not constrained to move in an exact prescribed path. In one respect, however, the MHD generator is simpler because the magnetic field due to the induced currents is negligible.

In comparison to the analysis of compressible flow in a duct, the flow in the MHD generator is also more complex because the Lorentz force and ohmic heating vary over a cross-section, which changes the boundary layer growth. Also, the Hall effect can, under certain circumstances, introduce strong cross-flow components. To make the analysis tractable, we will therefore make suitable simplifying assumptions as needed.

The basic principle of the MHD generator is that the electrical power $\underset{\sim}{E} \cdot \underset{\sim}{J}$ can be made negative by the presence of the magnetic field; that is, since $\underset{\sim}{j} = \underset{\approx}{\sigma} \cdot (\underset{\sim}{E} + \underset{\sim}{v} \times B)$, J can have a component in a direction opposite to $\underset{\sim}{E}$. The total generated power in an MHD generator is the integral of $\underset{\sim}{E} \cdot \underset{\sim}{J}$ over the entire volume of the generator, including the inlet and exhaust. Since $\underset{\sim}{E} = -\nabla\varphi - (\partial \underset{\sim}{A}/\partial t)$, this can be written as:

$$P = -\int \underset{\sim}{E} \cdot \underset{\sim}{J}\, d\mathcal{V} = \int \underset{\sim}{J} \cdot \nabla \varphi\, d\mathcal{V} + \int \frac{\partial \underset{\sim}{A}}{\partial t} \cdot \underset{\sim}{J}\, d\mathcal{V}$$

or, since $\nabla \cdot (\varphi \underset{\sim}{J}) = \varphi \nabla \cdot \underset{\sim}{J} + \underset{\sim}{J} \cdot \nabla \varphi$,

$$P = \int \nabla \cdot (\varphi \underset{\sim}{J})\, d\mathcal{V} - \int \varphi \nabla \cdot \underset{\sim}{J}\, d\mathcal{V} + \int \frac{\partial \underset{\sim}{A}}{\partial t} \cdot \underset{\sim}{J}\, d\mathcal{V}$$

Finally, the first integral is converted to a surface integral; and in the second integral $\nabla \cdot \underset{\sim}{J} = -\partial \rho_e/\partial t$, where ρ_e is the excess charge density, so that

$$P = \int \varphi \underset{\sim}{J} \cdot d\underset{\sim}{S} + \int \varphi \frac{\partial \rho_e}{\partial t}\, d\mathcal{V} + \int \frac{\partial \underset{\sim}{A}}{\partial t} \cdot \underset{\sim}{J}\, d\mathcal{V} \qquad (14.1)$$

In an MHD generator in which the flow is steady, the last two terms of (14.1) are zero. In the first term, the normal component of the current on all insulator surfaces is zero. Thus, the power appears as current to the electrodes if the potential on the different electrodes is not the same. The potential difference between electrodes is, of course, the ratio of the electrode current to the load resistance.

In an electrodeless induction type generator, the first term of (14.1) is zero. Also, it is common to design it in such a way that the potential is zero. Thus, the power delivered to the field coils comes from the last term.

The second term in (14.1) corresponds to capacitive coupling with the flow and corresponds to electrodeless electrohydrodynamic power generation.

14.1a Electrical Conductivity in MHD Generators

To make the working fluid electrically conducting, there are three general methods as follows:

(i) Non-Thermal Ionization

For a working fluid which is normally unionized, ionization can be achieved by electron beams, d.c. or r.f. discharges, fission product ionization, etc. However, the applicability of any of these methods for MHD power generation has yet to be demonstrated. Historically, electron-beam ionization was the first method tried with combustion gases, but was not successful.[2] However, in pure or noble gases, where the recombustion rate for electrons is smaller, this method may be proved useful.

In combustion flames, there is always a small amount of chemionization as a result of the chemical reactions. Although this can be enhanced somewhat by the addition of small amounts of metals, generally the degree of ionization is insufficient to be useful for an MHD generator, and furthermore, there are usually a large proportion of negative ions present, so

that the number of free electrons present is very small. It, therefore, appears that non-thermal ionization can be achieved only in special cases, see Section 14.3e.

(ii) Thermal Ionization

Thermal ionization refers to thermochemical equilibrium such that the thermal energy of the gas is an appreciable fraction of the ionization potential of one of its constituents; then Saha's equation predicts that a high number density of electrons will be present. Now, in ordinary flames, which burn a fuel with an oxidizer, the flame temperature is rarely high enough to cause appreciable thermal ionization of the products of combustion, mainly because of the relatively high ionization potential of the products of combustion. Fortunately, a number of elements have lower ionization potentials, see Table 14.1. If a small fraction of alkali metal "seed" is added to a combustion flame, then sufficient ionization may be obtained. Unfortunately, in flames of fossil fuels with air, the flame temperature is too low to ionize even the "seed"; the air must be either preheated or enriched with oxygen to obtain the required temperatures of $4000-5000^{\circ}F$.[3]

For working fluids which are heated by solid fuel rods in a nuclear reactor, it is unlikely that sufficiently high temperatures for thermal ionization can be achieved in the near future; hence, techniques for non-thermal ionization will have to be developed for this application. This problem will be alleviated if high-temperature gaseous nuclear reactors are developed. The application of MHD generators to controlled nuclear fusion has not been analyzed.

(iii) Liquid Metal Conductors

Even if the gas is non-conducting, there is a possibility that it may be mixed mechanically with liquid metals as a foam or droplets. If the liquid metal is foamed with the gas, then the entire mixture may be passed through the generator. If the liquid metal is mixed with the working gas as droplets, then the mixture must be expanded to accelerate the drops; that

is, the thermal energy of the gas must be converted into directed kinetic energy. This directed kinetic energy must then be exchanged with the liquid metal droplets. Next, the kinetic energy of the liquid metal droplets must be converted into a pressure head in a seperator, since this pressure head must be used to flow the liquid metal through the generator against the Lorentz force. This technique has not yet been demonstrated experimentally.

14.1b MHD Generator Geometries

There are also several different MHD generator geometries presently under consideration. The chief requirement for any geometry is that there be a component of the gas velocity which is not parallel to the magnetic field, so that a Faraday electric field $\underset{\sim}{v} \times \underset{\sim}{B}$ is created. This field will then cause electric currents and fields in the plane normal to the magnetic field. The second requirement is that there be electrodes in this plane which collect the current for the electrical load. The simplest geometries for accomplishing this are the linear (together with its many variations), vortex, and radial outflow, see Figure 14.1. These are described qualitatively below, and the linear geometry is examined more thoroughly in the remaining sections of this chapter.

(i) Linear MHD Generator - "Duct or Channel" Geometry

The simplest MHD generator geometry is the "linear" geometry in which the gas flows through a linear duct or channel, see Figure 14.1. The magnetic field is at right angles to the gas flow velocity, which induces a Faraday electric field at right angles to both the flow velocity and magnetic field. If suitable electrodes are placed on either side of the channel and connected through an electrical load or resistance, then current will flow through the gas, electrodes, and load.

In addition to the Faraday electric field, the magnetic field causes a Hall current to flow in the direction of fluid flow; that is, the current does not flow straight across the duct. This phenomena can be prevented

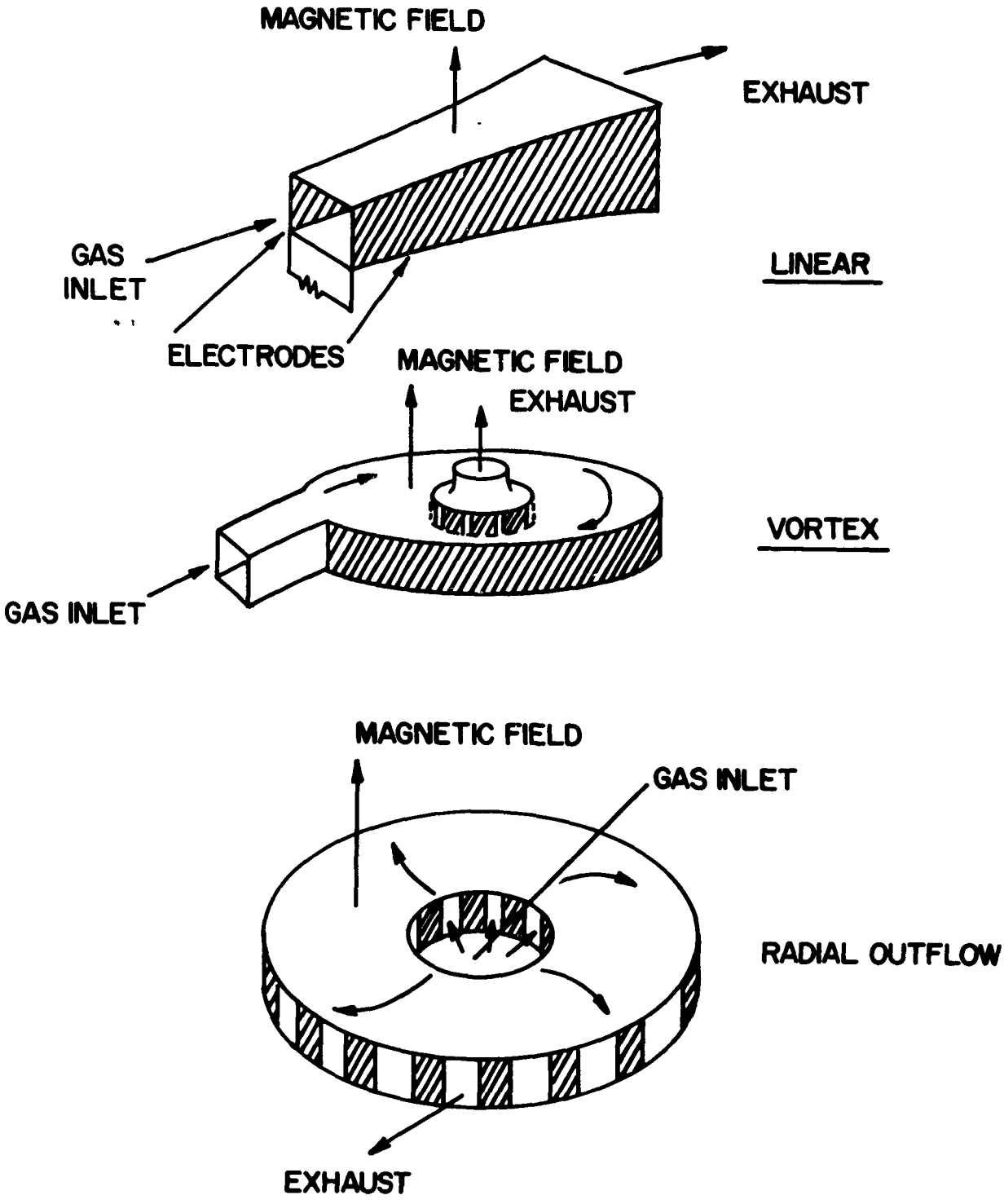

Figure 14.1. MHD Generator Geometries

by employing "segmented electrodes" which is a variation of the linear generator. This allows a Hall electric field to develop in the flow direction. In still another variation of the linear generator, the Faraday current is shorted, and the Hall current is allowed to flow through the electrical load. Other variations are also possible, see Section 14.3.

(ii) Vortex MHD Generator

In addition to the linear geometry with its many variations, there is also interest in the vortex or spiral geometry in which the gas is introduced tangentially into a cylindrical geometry, and withdrawn along the surface of an inner coaxial cylinder, see Figure 14.1. The magnetic field is in the axial direction, and the inner and outer cylinder are the two electrodes. Under open circuit conditions, free-vortex flow should result; that is, the tangential velocity should be inversely proportional to the radial position. Under load, the tangential velocity is practically constant in the radial direction. When the inner cylindrical diameter is much smaller than the outer cylinder, the gas makes several revolutions in the generator; thus, this geometry permits a longer magnetic interaction length; or alternately, for a given interaction length, the vortex generator has a more compact magnetic field. On the other hand, the Hall currents tend to flow in the tangential direction; thus, to prevent the Hall reduction in electrical conductivity, the gas pressure must be sufficiently high that $\omega_e \tau_e < 1$ at the exit. (Note that when the inner radius is almost equal to the outer radius, the vortex geometry is very similar to the linear geometry.) Up until the present time, the vortex geometry has not been demonstrated experimentally, and will not be considered in this chapter.

(iii) Radial Outflow MHD Generator

A variation of the vortex generator is one in which the gas is injected radially outward from the inner cylinder. In this case, the Faraday current flows tangentially and the Hall current flows radially; the latter interacts with the magnetic field to rotate the flow, so that flow becomes a spiral

outward. This variation is essentially the same as the Hall geometry, with the duct bent so that the Lorentz force caused by the Hall current is equal to the centrifugal force in the fluid.

(iv) Other Considerations

All of the geometries considered above generate dc power. However, by switching the magnetic field or by using a traveling magnetic field, it may be possible to generate ac power. Although this has not yet been demonstrated experimentally, the general principles for electrodeless ac "induction" generators also will be covered in this chapter.

In order that the ionized fluid behave as a continuum conductor in an MHD generator, the Debye length must be much smaller than the size of the apparatus; otherwise, charge separation will occur.

To prevent ion slip, the magnetic field must not be so large, nor the density so low that $\omega_e \tau_e \omega_I \tau_I$ exceeds unity. This will be explained later.

The pressure, conductivity, gas velocity, and magnetic field must be such to make the interaction length L, defined as

$$L = \frac{p_1}{\sigma u B^2} \tag{14.2}$$

equal to the length of the path of the gas through the generator, where p_1 is the inlet static pressure, and σ, u, and B^2 are average values in the generator. This condition insures that an appreciable fraction of the inlet enthalpy is converted into electrical energy.

Finally, if electrodes are used, the current density from the cathode must equal or exceed the current density in the gas; otherwise, the effective electrical resistivity of the gas will be increased.

14.2 OPTIMUM SEEDING RATIO

As indicated in Section 14.1, to make a combustion gas (or working fluid) electrically conducting, it is necessary to add to it a small amount of seed material which has a low ionization potential, see Table 14.1. There are two ways in which this may be done, either as a pure element, or as a compound. To determine the degree of ionization, Saha's equation may be used; thus, it is generally necessary to determine both the depletion of electrons due to electron attachment to gas atoms, and the depletion of seed atoms due to chemical combination with the other atoms present in the gas. This generally requires the simultaneous solution of Saha's equation, the electron attachment, and the chemical equilibrium equations.[4] This may be represented as follows:

$$S \rightleftarrows S^{+} + e$$

$$e + A \rightleftarrows A^{-}$$

$$S + B \rightleftarrows SB$$

$$C + B \rightleftarrows D$$

etc.

where S is a seed atom, and A, B, C, D, etc., are gas molecules.

At temperatures of about $3000^{\circ}K$, all reactions except the first generally can be neglected; thus, simplified equations can be obtained for the optimum seed concentration. Generally, the upper limit for the seed concentration can be obtained by two different sets of approximations, as follows:

14.2a Isothermal Optimum Seeding

The temperature of the mixture is assumed to be unaffected by the addition of seed material. This is true in combustion gases if the seed percentage is very small, or for the working fluid of a closed cycle, if the seed plus working fluid is heated to the same uniform temperature. From Chapter V, the scalar resistivity of the gas is given by:

TABLE 14.1. MOLECULAR WEIGHTS AND IONIZATION POTENTIALS

(From 33rd Ed., Handbook of Chemistry and Physics, Chemical Rubber Publishing Co.)

Gas	Molecular Weight	Ionization Potential (electron-volts) I	II
Noble Gases			
Helium	4.03	24.46	54.14
Neon	21.83	21.47	40.9
Argon	39.4	15.68	27.76
Krypton	83.7	13.93	26.4
Xenon	130.2	12.08	21.1
Common Gases			
H	1.008	13.53	-
H_2	2.016	15.6	-
N	14.008	14.48	29.47
N_2	28.016	15.51	-
O	16.000	13.55	34.93
O_2	32.000	15.51	-
CO	28.01	14.1	
CO_2	40.02	14.4	
NO	30.008	9.5	
Metal Vapors (Atoms)			
Lithium	6.940	5.363	75.26
Sodium	23.00	5.12	47.06
Aluminum	26.97	5.96	18.74
Potassium	39.10	4.318	31.66
Calcium	40.8	6.09	11.82
Rubidium	85.48	4.16	27.36
Cesium	132.91	3.87	14.8
Barium	137.36	5.19	9.95
Mercury	200.61	10.39	18.65

$$\eta \simeq \frac{m_e \langle c \rangle}{e^2} \left[\frac{n_{ns} Q_{es}}{n_e} + \frac{n_g Q_{eg}}{n_e} \right] + \eta_{eI} \qquad (14.3)$$

where n_{ns} is the number density of neutral seed atoms; Q_{es} is their average cross section; n_g is the number density of the rest of the gas atoms and Q_{eg} is their average cross section; η_{eI} is the electron-ion resistivity, which from Chapter V is:

$$\eta_{eI} = 65.3 \times T^{-3/2} \left\{ \ell n \left[1.24 \times 10^4 \, T^{3/2} \right] - \ell n \, n_e^{1/2} \right\} \qquad (14.4)$$

From Chapter VI, the number density of electrons for thermal ionization of a single species is given by:

$$n_e = \sqrt{n_{ns}} \sqrt{2G} \, (2\pi m_e k T/h^2)^{3/4} e^{-T_I/2T} \qquad (14.5)$$

where $T_I = e E_i/k$ and E_i is the ionization potential. Substitution of (14.4, 14.5) into (14.3) yields:

$$\eta = \frac{m_e \langle c \rangle_e}{e^2 \sqrt{2G}} \left(\frac{h^2}{2\pi m_e k T} \right)^{3/4} e^{\frac{T_I}{2T}} \left[n_{ns}^{1/2} Q_{es} + \frac{n_g}{n_{ns}^{1/2}} Q_{eg} \right]$$

$$- 65.3 \, T^{-3/2} \left[\frac{1}{4} \ell n \, n_{ns} \right] + \text{other terms} \qquad (14.6)$$

where the other terms do not depend on n_{ns}.

To obtain the optimum seed atom concentration, (14.6) must be differentiated with respect to n_{ns}, and the resulting expression set equal to zero. The result is:

$$\frac{n_{ns}}{n_g} = \frac{(1+\beta)}{(1-\beta)} \frac{Q_{eg}}{Q_{es}} \tag{14.7}$$

where

$$\beta = \sigma_{en} / 2\sigma_{eI} \ell n \Lambda \tag{14.8}$$

and where σ_{en} σ_{eI}, and $\ell n \Lambda$ are defined in Ch. V.

Equations (14.7, 14.8) must be solved iteratively, by first assuming $\beta = 0$, then obtaining n_{ns} from (14.7). Then n_e is obtained from Saha's equation and β is calculated from (14.8). This value is then substituted back into (14.7) and a new value of n_{ns} is calculated, etc. The total required seed n_s' is the sum of the final value of n_{ns} and n_e.

This simplified procedure works well for mixtures of pure seed and pure noble gases, see Figure 14.2, where the conductivity of a mixture of cesium and argon has been plotted against mixture ratio. For small mole fractions of cesium, the electrical conductivity increases rapidly with increasing cesium fraction. Beyond the maximum, the conductivity decreases slightly because the cross-section of cesium is larger than that of argon. Note, however, that the value of $\omega_e \tau_e$ decreases monotonically, because τ_e depends on the average cross-section, which increases with increasing cesium fraction. Some average values of the cross section are shown in Table 14.2

14.2b Isoenergetic Optimum Seeding

Equations (14.7, 14.8) can be used with combustion gases only if the seed atom cross-section is much larger than the average cross-section for the combustion gas; for otherwise. (14.7 predicts a large fraction of seed atoms, which will

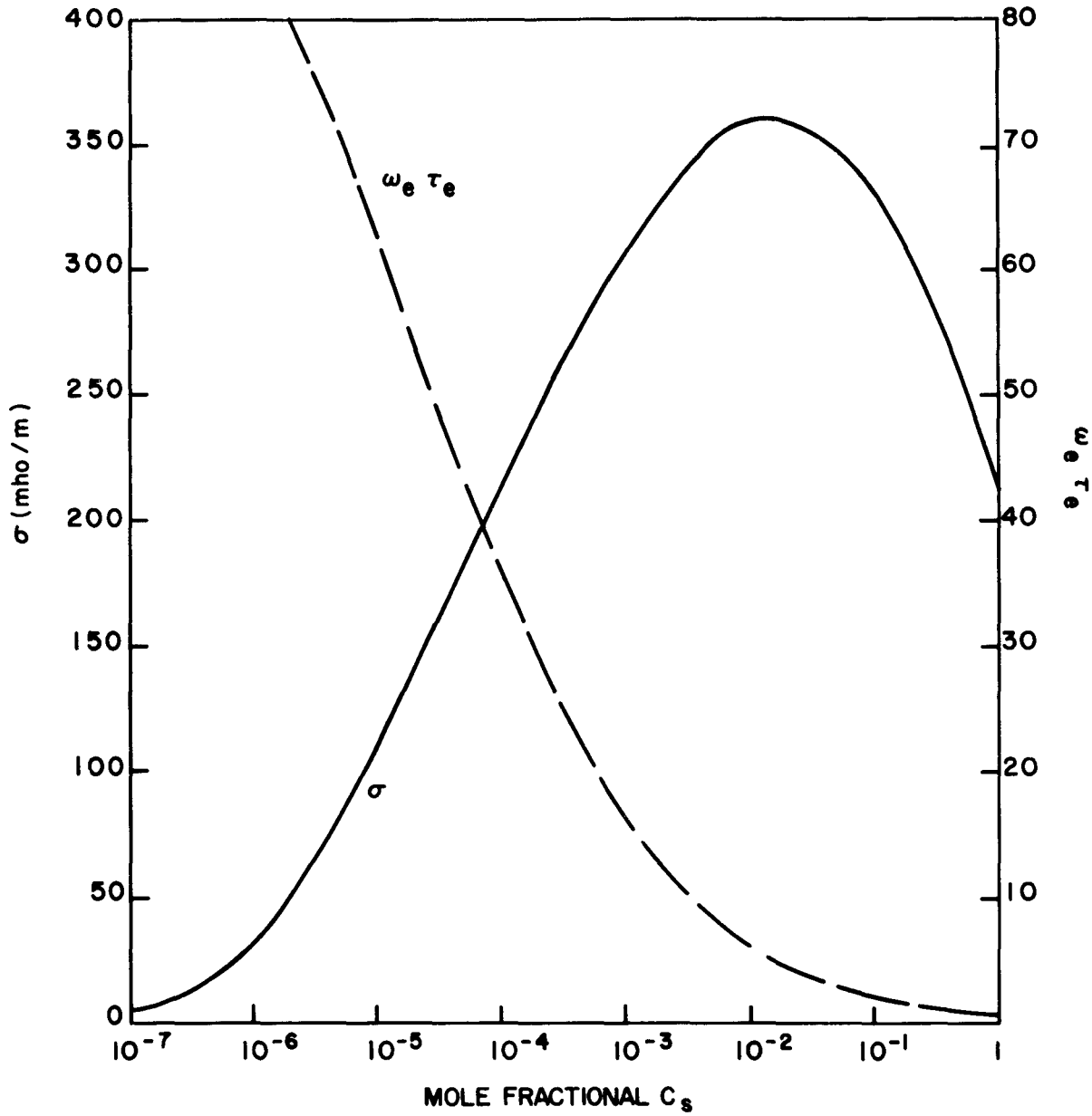

Figure 14.2. Electrical Conductivity and Hall Parameter in a Mixture of Cesium and Argon at 1 Atm. Pressure and 2500°K. $Q_{e_{C_s}} = 3.5 \times 10^{-15}\,cm^2$, $Q_{eA} = 2 \times 10^{-17}\,cm^2$. B = 10,000 gauss

TABLE 14.2. AVERAGE VALUES OF ELASTIC ELECTRON CROSS-SECTIONS WITH VARIOUS ATOMS AND MOLECULES

Particle	Elastic Cross-Section, in 10^{-15} cm^2	Electron Temperature 10^3 °K
Noble Gases[1]		
A	0.02	2-3.5
	.11	7.7
	2.38	50
He	0.54	0-30
Ne	.142	0-8
Alkali Metals[2]		
K	1.0	2.4
C_S	3.6	1.1
Combustion Gas Constituents[3]		
O_2	.31	3-4
N_2	.6	3-4
H_2	.85	3-4
CO	.81	3-4
CO_2	1.2	3-4
H_2O	3.6	5
N	1.4	3-4
O	1.7	3-4

1. S. Brown, Basic Data of Plasma Physics, Wiley, 1959.
2. G. J. Mullaney and N. Dibelius, ARS Journal, 31, 1575 (1961); G. J. Mullaney, P.H. Kydd, N. Dibelius, J. Appl. Physics, 32, 668 (1961).
3. Data Compiled by W. Chinitz, L. Eisen, R. Gross, Am. Rocket Society preprint 706-58, 1958.

lower the flame temperature by dilution and therefore violates the assumption that the gas temperature remains constant. For this latter case, the analysis must include the effect of the seed atom dilution on the gas temperature.

To analyze this case, the following assumptions are made:

i) the percentage of seed is small and the degree of ionization is small;

ii) the seed atoms and electrons do not react chemically with the rest of the gas. Let the initial enthalpy of the gas be h_{og}; and the initial enthalpy of all the added seed be $h_{os'}$. It is assumed that the seed is added as an unionized element. Then conservation of enthalpy yields:

$$n_{s'} h_{s'} + n_g h_g = n_g h_{og} + n_s h_{os'} \tag{14.9}$$

If the seed atoms are atomic, then the enthalpy per seed particle is:

$$h_{s'} = \frac{5}{2} k T + \alpha k T_I \tag{14.10}$$

where α is the degree of ionization defined as:

$$\alpha = \frac{n_e}{n_I + n_s} = \frac{n_e}{n_{s'}} \tag{14.11}$$

and where electronic exitation has been neglected. The enthalpy of the combustion gas is $\frac{1}{2}$ (N + 2) k T; where N is the average degrees of freedom of the gas; thus the ratio of specific heats of the combustion gas is $\gamma = (N + 2)/N$. Finally, it may be assumed that the seed material has zero enthalpy when added to the flow. The temperature of the gas, after addition of the seed material, is therefore given by:

$$T = \frac{\frac{\gamma}{\gamma-1} T_o - \alpha\beta T_I}{\frac{5}{2}\beta + \frac{\gamma}{\gamma-1}} \tag{14.12}$$

where $\beta = n_{s'}/n_g$ is the mole fraction of added seed. The upper limit for β can be obtained by assuming $\alpha \ll 1$. Then for $\beta \ll 1$, (14.12) reduces to:

$$T = T_o \left[1 - \frac{5\,(\gamma-1)}{2\gamma}\,\beta\right] \tag{14.13}$$

and

$$\frac{\partial T}{\partial \beta} = -\frac{5\,(\gamma-1)}{2\gamma}\,T_o \tag{14.14}$$

where T_o is the flame temperature without seed. Next, (14.6) is differentiated with respect to β using (14.14), and equated to zero, but the terms $T^{-3/4}$ and η_{eI} may be neglected in comparison to the exponential term. The result is:

$$0 = \frac{1}{2}\,\beta^{-\frac{1}{2}}\,Q_{es} - \frac{1}{2}\,\beta^{-3/2}\,Q_{eg} + \left[\beta^{\frac{1}{2}}\,Q_{es} + \beta^{-\frac{1}{2}}\,Q_{eg}\right]\frac{5\,(\gamma-1)}{2\gamma}\,\frac{T_I\,T_o}{T^2} \tag{14.15}$$

Finally, if Q_{es} is of the order of Q_{eg} and $\beta \ll 1$, then Q_{es} may be neglected. Also, after the seed addition, $T \approx T_o$ if β is small. Then, solving (14.15) for β one obtains:

$$\beta = \frac{5(\gamma-1)}{\gamma}\,\frac{T_o}{T_I} \tag{14.16}$$

Now, in combustion gases $\gamma \approx 1.2$; thus, the final expression for the maximum seed concentration is

$$\beta \approx \frac{T_o}{T_I} = \frac{k\,T_o}{e\,E_I} \tag{14.17}$$

As an example, consider a flame temperature of $3000^{o}K$ so that T_o is about 0.25 volts; the ionization potential of cesium or potassium is about four volts; thus, the mole fraction of pure seed should be less than 1/16 or 6%. It therefore appears that the seed fraction for combustion gases must be small; in fact up to the present time concentrations of only 0.1% to 4% have been considered. Of course, another factor in keeping the seed ratio small is the cost of the seed material. Also, if it is desired to minimize the Hall parameter, seed concentrations greater than 6% could be used, since electron cross-section of ions is very large.

14.3 LOCAL INVISCID ANALYSIS OF LINEAR MHD GENERATORS

The local analysis of an MHD generator refers to the performance between two adjacent cross-sections in the downstream direction in a linear geometry. The advantage of a local analysis is that compressibility and area changes generally can be neglected, if the two cross-sections are sufficiently close. It is also usual to neglect viscous and thermal losses to the walls, in comparison to the Lorentz force and electrical energy extraction, respectively. This assumption is valid if the viscous Reynolds number of the flow, based on the hydraulic diameter, is very large, compared to the magnetic interaction parameter. The effect of these losses is discussed in Section 14.4. In addition, the magnetic Reynolds number in most MHD generators will be small so that the induced magnetic field may be neglected. With these two assumptions the velocity U is taken constant in the x direction and the magnetic field in the z direction is taken to be constant, see Figure 14.3a. The induced electric field $\underline{v} \times \underline{B}$ is then UB in the negative y direction. Then from Chapter V, ohm's law, including the effects of ion slip, becomes:

$$j_x = \frac{\sigma}{(1 + \beta_I \beta_e)^2 + \beta_e^2} \left[(1 + \beta_I \beta_e) E_x - \beta_e (E_y - UB)\right]$$

$$j_y = \frac{\sigma}{(1 + \beta_I \beta_e)^2 + \beta_e^2} \left[(1 + \beta_I \beta_e) (E_y - UB) + \beta_e E_x\right] \qquad (14.18)$$

where σ is the scalar electrical conductivity $n_e e^2 \tau_e / m_e$, $\beta_I = \omega_I \tau_{In}$, and $\beta_e = \omega_e \tau_e$.

In the absence of velocity or thermal boundary layers both E_x and E_y may be considered constant (although more generally they may be a function of x). Then

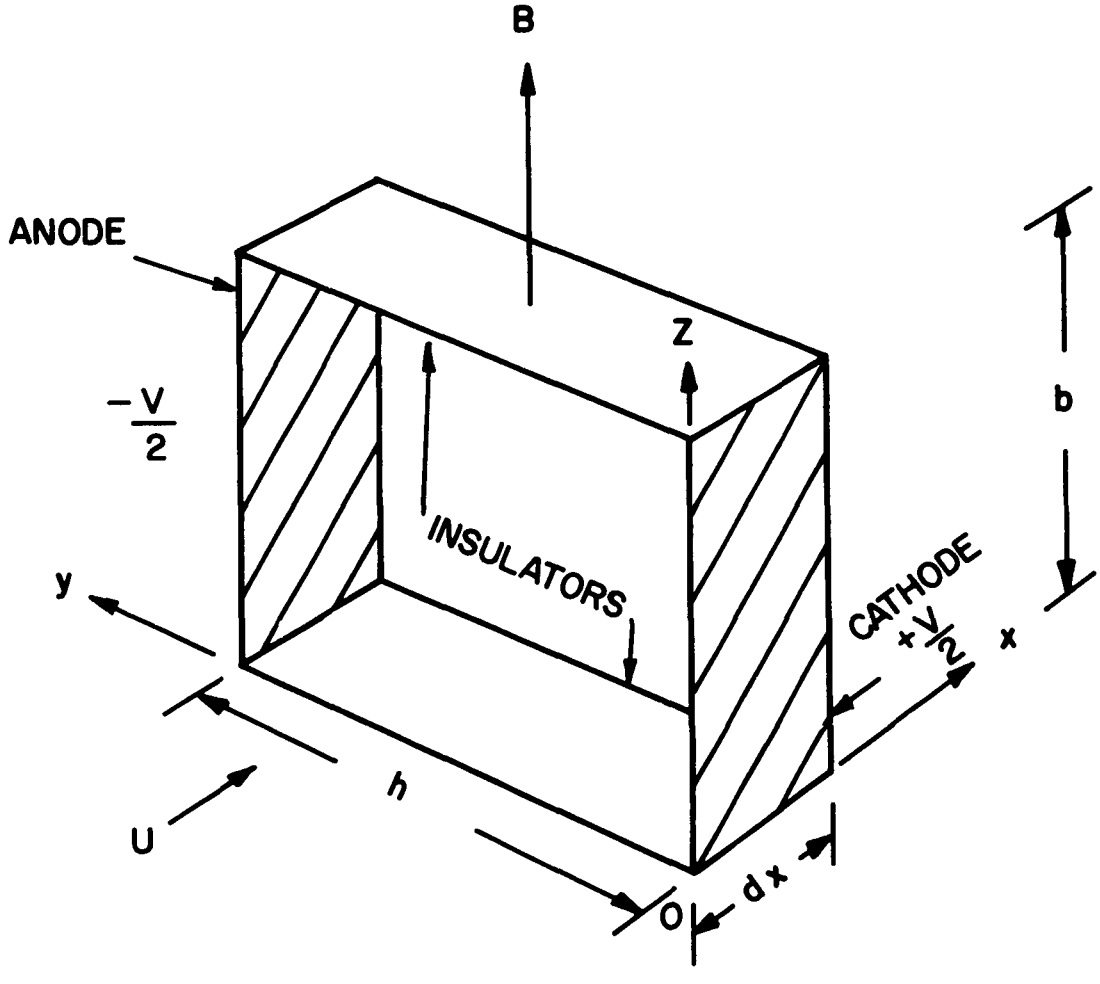

Figure 14.3a. Schematic Diagram for "Local Analysis" of Linear MHD Generators

all variables are constant across a cross-section, so that the electric field and current in the direction of the magnetic field is zero.*

We will next use this simple model to analyze the three most common types of linear generators: continuous electrodes, segmented electrodes, and the Hall generator, see Figure 14.3b; and a variation of the segmented electrode geometry, in which the flow is helical through an annulus.

14.3a Continuous Electrodes

With the electrodes continuous along each side of the generator with a different constant potential on each, no axial electric field can develop and therefore $E_x = 0$. Then from (14.18), the transverse component of the current is:

$$j_y = \frac{\sigma}{(1 + \beta_e \beta_I)^2 + \beta_e^2} \left[(1 + \beta_e \beta_I) (E_y - UB) \right] \qquad (14.19)$$

The open circuit condition implies that $j_y = 0$; thus, from (14.19), the open circuit electric field is E_y (open circuit) = UB. Under short circuit conditions, $E_y = 0$ (except for the finite electrical resistance of the electrodes and external connection). Thus, in general, $0 < E_y < UB$. It is common to express the electric field under load as a fraction K of the open circuit electric field; thus, for the continuous electrode geometry:

$$K = \frac{E_y}{UB} \qquad (14.20)$$

where for generation of electrical power, $0 < K < 1$. Note that j_y is then negative, and the Lorentz force $\underset{\sim}{j} \times \underset{\sim}{B}$ is in the negative x direction; that is,

*Velocity boundary layers on the insulators cause the induced field $\underline{v} \times \underline{B}$ within the boundary layer to be less than that at the centerline. Under these conditions, the current in the boundary layer may be in the opposite direction as that in the main flow and thus constitute a "leakage" current. However, if the electrical conductivity is constant, then the average axial velocity across a cross-section may be used instead of U.

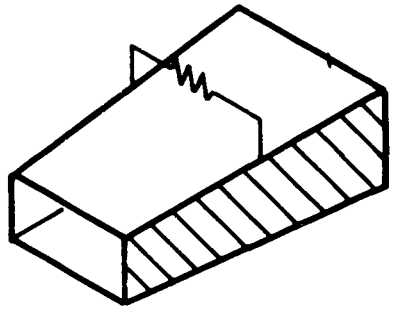

CONTINUOUS ELECTRODES

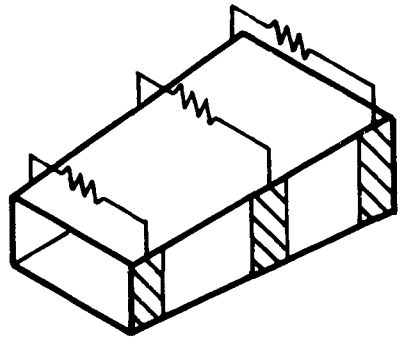

SEGMENTED ELECTRODES

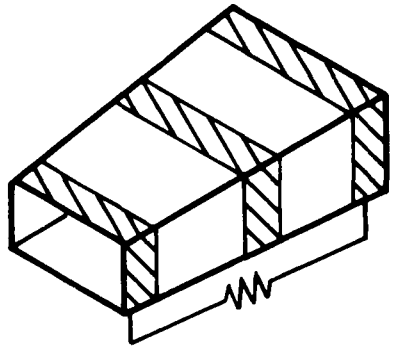

HALL GENERATOR

Figure 14.3b. Linear Generator Geometries Having Rectangular Cross Sections

opposite to the flow direction. Thus, in the generator, the Lorentz force tends to retard the flow. (If, on the other hand, the electrodes were attached to a voltage source so that $E_y > UB$, that is, $K > 1$, then j_y is positive and the Lorentz force tends to accelerate the flow. If the polarity of the imposed voltage is reversed so that $E_y < 0$, the Lorentz force will retard the flow; the energy added to the flow from the voltage source then increases the thermal energy of the gas.)

In addition to the transverse component of the electric current, there is also a component in the downstream direction given by:

$$j_x = \frac{\sigma \beta_e (1-K) UB}{(1 + \beta_I \beta_e)^2 + \beta_e^2} \tag{14.21}$$

where use has been made of (14.20). Thus, the current, as it flows across the generator, also tends to flow downstream. Actually, it is the current in the downstream direction (14.21) which is responsible for the Lorentz force on the gas. This may be seen by simplifying the problem somewhat: let $\omega_I \tau_{In} \equiv \beta_I = 0$, so that the average ion motion is exactly equal to the gas velocity U_1. The current given by (14.21) is the total downstream current; if the average ion velocity is equal to the gas velocity, then with $\beta_I = 0$ (14.21) is also the expression for the electron conduction current relative to the gas motion, since the gas is electrically neutral. Thus, the diffusion velocity of the electrons is in the downstream direction relative to the gas, that is:

$$V_{e_x} = \frac{\sigma \omega_e \tau_e (1-K) UB}{n_e e (1 + \beta_e^2)} \tag{14.22}$$

The drag force exerted on the gas by the electrons is $F_x = n_e m_e V_{e_x} / \tau_e$, with the use of (14.22) this becomes:

$$F_x = \frac{-\sigma (1-K) UB^2}{1 + \beta_e^2} \tag{14.23}$$

This is identical to the Lorentz force $j_y B$, calculated from (14.19) when β_I is neglected.

(i) Power Density, Continuous Electrodes

The power generated per unit volume is $P = -\underset{\sim}{E} \cdot \underset{\sim}{j}$ which becomes just $j_y E_y$ since $E_x \approx 0$. From (14.19), (14.20), this becomes:

$$P = \frac{\sigma K (1-K) U^2 B^2 (1 + \beta_e \beta_I)}{(1 + \beta_e \beta_I)^2 + \beta_e^2} \qquad (14.24)$$

Equation 14.24 can also be written as:

$$P = \frac{n_e m_e U^2 K (1-K)}{\tau_e} \cdot \frac{\beta_e^2 (1 + \beta_e^2 \frac{\mu_I}{\mu_e})}{(1 + \beta_e^2 \frac{\mu_I}{\mu_e})^2 + \beta_e^2} \qquad (14.25)$$

where μ_I, μ_e are the electron and ion mobilities $e \tau_{In}/m_I$, $e \tau_e/m_e$, respectively. From (14.25) it is also obvious that $0 < K < 1$ for power generation. The coefficient of (14.25) $\left(n_e m_e U^2 \nu_e\right)$ has a simple interpretation: consider that after each collision with a heavy particle the electron acquires the gas velocity U in the downstream direction. But then the magnetic field turns the electron velocity in the +y direction parallel the electric field, so that its kinetic energy is transformed into potential energy. If the electron is then hit again by a heavy particle, it again acquires a velocity U in the downstream direction. The rate at which an electron acquires kinetic energy from the gas is thus approximately $\left(\frac{1}{2} m_e U^2 \nu_e\right)$; the total rate at which all electrons acquire energy from the gas is therefore $\approx \frac{1}{2} n_e m_e U^2/\tau_e$.

This same result can be obtained from a different point of view: between collisions, the magnetic field turns an electron in the y-direction

a distance of order of magnitude equal to the Larmor radius, which may be taken as approximately U/ω_e, thereby acquiring a potential energy due to the stationary electric field equal to EU/ω_e. The total rate at which the electrons acquire potential energy is then $\left(n_e \nu_e EU/\omega_e\right)$. Since $E \propto UB$, and $\omega_e = eB/m_e$, this rate is again equal to $\left(n_e m_e U^2 \nu_e\right)$, which agrees with the previous argument.

The factor on the right side of (14.25) represents the effects of the Hall reduction in electrical conductivity and ion slip for this geometry, and has two asymptotes. The first asymptote is obtained by taking μ_I or equivalently τ_I or β_I equal to zero, which is equivalent to stating that the ion velocity is equal to the gas velocity. This factor then becomes $\beta_e^2/(1 + \beta_e^2)$. Thus, for a given value of τ_e, the power P initially increases quadratically with the magnetic field, since $\beta_e \equiv \mu_e B$. This is shown in Figure 14.4. As the magnetic field is increased further, the first asymptote is reached as $\beta_e^2/(1 + \beta_e^2) \longrightarrow 1$. Thus, the maximum energy transfer or power generation due to the electrons is $\left(n_e m_e U^2 \nu_e\right)$ modified, of course, by the loading factor term K (1-K). In Figure 14.4 the inflection point near unity represents this first asymptote. Since magnets generally consume power and are expensive or heavy, it is desirable to operate at a point somewhat below this point; suppose the power level is set at $P \tau_e / n_e m_e U^2 K(1-K)$ equal to 80% of the first asymptote, then $\beta_e^2/(1 + \beta_e^2) = 0.8$, so that $\beta_e = \sqrt{5} = 2.24$. Thus, a magnetic field which corresponds to a value of the Hall parameter greater than two will not lead to substantially greater power generation by electrons.

(ii) Magnetic Interaction Length

With $\beta_I = 0$, the interaction length can be written in terms of the electron mean free path as follows:

$$L = \frac{p_i}{\sigma U B^2} \approx \left(\frac{1 + \beta_e^2}{\beta_e^2}\right) \frac{n}{n_e} \sqrt{\frac{m_g}{m_e}} \frac{\lambda_e}{\mathcal{M}} \qquad (14.26)$$

where $\mathcal{M}$ is the gas Mach number.

Again, as β_e^2 is increased from zero, the interaction length decreases and then becomes asymptotic. Since the degree of ionization will be of the order of 10^{-2} to 10^{-4}, the square root of the mass ratio is about 10^{-2}, and the Mach number is of order of magnitude unity, the interaction length of the generator is 10^4 to 10^6 electron mean-free paths, multiplied by $(1 + \beta_e^2)/\beta_e^2$. For constant electron mean-free path, increasing the magnetic field decreases the interaction length, but values of β_e beyond about two will not lead to any appreciable further reduction. On the other hand, with the magnetic field constant, if β_e is increased by decreasing the gas pressure, then the electron mean-free path will increase, which increases the interaction length. This may be seen by substitution of $\lambda_e = m_e \langle C_e \rangle \beta_e / e B$ into (14.26). The interaction length then varies as $(1 + \beta_e^2)/\beta_e$, which has a minimum at $\beta_e = 1$.

With β_I non-zero, (14.25) predicts a second asymptote when $\beta_e > \mu_e/\mu_I$ for the right hand factor, equal to the mobility ratios μ_e/μ_I which is generally much greater than unity. This is shown on the right side of Figure 14.4 for very large values of $\omega_e \tau_e$. The power extraction is then of the order of $P \approx n_I m_I U^2/\tau_{In}$, which shows that for very large values of $\omega_e \tau_e$, the positive ions are responsible for the power generation. Because the mobilities vary roughly as the inverse square root of the mass ratio, the asymptotic interaction length for β_e large becomes $L = n \lambda_e / n_e m_I$. However, values of β_e larger than 10^3 cannot be obtained except by reducing the pressure, which again increases the interaction length because of the dependence on the mean-free path. For example, consider $\mu_e/\mu_I = 200$; from Figure 14.4, values of $\omega_e \tau_e$ greater than 2×10^4 are required to approach the asymptote, while the first asymptote is reached when $\omega_e \tau_e > 2$. Thus, if one lowers the density to obtain 2×10^4, then the electron mean-free path has been increased by a factor of 10^4, so that the interaction length is increased by two orders of magnitude. It, therefore, appears unlikely that an MHD generator can be designed to utilize the ion current with continuous electrodes.

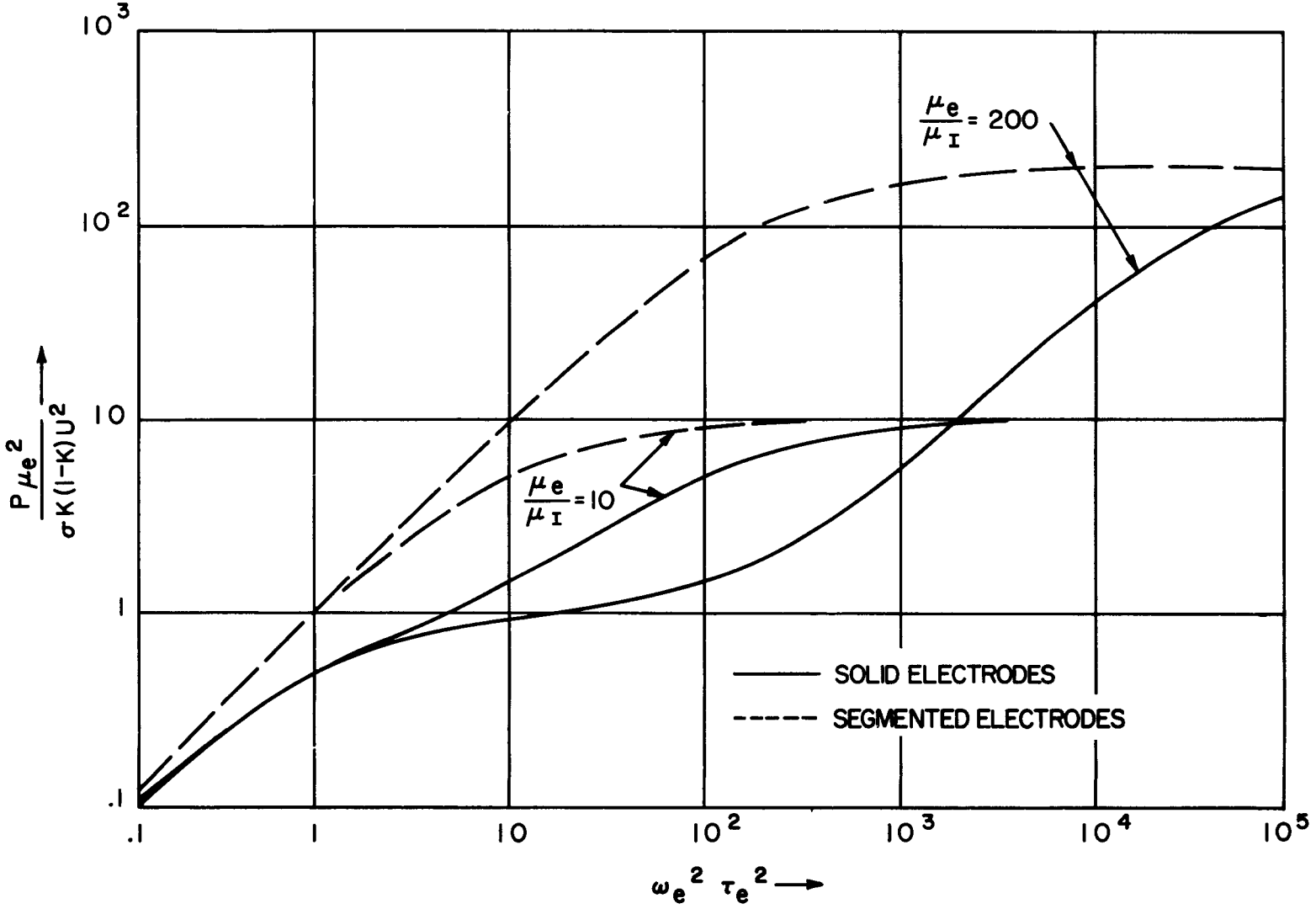

Figure 14.4. Power Density For Continuous and Segmented Electrodes

(iii) Efficiency, Continuous Electrodes

From (14.24), it is obvious that the power generation density is a maximum when $K = \frac{1}{2}$ which obviously corresponds to matched impedance; that is, when the load resistance is equal to the generator internal resistance. However, for some applications, it may not be desirable to operate at maximum power density, but instead, closer to maximum efficiency. For the purpose of a local analysis, a local conversion efficiency may be defined as the ratio of the generated power to the flow work which is required to overcome the Lorentz force, or:

$$\eta_L = \frac{P}{\underset{\sim}{v} \cdot \underset{\sim}{j} \times \underset{\sim}{B}} \tag{14.27}$$

In the present geometry, the denominator of (14.27) is $U j_y B$, while the numerator is $E_y j_y$; thus, the local efficiency for this geometry is $E_y/UB = K$, from (14.20).

The local efficiency, as defined by (14.27), is also equal to the local adiabatic or polytropic efficiency (also called the "stage" efficiency) when $\frac{\gamma-1}{2}\mathcal{M}^2$ (1-K) is small compared to unity, see Section 14.4. Thus, if a high polytropic efficiency is required, it is necessary to operate at values of K near unity.

Since the load voltage is KUBh, and the load current per unit length of generator is σ_e (1-K) UBb where σ_e is the "effective" electrical conductivity; the external load resistance per unit length of generator is, therefore,

$$R_L = \frac{V}{J} = \frac{Kh}{(1-K)\,\sigma_e b} = \frac{K}{1-K} R_i \tag{14.28}$$

where R_i is the effective internal resistance of the generator, $h/\sigma_e b$, see fig. 14.3a. Solving (14.28) for the value of K, one obtains:

$$K = \frac{1}{1 + R_i/R_L} \tag{14.29}$$

which, for this geometry is also equal to the conversion efficiency. One therefore obtains the familiar result that the conversion efficiency increases as the ratio of external to internal load increases.

(iv) Voltage Control, Continuous Electrodes

In general, the continuous electrode geometry will be operated such that $\frac{1}{2} < K < 1$; since the power generated is a parabolic function of K, this means that operation will be on the falling side, see Figure 14.5. This means that as the generator is unloaded (load resistance increases) the power to the remaining load decreases although the load voltage increases slightly. If the magnetic field is kept constant, then the effective electrical conductivity and therefore R_i will remain constant, so that the local conversion efficiency is still given by (14.29).

If it is desired to keep the load voltage constant as the load is changed, this may be accomplished by varying the magnetic field, but this will change the internal resistance. For example, if the load resistance is increased, the load voltage will increase; to keep the load voltage constant, the magnetic field is then decreased. However, this reduces the Hall parameter β_e and therefore increases the effective electrical conductivity, thereby simultaneously decreasing the internal resistance. One, therefore, expects that the local efficiency will increase more than if the magnetic field were held constant. It is easily shown that the load parameter and, hence, efficiency is given by:

$$K = \frac{Z + \sqrt{Z^2 - 4(1+Z)\beta_o^2 K_o^2}}{2(1+Z)} \qquad (14.30)$$

where β_o is the initial value of β_e; β_I was assumed to be zero, K_o is the initial value of the loading factor, and Z is defined as:

$$Z = \frac{K_o}{1-K_o}(1+\beta_o^2)\frac{R_L}{R_{L_o}} \qquad (14.31)$$

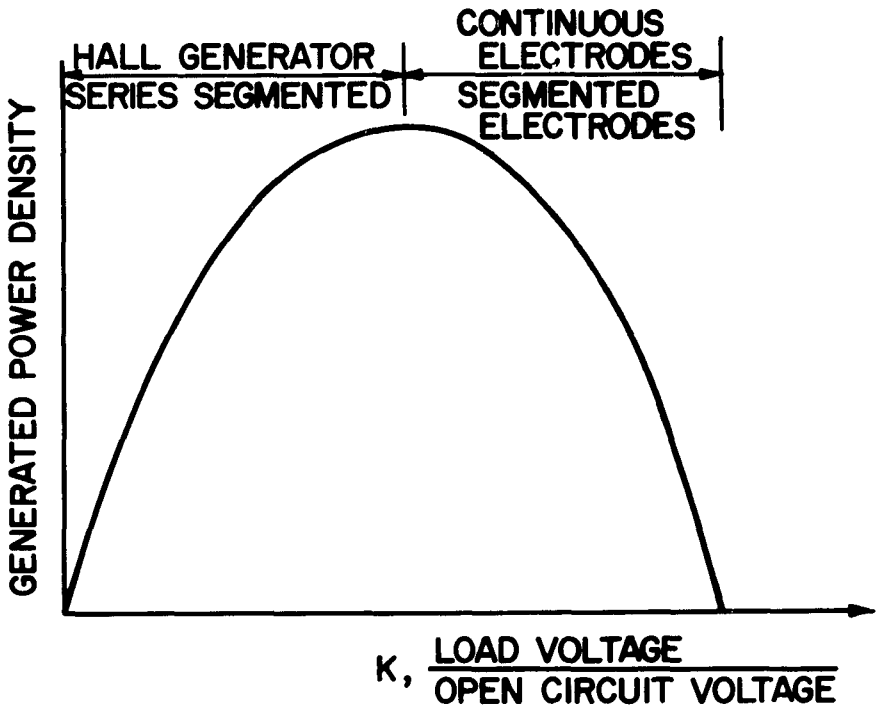

Figure 14.5. Local Power Density For Several Generator Geometries as a Function of the Ratio of Load Voltage to Open Circuit Voltage

where R_L is the new load resistance, and R_{L_o} was the initial value of the load. For example, consider $K_o = 0.6$, $R_{L_o}/R_{i_o} = 1.5$, $\beta_o = 2$. If the load resistance is doubled, while the magnetic field is decreased to keep the load voltage constant, then K becomes 0.83. On the other hand, if the magnetic field were kept constant, doubling the load would only increase the value of K to 0.75.

In addition to the Lorentz force, which acts to retard the flow, there is a component of the Lorentz force in the direction of the cathode which is the product of $\beta_e/(1 + \beta_e \beta_I)$ and the retarding Lorentz force. This is balanced by a transverse pressure gradient; if the magnetic interaction parameter, based on the channel width is large, this transverse pressure gradient could become quite large, and would alter the density or temperature across a cross-section.

14.3b Segmented Electrodes

In the previous section, it was shown that with increasing magnetic field, the generated power density due to electrons becomes asymptotic to $\left[n_e m_e U^2 K(1-K) \nu_e\right]$, because of the Hall reduction in electrical conductivity in the direction of the electric field. To remedy this situation, the segmented electrode generator has been devised[5,6] in which each opposite pair of electrodes is connected to a single load, see Figure 14.3. In this arrangement, the current flow is essentially transverse to the gas flow, and no net Hall current exists in the downstream direction. Since the gas is electrically neutral, this means, of course, that the electron and ion velocities in the downstream direction are equal to each other and are also equal to the gas velocity in the downstream direction, in the absence of ion slip.

With the Hall current j_x equal to zero, (14.18) predicts that an electric field will develop in the axial direction given by

$$E_x = \frac{\beta_e}{1 + \beta_e \beta_I} (E_y - UB) \qquad (14.32)$$

so that the current in the y direction becomes:

$$j_y = \frac{\sigma}{1 + \beta_e \beta_I} (E_y - UB) \tag{14.33}$$

As in the previous section, the open circuit voltage corresponding to $j_y = 0$ is UB; we therefore take the electric field under load as KUB. The Lorentz force $\underset{\sim}{j} \times \underset{\sim}{B}$ now acts only in the negative x direction so that it acts only to retard the flow. This force is exerted purely on the ions and not the electrons, as shown in the following argument. The electron velocity with respect to the generator may be resolved into two parts, one due to the electron drift motion $\underset{\sim}{E} \times \underset{\sim}{B}$ and the other in the downstream direction due to collisions with the gas, v_{e_c}

$$\underset{\sim}{v}_e = \frac{\underset{\sim}{E} \times \underset{\sim}{B}}{B^2} + \underset{\sim}{i} v_{e_c} \tag{14.34}$$

see Figure 14.6. In the y-direction, (14.34) becomes with the use of (14.32):

$$v_{e_y} = - E_x B^{-1} = (1-K)\, \omega_e \tau_e U/(1 + \beta_e \beta_I) \tag{14.35}$$

in agreement with (14.33). The electron velocity in the downstream direction is equal to the ion velocity, which for $\beta_e \beta_I \ll 1$ is the gas velocity; thus, from (14.34):

$$v_{e_x} = E_y B^{-1} + v_{e_c}$$

or

$$U = KU + v_{e_c} \tag{14.36}$$

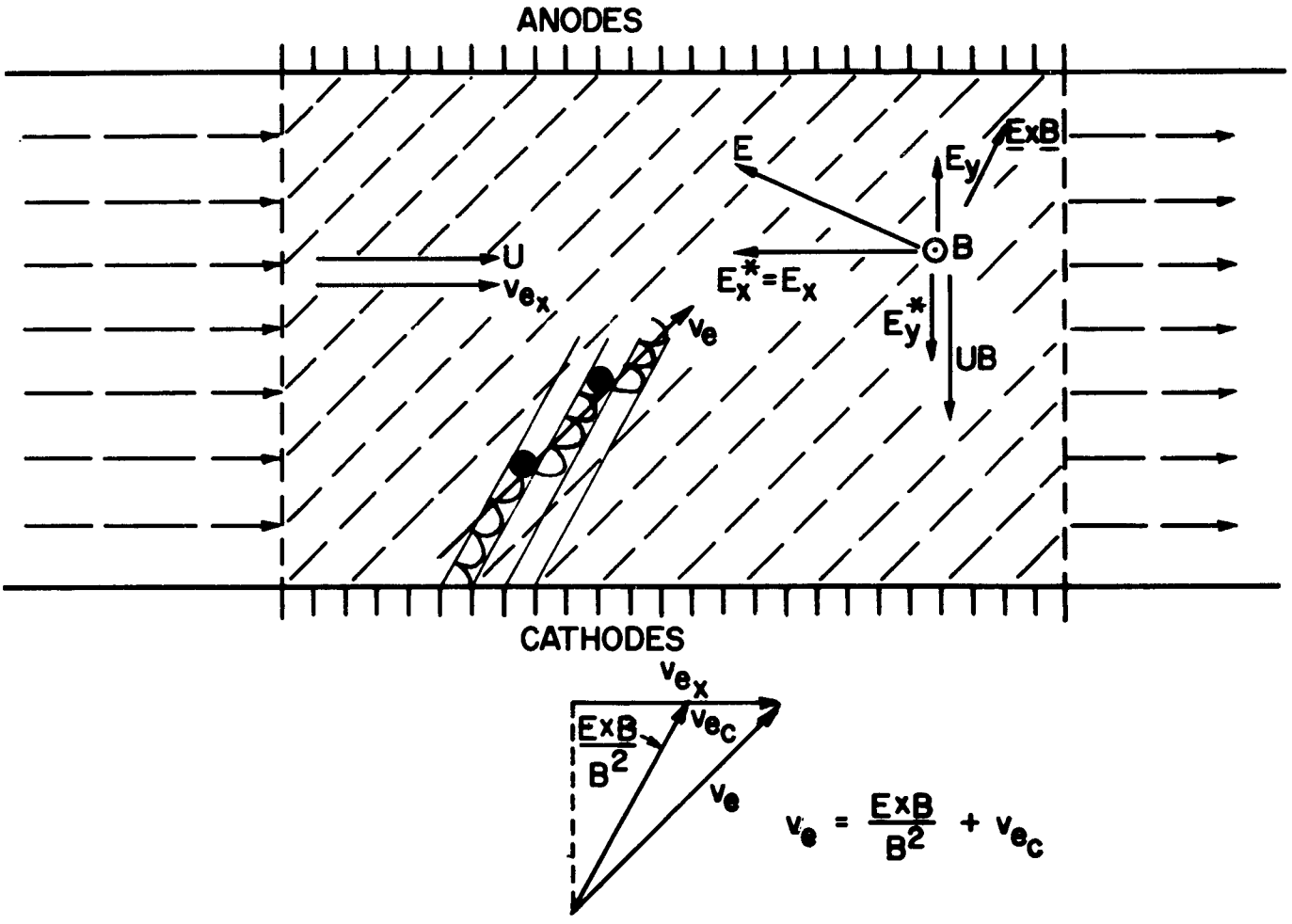

Figure 14.6. Electron Motion and Electric Fields in a Segmented Electrode Geometry

so that the velocity increment in the downstream direction is $v_{e_c} = (1-K)\,U$. Now, the total force on electrons in the x direction is given by:

$$F_{e_x} = -ne\,(E_x + v_{e_y} B) \tag{14.37}$$

Substitution of E_x from (14.32) (with $\beta_e \beta_I$ neglected) and v_{e_y} from (14.35) shows that the net axial force on the electrons is zero. On the other hand, the force on ions* in the x direction is $F_{I_x} = n_e e E_x$; use of (14.32) then yields $F_{I_x} = ne\,\beta_e\,(K-1)\,UB/(1 + \beta_e \beta_I)$ which is identical to $\underset{\sim}{j} \times \underset{\sim}{B}$ as obtained from (14.33).

(i) Power Density and Efficiency, Segmented Electrodes

The power density is $-\underset{\sim}{E} \cdot \underset{\sim}{j} = -E_y j_y$, or:

$$P = \frac{K(1-K)\,\sigma\,U^2 B^2}{1 + \beta_e \beta_I}$$

$$= \frac{n_e m_e U^2 K(1-K)}{\tau_e} \quad \frac{\beta_e^2}{1 + \beta_e^2 \mu_I/\mu_e} \tag{14.38}$$

As in the case of continuous electrodes, the power density initially increases quadratically with increasing magnetic field (since $\beta_e = e \tau_e B/m_e$); and the last factor of (14.38) becomes asymptotic to μ_e/μ_I, see Figure 14.4. However, for intermediate values of β_e, no first asymptote appears in the power density as was the case for continuous electrodes. Thus, for $1 < \beta_e < (\mu_e/\mu_I)$, the generated power of the segmented electrode geometry greatly exceeds that for the continuous electrode geometry. The generated power comes from the ions for this geometry; in fact, the electrons actually

*It has been assumed that all ions are positively charged. If some have negative charges, the force is $e\,(n_I^+ - n_I^-)\,E_x$. But $n_I^+ - n_I^- = n_e$ in an electrically neutral gas, therefore, this same expression applies.

decrease the power generation. The power is obtained from the ions by their motion against the x-component of the electric field:

$$P_I = -n_e e U E_x = n_e e \beta_e (1-K) U^2 B/(1 + \beta_e \beta_I) \qquad (14.39)$$

The power generated by the electrons is:

$$P_e = n_e e \underset{\sim}{v}_e \cdot \underset{\sim}{E}$$

Now, from (14.34) the electron velocity consists of two parts: $\underset{\sim}{E} \times \underset{\sim}{B}/B^2$ and $\underset{\sim}{i} v_{e_c}$. The drift velocity $\underset{\sim}{E} \times \underset{\sim}{B}/B^2$ generates zero power since $\underset{\sim}{E} \times \underset{\sim}{B} \cdot \underset{\sim}{E} = 0$; while the part due to v_{e_c} in the x-direction yields

$$P_e = -n_e e (1 - K)^2 U^2 \beta_e B/(1 + \beta_e \beta_I) \qquad (14.40)$$

so that the electrons actually consume power; that is, power must be expended in order for the electrons to move with the gas velocity U. The sum of (14.39), (14.40) is identical to that given by (14.38).

The local efficiency is still equal to K, since $\eta_L = E_y j_y/U B j_y$. Thus, the increase in power density has been obtained with no sacrifice in efficiency. Since the power density is still a maximum when $K = \frac{1}{2}$, this geometry will also be operated on the downward side of the power curve, see Figure 14.5.

14.3c Hall Generator[7]

When the electrodes are segmented it was shown in the previous section that an electric field develops in the flow direction, see (14.32). This electric field is maximum when the opposite electrodes are short-circuited; that is, when

$E_y = 0$. If the electrode pair at the inlet is connected through a load to the pair at the exit, a current should then flow through the load. With $E_y = 0$, the current density in the +x direction is obtained from (14.18):

$$j_x = \frac{\sigma}{(1 + \beta_e \beta_I)^2 + \beta_e^2} \left[(1 + \beta_e \beta_I) E_x + \beta_e UB\right] \tag{14.41}$$

When open-circuited, the axial electric field is $-\beta_e UB/(1 + \beta_e \beta_I)$; under load the axial electric field will be some fraction K_H of this value, $E_x = -\beta_e K_H UB/(1 + \beta_e \beta_I)$, so that:

$$j_x = \frac{\sigma \beta_e (1-K_H) UB}{(1 + \beta_e \beta_I)^2 + \beta_e^2} \tag{14.42}$$

Note that the definition of K_H is different than K for the continuous and segmented electrode geometry.

(i) Power Density Hall Generator

The generated power density is:

$$P = -E_x j_x$$

$$= \frac{K_H (1-K_H) \sigma \beta_e^2 U^2 B^2}{(1 + \beta_e \beta_I) \left[(1 + \beta_e \beta_I)^2 + \beta_e^2\right]}$$

$$= \frac{n_e m_e U^2 K_H (1-K_H)}{\tau_e} \frac{\beta_e^4}{\left(1 + \beta_e^2 \frac{\mu_I}{\mu_e}\right) \left[\left(1 + \beta_e^2 \frac{\mu_I}{\mu_e}\right)^2 + \beta_e^2\right]} \tag{14.43}$$

In this geometry, as the magnetic field is increased from zero, the power increases as the fourth power of the magnetic field, in contrast to the

quadratic dependence of the continuous and segmented electrode geometries. An asymptote is reached when $\beta_e > \mu_e/\mu_I$, equal to $(\mu_e/\mu_I)^3 \beta_e^{-2}$, which is considerably smaller than the asymptote of μ_e/μ_I obtained in the continuous and segmented geometry generators. However, for $2 < \beta_e < (\mu_e/\mu_I)^{1/2}$, the power density approaches that of the segmented electrode geometry.

The retarding Lorentz force, $j_y B$ becomes:

$$F_x = \frac{-\sigma U B^2}{1 + \beta_e \beta_I} \cdot \frac{1 + \beta_e'^2 K_H}{1 + \beta_e'^2} \tag{14.44}$$

where β_e' is an effective Hall parameter for electrons defined as:

$$\beta_e' = \frac{\beta_e}{1 + \beta_e \beta_I} \tag{14.45}$$

Note that the retarding Lorentz force is a minimum when the load is short-circuited; that is, when $K = 0$. This is in sharp contrast to the previous geometry, where the retarding force is a maximum when short-circuited. This effect is again due to the force on the ions: in the segmented electrode generator, the axial electric field is a maximum when short-circuited; in the Hall geometry when $K = 0$, there is no axial electric field and therefore no net axial force on the ions. This may be seen as follows: the axial force on the ions is (neglecting ion slip):

$$F_{Ix} = n_I e E_x = -n_e e \beta_e U B K_H \tag{14.46}$$

The electron current relative to the gas is:

$$j_{ex} = \frac{\sigma}{1 + \beta_e^2} \left[E_x + \beta_e U B \right] \tag{14.47}$$

so that the electron velocity relative to the gas is

$$\overline{V}_{e_x} = \frac{-e\tau_e \beta_e UB}{(1+\beta_e^2)\, m_e} (1-K)_H \tag{14.48}$$

The motion of the electrons relative to the gas exert a friction drag on the gas given by:

$$F_{g_x} = -\frac{n_e m_e \overline{V}_{e_x}}{\tau_e} = -\frac{n_e e \beta_e UB}{1+\beta_e^2} (1-K)_H \tag{14.49}$$

The sum of (14.46, 14.49) then yields the total force on the gas heavy particles. This expression is identical to the expression (14.44), neglecting ion slip.

(ii) Efficiency, Hall Generator

The local efficiency of the Hall generator is the ratio of the power (14.43) to the flow work UF_x when F_x is given by (14.44). Thus,

$$\eta_L = \frac{\beta_e'^2 K_H (1-K)_H}{1+\beta_e'^2 K_H} \tag{14.50}$$

For small values of $\beta_e'^2$, the efficiency is proportional to $\beta_e'^2$ and is maximum when $K = \frac{1}{2}$. For large values of $\beta_e'^2$, the efficiency becomes:

$$\beta_e'^2 \longrightarrow \infty, \quad \eta_L \longrightarrow (1-K)_H, \tag{14.51}$$

that is, the efficiency is a <u>maximum</u> when K_H is small, that is, when close to short-circuited. For arbitrary values of β_e', as K is increased, the

efficiency at first increases, then decreases, as shown in Figure 14.7. Thus, for any given value, there is a value of K_m which yields the maximum efficiency. This value is obtained by differentiation of (14.50) with respect to K; the result is:

$$\beta_e'^2 K_m^2 + 2 K_m - 1 = 0 \tag{14.52}$$

which yields

$$K_m = \beta_e'^{-2} \left[\sqrt{\beta_e'^2 + 1} - 1 \right] \tag{14.53}$$

Also, from (14.52):

$$\beta_e'^2 = \frac{1-2 K_m}{K_m^2} \tag{14.54}$$

Substitution of (14.54) into (14.50) yields η_{L_m} in terms of K_m:

$$\eta_m = 1 - 2 K_m \tag{14.55}$$

Substitution of K_m from (14.55) into (14.54) yields an alternate form for the maximum local efficiency:

$$\frac{4 \eta_{L_m}}{(1-\eta_{L_m})^2} = \beta_e'^2 \tag{14.56}$$

Thus, β_e' must be large in order for the local efficiency to be close to unity. Figure 14.8 shows the maximum efficiency as a function of β_e' given by

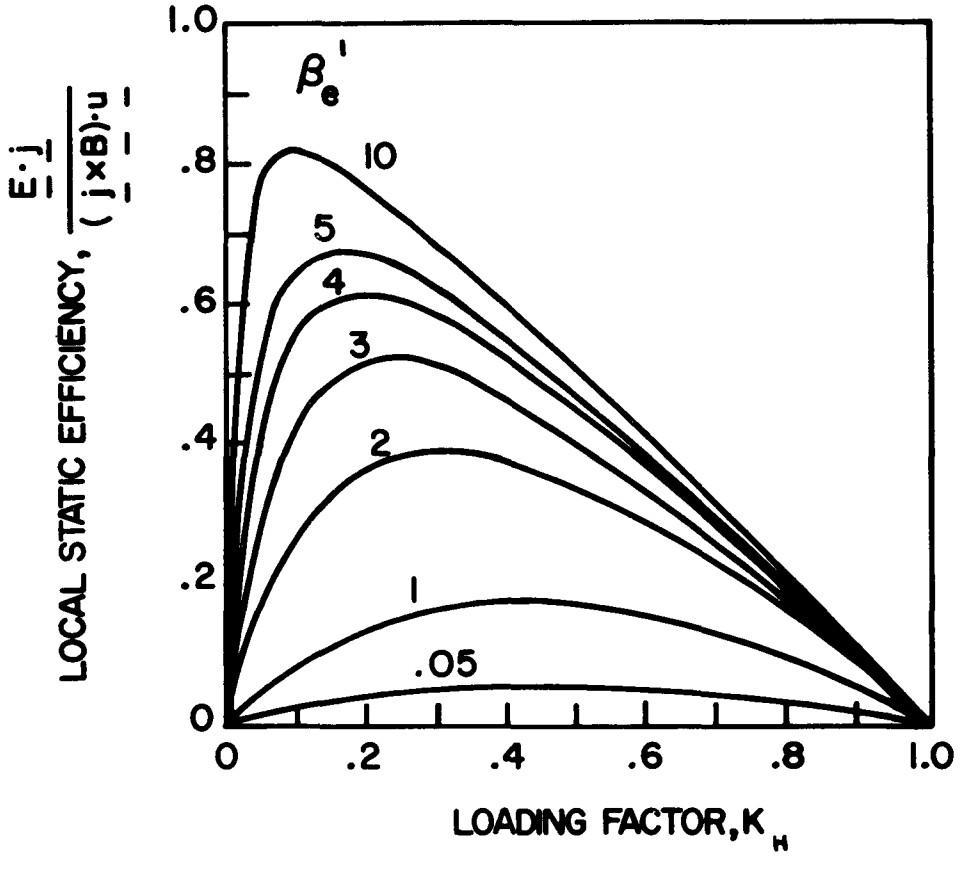

Figure 14.7. Local Static Efficiencies, Hall MHD Generator, for Various Values of $\beta_e' = \omega_e\tau_e/(1+\omega_e\tau_e\omega_I\tau_{In})$

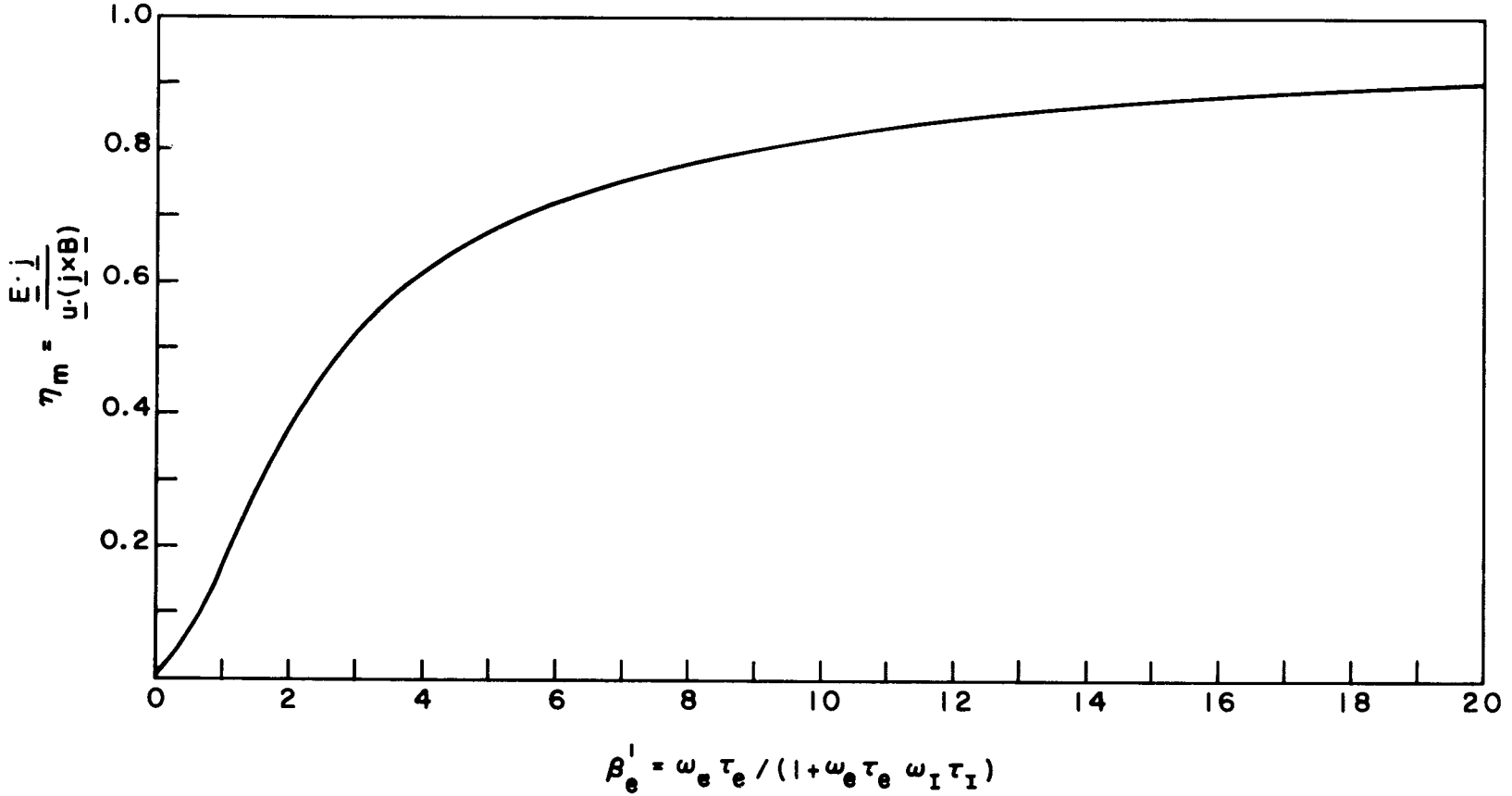

Figure 14.8. Maximum Local Static Efficiency For Hall Generator

(14.56). Note, however, that as the magnetic field is increased from zero, that is, as β_e is increased, β_e' first increases, reaches a maximum, and then decreases. The maximum value of β_e' is obtained by setting equal to zero the derivative with respect to β_e of $\beta_e/(1 + \beta_e^2 \mu_e/\mu_I)$. The result is:

$$\beta'_{e\,max} = \sqrt{\mu_e/\mu_I} \tag{14.57}$$

Thus, if the mobility ratio is 100, the maximum value of β_e' is 10 and the maximum local efficiency is slightly over 80%.

(iii) Comparison With Segmented Electrodes

It was shown in the previous section that the segmented electrode generator has a higher power density than the continuous electrode generator for $1 < \beta_e < \mu_e/\mu_I$, for the same value of local efficiency. It is therefore desirable to compare the power densities of the Hall generator to that of the segmented electrode generator for the same values of η_L. From (14.38, 14.43),

$$\frac{P_{Hall}}{P_{Seg}}\,(\eta_L) = \frac{K_H(1-K_H)\,\beta_e'^{\,2}}{\eta_L(1-\eta_L)(1+\beta_e'^{\,2})} \tag{14.58}$$

where $K_H = K_H(\eta_L)$, given by (14.50). This ratio is shown in Figure 14.9 as a function of the parameter β_e'. It is seen that for the same efficiency, the power density of the Hall generator approaches that of the segmented electrode generator. Of course, the latter generator can be operated at any local efficiency, while the maximum efficiency of the Hall generator depends on the value of β_e'; this maximum efficiency is shown as the dashed line in Figure 14.9.

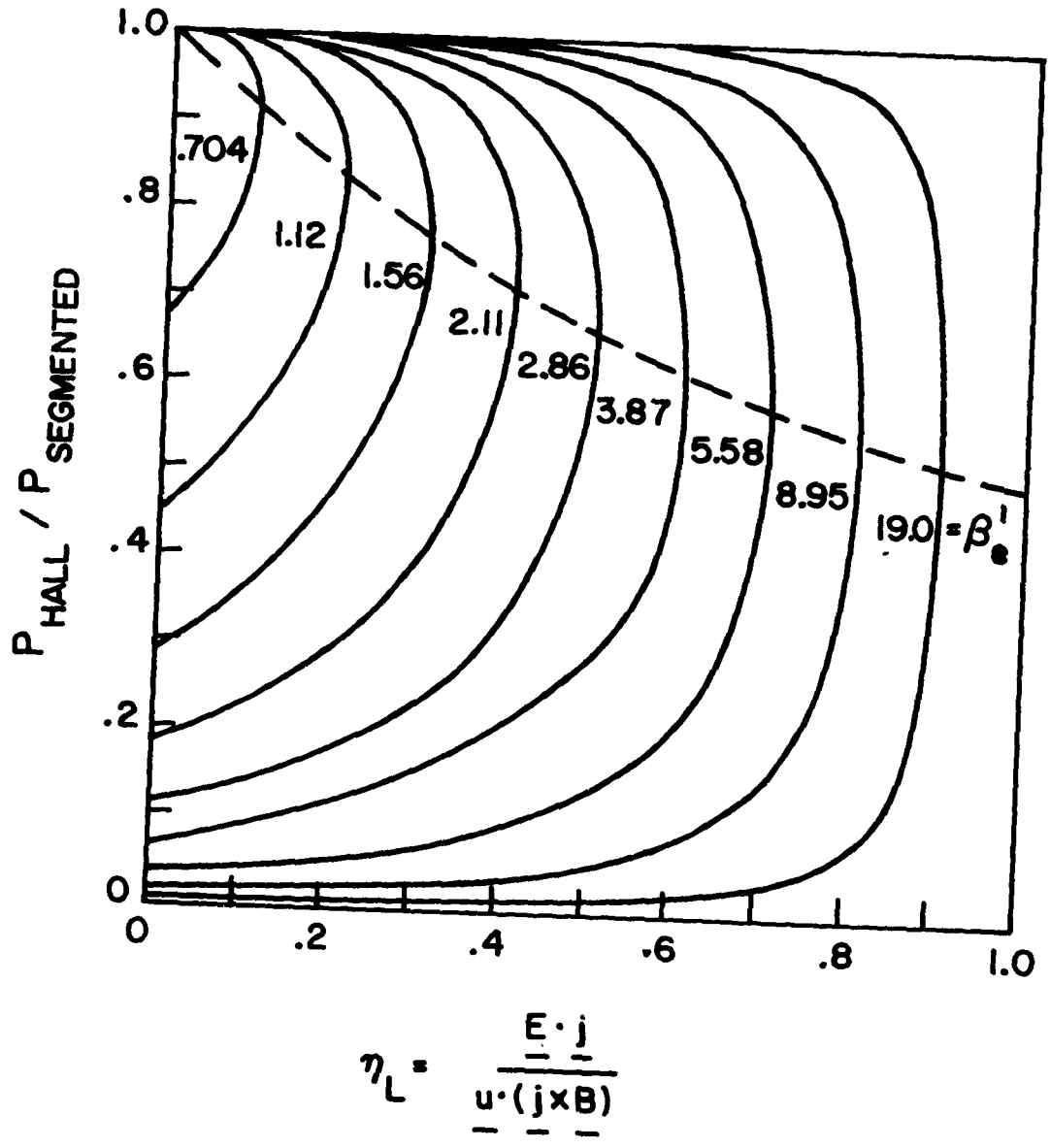

Figure 14.9. Comparison of Power Density of Hall Generator to Power Density of Segmented Electrode Generator, For Various Values of $\beta'_e = \omega_e \tau_e / (1 + \omega_e \tau_e \omega_I \tau_I)$

Since the Hall current is allowed to flow, a Lorentz force will exist in the -y direction, as in the case of continuous electrodes. The ratio of this transverse force to the retarding Lorentz force is j_x/j_y, or

$$\frac{F_y}{F_x} = \frac{\beta_e' (1-K_H)}{1 + \beta_e' K_H}$$

which is of order of magnitude unity, for $\beta_e > 1$; this must be balanced by a pressure gradient of the gas normal to the plane of the electrodes similar to continuous electrodes.

(iv) Voltage Control, Hall Generator

Since the maximum power density is developed when $K_H = \frac{1}{2}$, see (14.43), and the efficiency is a maximum when $K_H < \frac{1}{2}$ (see Figure 14.7), the Hall generator will generally be operated on the rising part of the power curve, see Figure 14.5. This means that if the generator load consists of resistances in parallel, as the load is reduced by removing resistances, the total load resistance will increase, increasing the load voltage. If the initial point of operation was $K_H \ll \frac{1}{2}$ then the new value of the loading factor may still be less than $\frac{1}{2}$, so that the power to the remaining load is now greater than the original power to all resistances. Morever, as K_H increases, the efficiency decreases, in contrast to the previous two geometries. This may be seen as follows: The load voltage is given by $K_H \beta_e' UBL$, where L is the generator length; the load current is $\sigma h b \beta_e UB \cdot (1-K_H) \left[(1 + \beta_e \beta_I)^2 + \beta_e^2\right]^{-1}$: thus, the load resistance $R_L = V/I$, is given by

$$R_L = R_i \frac{K_H}{1-K_H} \qquad (14.59)$$

where the internal resistance of the Hall generator is defined as:

$$R_i = \frac{L\left[(1+\beta_e\beta_I)^2+\beta_e^2\right]}{\sigma b h (1+\beta_e\beta_I)} \tag{14.60}$$

Solving (14.59) for K_H, one obtains:

$$K_H = \frac{1}{1+\frac{R_i}{R_L}} \tag{14.61}$$

For $K_H < \frac{1}{2}$, $R_i > R_L$; thus, the external resistance must be <u>less</u> than the internal resistance to obtain good local efficiencies. This is also in contrast to the previous cases. Thus, as R_L increases, K_H will also increase, and η_L will decrease. To remedy this situation, the load resistances can be connected in series and resistances can be removed from the circuit by shunting them, or the magnetic field can be reduced to keep the load voltage constant, if the load resistances are in parallel. The analysis of the voltage control is simplified if the ion slip is neglected. Then, to keep the axial electric field constant, the magnetic field must be varied so that

$$\left(\frac{B}{B_o}\right)^2 = \frac{K_o}{K_H} \tag{14.62}$$

where K_o, B_o are the initial or design values of the loading factor and magnetic field, respectively. From (14.59, 14.60), the load resistance is given by:

$$R_L = \frac{L(1+\beta_e^2)K_H}{\sigma b h (1-K_H)} \tag{14.63}$$

and the design load is

$$R_{L_o} = \frac{L}{\sigma b h} \frac{(1 + \beta_o^2) K_o}{(1-K_o)} \tag{14.64}$$

The ratio of off-design load resistance to load resistance is obtained by dividing (14.63) by (14.64). Thus, the off-design load factor K_H is given by:

$$\frac{R_L}{R_{L_o}} = \frac{\frac{K}{1-K}\left(\frac{1}{\beta_o^2} + \frac{K_o}{K_H}\right)}{\frac{K_o}{1-K_o}\left(\frac{1}{\beta_o^2} + 1\right)} \tag{14.65}$$

where use has been made of $\beta_e^2 K = \beta_o^2 K_o$. From (14.5c) The off-design efficiency is given by:

$$\eta_L = \frac{K_H(1-K_H)}{\frac{1}{\beta_e^2} + K_H} = \frac{1-K_H}{\frac{1}{\beta_o^2 K_o} + 1} \tag{14.66}$$

For example, consider a Hall generator which has been designed for $\beta_o = 5$, $K_o = 0.2$, $\eta_L = \frac{2}{3}$. Suppose the load resistance is increased by 38.5%, and the magnetic field is reduced to keep the load voltage constant. From (14.65) the off-design value of K_H becomes 0.4; from (14.62), the magnetic field and β_e are reduced by 0.707, and the efficiency drops to 0.5, from (14.66). If the magnetic field had been kept constant while the load resistance was increased by the same amount, the load factor would have increased to 0.53, and the efficiency would have been reduced to 0.436.

(v) Annular Hall Generator

Since there is no electric field in the y-direction, it is possible to "wrap" this geometry into a cylindrical annulus; the axial coordinate is then x; the y coordinate becomes the circumferential coordinate Θ, and the z-coordinate becomes the radial coordinate, see Figure 14.10. In this device, the flow is introduced in the axial direction and the magnetic field is in the radial direction. In practice, it is not possible to make radial magnetic fields which have large axial lengths; it is necessary to periodically reverse the direction of the radial magnetic field, see Reference 2 for one method of accomplishing this. However, the power generation or efficiency does not depend on the direction of the radial magnetic field; in fact, it may be shown that the power density depends only on the average of the square of the magnetic field.

On the other hand, the circumferential Lorentz force on the gas, which is caused by the axial current j_x, does depend on the direction of the radial magnetic field. If the radial magnetic field were to be in the same direction, this circumferential force would cause the gas to rotate; that is, the flow would become helical. But if the direction of the radial magnetic field were alternated, then the direction of the circumferential force would also alternate in the x direction. This would tend to minimize the rotation of the gas.

For this geometry, the local performance is given by the previous formula, if the annulus is narrow.

14.3d Series-Segmented and Helical Flow Generators

In the preceding sections it has been shown that the segmented electrode has the combination of the highest power density and highest efficiency of the three configurations which have been discussed; however, it suffers from the requirement of multiple loads. This problem can be relieved by connecting the electrodes which are at the same potential in series, see Figure 14.11. The lines of constant

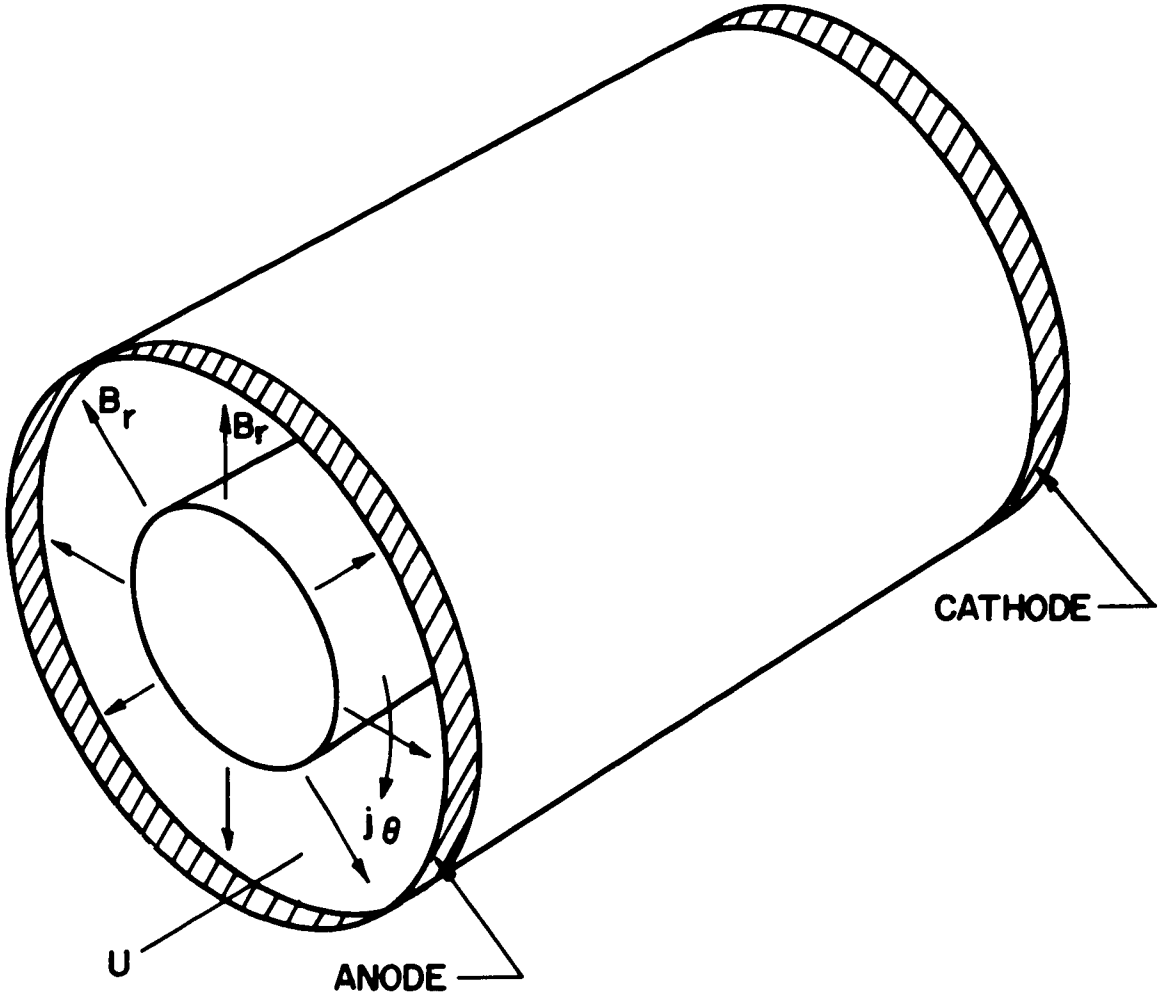

Figure 14.10. Schematic Diagram of Annular Hall Generator

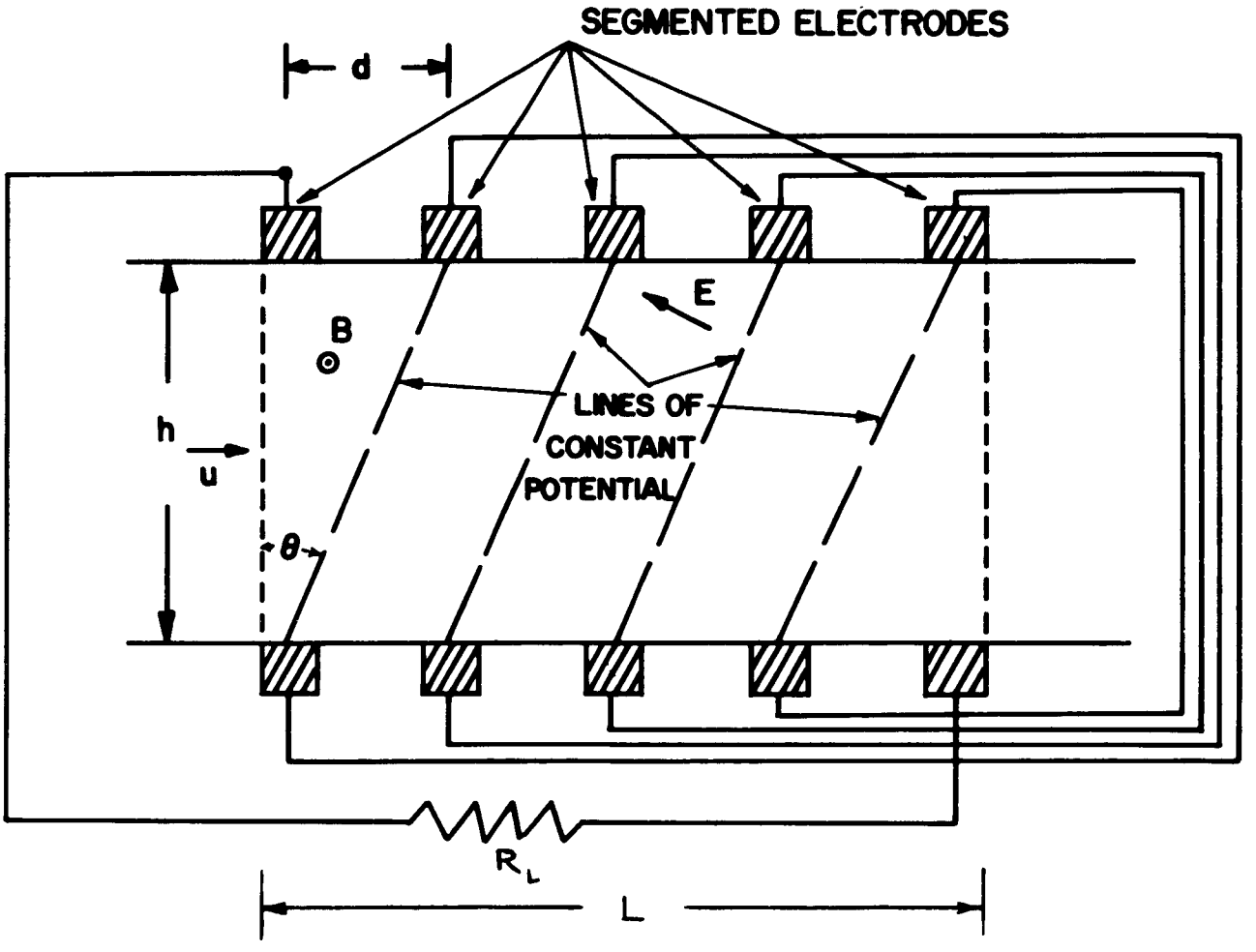

Figure 14.11. Connection Diagram For the Series - Segmented Electrode Geometry. $\tan\theta = \alpha^{-1} = (1-\eta_o)/\eta_o\beta_e'^2$

potential are normal to the electric field shown in Figure 14.6. The requirement for connection of electrodes is that $\Delta\varphi_y = \Delta\varphi_x$, or $E_y h = E_x d$, which from (14.32) becomes:

$$\frac{d}{h} = \frac{K}{(1-K)\,\beta'_e} \tag{14.67}$$

The connections shown in Figure 14.11 are for a single load; if additional electrodes are inserted between those shown and connected in series, two loads may be used, and so forth.

(i) Maximum Power Density

Now it is natural to inquire whether there is some other linear geometry which can have a higher power density than the three geometries which have been considered for a given efficiency. To determine this, let

$$\begin{aligned} E_x &= K_1\, UB \\ E_y^* &= K_2\, UB \end{aligned} \tag{14.68}$$

so that $E_y = UB + E_y^* = (K_2 + 1)\, UB$. The current can be obtained in terms of K_1, K_2 from (14.18), and the power becomes:

$$P = \eta_L\, j_y\, B = \frac{\eta_L \sigma\, UB^2}{(1 + \beta_e \beta_I)(1 + \beta'^2_e)} \left[K_2 + \beta'_e\, K_1\right] \tag{14.69}$$

For η_L constant, differentiation of (14.69) with respect to K_2 shows that the power density is a maximum when

$$\frac{dK_1}{dK_2} = -\frac{1}{\beta'_e} \tag{14.70}$$

Now, the efficiency is also given by $(-E_x j_x - E_y j_y)/j_y$ UB, or:

$$\eta_L = \frac{K_1^2 + K_2 (K_2 + 1) + \beta_e' K_1}{K_2 + \beta_e' K_1} \tag{14.71}$$

For η_L constant, differentiation of (14.71) yields:

$$2 K_1 \frac{d K_1}{d K_2} = - \beta_e' (1 - \eta_L) \frac{d K_1}{d K_2} - 2 K_2 - 1 + \eta_L \tag{14.72}$$

Finally, substitution of K_1 from (14.71) and $(d K_1/d K_2)$ from (14.70) yields:

$$K_2 = \eta_L - 1 \tag{14.73}$$

Substitution of this value of K_2 into (14.71) yields the following value of K_1:

$$K_1 = \beta_e' (\eta_L - 1) = \beta_e' K_2 \tag{14.74}$$

Use of (14.68) then shows that

$$E_x = \beta_e' E_y^* \tag{14.75}$$

so that the axial current j_x is zero, which is precisely the condition in the segmented electrode geometry. Thus, for a linear generator, the segmented electrode geometry yields the highest power density for any given efficiency. This condition may also be interpreted as follows: the highest power density and efficiency is obtained when the Lorentz force exactly opposes the gas velocity.

(ii) Load Variation - Series Segmented

The series-segmented geometry is designed for just one loading, since the electrode pitch d is selected on the basis of the loading factor K. Thus, once K is selected,

$$\frac{-E_x}{E_y} = \frac{h}{d} = \alpha \tag{14.76}$$

remains constant regardless of the loading, where

$$\alpha = \left(\frac{1-\eta_o}{\eta_o}\right) \beta'_e \tag{14.77}$$

and η_o is the local efficiency η_L for the design load, from (14.67). For an off-design load, $E_y = K\,U\,B$, so that $E_x = -\alpha\,K\,U\,B$, and the load voltage is

$$V = K\,U\,B\,h\,(1 + L/d) \tilde{\sim} K\,U\,B\,\alpha\,L \tag{14.78}$$

where L is the generator length. The load current is the sum of the current to an electrode plus the axial current:

$$I = \left(-j_y d + j_x h\right) b \tag{14.79}$$

From (14.18, 14.76),

$$j_y = \frac{\sigma\,U\,B}{(1 + \beta_e \beta_I)(1 + \beta'^2_e)} \left[K - 1 - \beta'^2_e \left(\frac{1-\eta_o}{\eta_o}\right) K\right] \tag{14.80}$$

*This may also be shown by using I = P/V, where V is given by (14.78); $P = -(E_x j_x + E_y j_y) h\,Lb$; and use of (14.76).

$$j_x = \frac{\sigma \quad UB \ \beta_e'}{(1 + \beta_e \beta_I)(1 + \beta_e'^{\,2})} \quad \frac{(-K + \eta_o)}{\eta_o} \tag{14.81}$$

so that the load current is:

$$I = \frac{\sigma UBdb}{(1 + \beta_e \beta_I)(1 + \beta_e'^{\,2})} \left[1 - K + \beta_e'^{\,2} \frac{(1-\eta_o)}{\eta_o} K - \left(\frac{1-\eta_o}{\eta_o^{\,2}}\right) \beta_e'^{\,2} (K-\eta_o) \right] \tag{14.82}$$

The value of K which corresponds to open circuit is obtained by setting the bracket in (14.82) to zero:

$$K_{o.c.} = \frac{1 + \left(\frac{1-\eta_o}{\eta_o}\right) \beta_e'^{\,2}}{1 + \beta_e'^{\,2} \left(\frac{1-\eta_o}{\eta_o}\right)^2} \tag{14.83}$$

which can be greater than unity. In fact, for $\beta_e'^{\,2} \gg 1$, the open circuit value of $K_{oc} = \eta_o/(1-\eta_o)$. Thus, if the design value of η_o is greater than 1/2, K_{oc} is greater than unity. The power generated is given by the product of (14.78) and (14.82); the ratio of the off-design power to the design power (14.38) is given by:

$$\frac{P}{P_o} = -\frac{K}{(1 + \beta_e'^{\,-2})\, \eta_o (1 - \eta_o)} \left\{ \left(\frac{1-\eta_o}{\eta_o}\right) \left[\left(\frac{1-\eta_o}{\eta_o}\right) K + K - 1 \right] \right.$$

$$\left. + \beta_e'^{\,-2} (K-1) - K \left(\frac{1-\eta_o}{\eta_o}\right) \right\} \tag{a}$$

For $\beta_e'^2 \gg 1$, this reduces to

$$\frac{P}{P_o} = \frac{K}{\eta_o^2} \left[1 - \left(\frac{1-\eta_o}{\eta_o}\right) K\right] \qquad (b)$$

This has a maximum when K is equal to $\frac{1}{2}\ \eta_o/(1-\eta_o)$, that is, half the open-circuit voltage; this maximum is

$$\frac{P}{P_o} = \frac{1}{4\,\eta_o\,(1-\eta_o)} \qquad (c)$$

Since $\left[\eta_o\,(1-\eta_o)\right]^{-1}$ is always greater than 4, the maximum power is always greater than the design power. Now, if $\eta_o > \frac{1}{2}$, the operating point will always be less than half the open-circuit voltage. Thus, the design point will be on the rising part of the power curve, see Figure 14.5. In this respect, the series-segmented electrode generator resembles the Hall generator. If, however, the design value of η_o is less than $\frac{1}{2}$, the design point lies on the falling side of the power curve.

The load resistance is given by the ratio of the load voltage to the current; the design value corresponding to $K=\eta_o$ is given by:

$$R_{L_o} = \left(\frac{1-\eta_o}{\eta_o}\right) \frac{L}{\sigma b h}\ \beta_e'^2\,(1+\beta_e\beta_I) = \frac{L}{\sigma b d}\ \beta_e'\,(1+\beta_e\beta_I) \qquad (d)$$

while the off-design load is related to the load factor K by:

$$\frac{R_L}{R_{L_o}} = \frac{K\,(1+\beta_e'^{-2})}{1+\beta_e'^{-2}\,\eta_o\left(\frac{1-K}{1-\eta_o}\right) - \left(\frac{1-\eta_o}{\eta_o}\right) K} \qquad (e)$$

For $\beta_e'^2 >> 1$, the reciprocal of (e) becomes:

$$\frac{R_{L_o}}{R_L} = \frac{1}{K} + 1 - \frac{1}{\eta_o} \tag{f}$$

which shows that as the load resistance increases, the value of K increases.

The efficiency is the ratio of the power to j_y UB, or:

$$\eta_L = K - \frac{\frac{K}{\eta_o}\beta_e'^2\left[K - \eta_o\right]}{\eta_o\left(\frac{1-K}{1-\eta_o}\right) + \beta_e'^2 K} \tag{14.84}$$

For large values of $\beta_e'^2$ this becomes:

$$\eta_L = 1 - K\left(\frac{1-\eta_o}{\eta_o}\right) \tag{14.85}$$

Thus, as the load resistance increases, the load voltage will increase, and the efficiency will decrease. This behavior is also similar to that of the Hall generator.

(iii) Helical Flow Generator

It was shown in the preceding section that the series-segmented electrode geometry has the advantage of the high efficiency and power density of the segmented electrode geometry, but has only two terminals for a single load. In comparison to the annular Hall geometry, it is mechanically complex because of the necessity for having multiple electrodes and connections.

Consider the electrode arrangement shown in Figure 14.11, where the electrodes are along constant potential lines. If the electrodes were re-arranged, as shown in Figure 14.12, the power density and performance

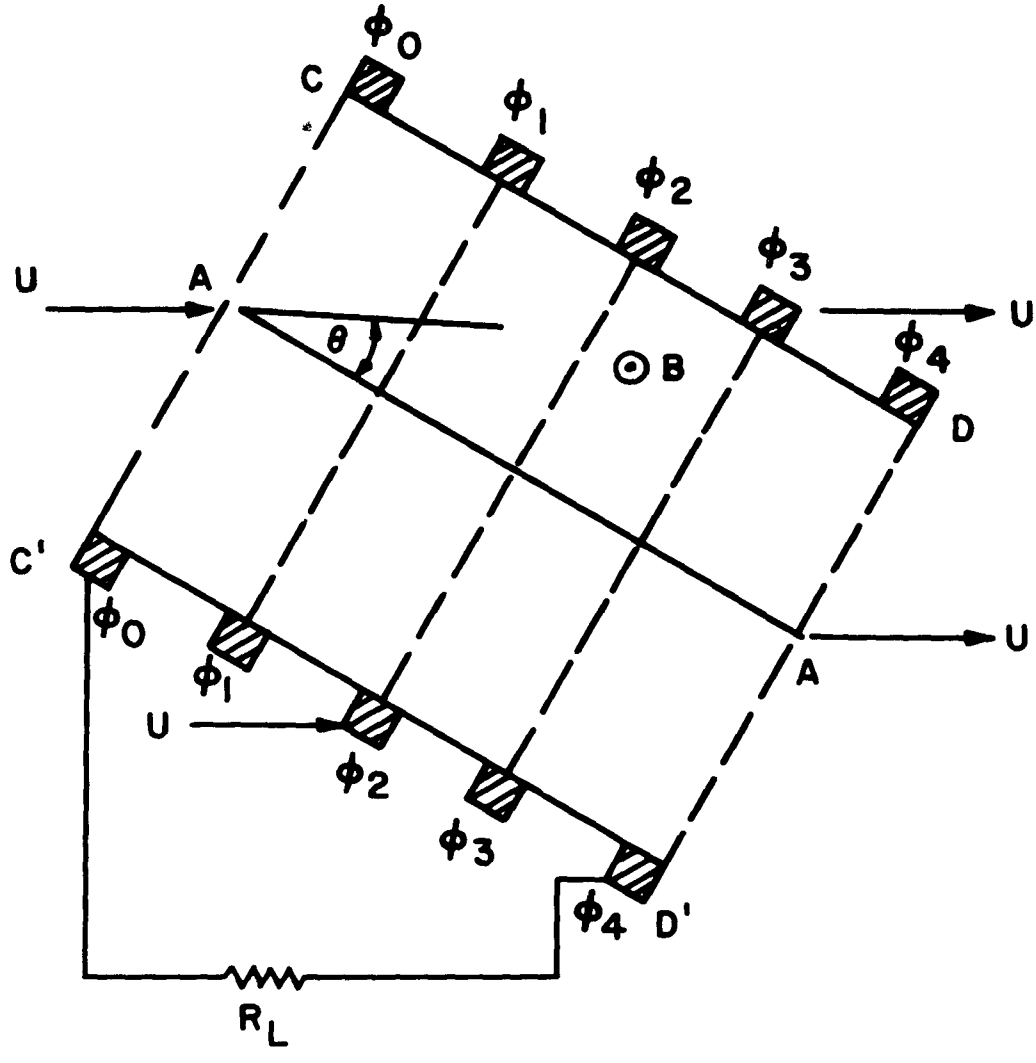

Figure 14.12. Rearrangement of Series - Segmented Electrode Geometry

would be the same as for Figure 14.11; that is, the total power and load voltage are identical. Note that the ionized gas must pass through the line of electrodes C-D. Now, this geometry is symmetrical about the line A-A. Thus, the performance is not changed if it is wrapped into an annulus with points C and C' meeting, and points D and D' also meeting. Since the equipotential lines now meet, the electrodes at φ_1-φ_3 may be dispensed with; only the electrodes at φ_0 and φ_4 are now needed for connection to the external load. This new geometry is shown in Figure 14.13; it is essentially the same as the annular Hall generator, except that now the gas must be admitted with a circumferential velocity v_θ, such that $v_\theta/u_x = d/h$, or:

$$\frac{v_\theta}{u_x} = \tan\theta = \frac{\eta_o}{(1-\eta_o)\,\beta'_e} \tag{14.86}$$

which can be accomplished by inlet turning vanes. The axial electric field is:

$$E_x = -\frac{u_x B \eta_o (1 + \tan^2\theta)}{\tan\theta} = -\frac{\beta'_e (1 + \tan^2\theta)\, u_x B}{1 + \beta'_e \tan\theta} \tag{14.87}$$

while the axial electric current density is given by:

$$j_x = \frac{\sigma(1-\eta_o)\, u_x B \tan\theta}{1 + \beta_e \beta_I} \tag{14.88}$$

The efficiency has been taken as η_o in (14.86 - 14.88), where the efficiency is now defined as:

$$\eta_o = \frac{E_x j_x}{\underset{\sim}{u} \cdot (\underset{\sim}{j} \times \underset{\sim}{B})} = \frac{E_x j_x}{(u_x j_y - v_y j_x) B} \tag{14.89}$$

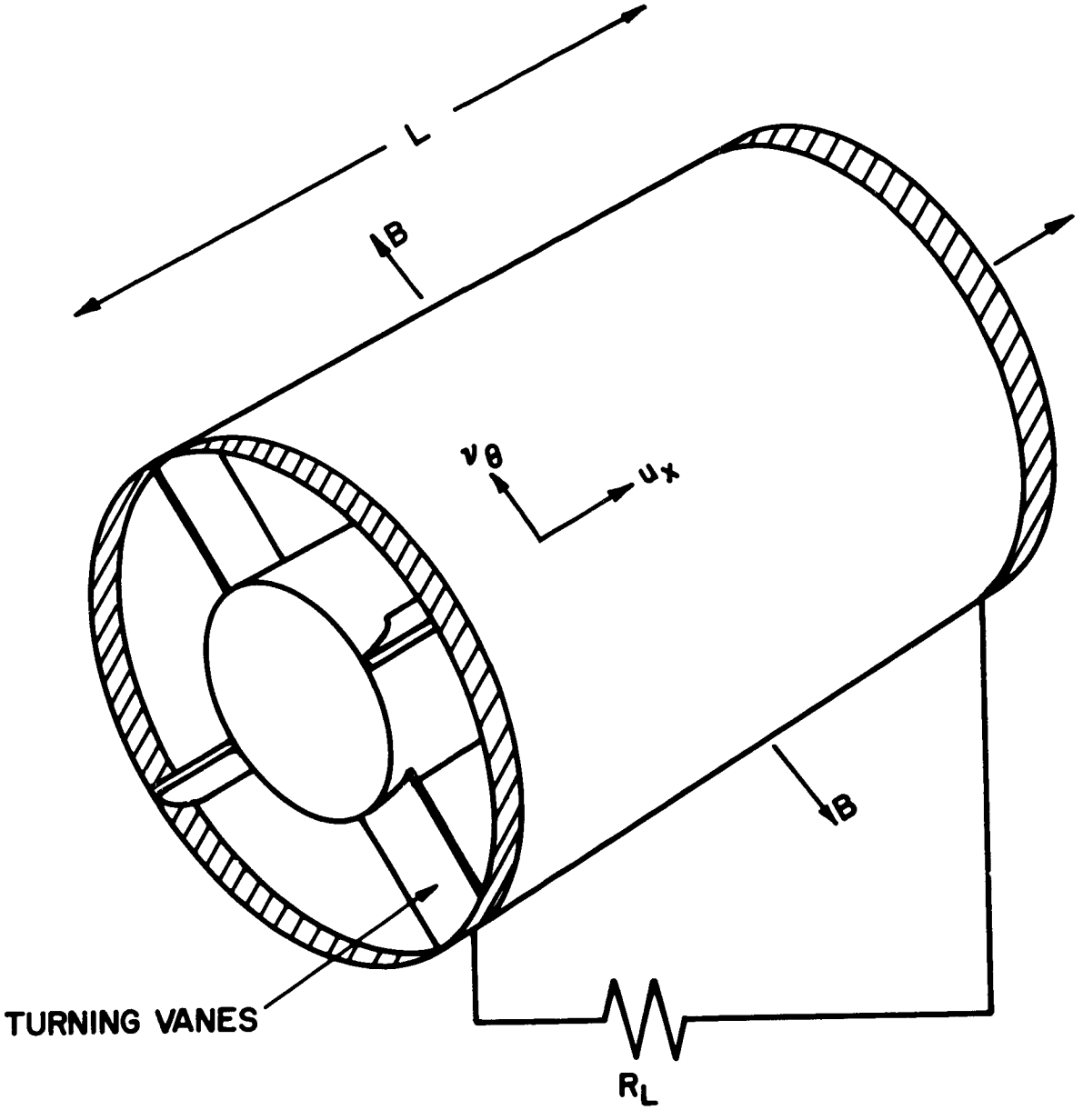

Figure 14.13. Helical Flow Generator

The power density is obviously $E_x j_x$, which is obtained from (14.87, 14.88), while (14.89) may be used to obtain j_y. The load voltage is $- E_x L$ and the load current is the product of j_x and the annular cross-sectional area. The load resistance is obviously equal to the ratio of load voltage to load current.

Although the flow is helical, the Lorentz force is parallel to the streamlines, so that the Lorentz force does not change the ratio of v_θ/u_x, that is, the helix angle θ will remain constant. The helix angle is determined by the selected efficiency η_o which in turn is determined by the load resistance. If the load resistance is changed, the current and voltage will change as described in the previous section; but also, the direction of the Lorentz force will be different than the flow helix angle θ. This can be remedied by changing the turning angle of the inlet stator vanes so that $\tan \theta_L = \eta_L/\beta_e' (1-\eta_L)$, where θ_L is the new helix angle. Also, voltage control may be obtained by varying the magnetic field which in turn changes β_e' and θ again.

The helical flow geometry has two possible disadvantages: first, the helical flow will cause a radial pressure gradient, which if sufficiently large will alter the performance. Also, to keep the helix angle small, large values of β_e' are necessary. Second, the radial magnetic field must be in the same direction; switching the direction of the magnetic field reverses the required helix angle. If it is necessary to reverse the direction of the radial magnetic field in the downstream direction as in the annular Hall geometry, then additional turning vanes are required at each point where the magnetic field is reversed. It will not be necessary to reverse the magnetic field if the generator length L is sufficiently short, which requires a large magnetic interaction parameter. It therefore appears that the helical flow generator is most applicable to large values of both the Hall parameter and magnetic interaction parameter.

14.3e Magnetically Induced Ionization[8]

Whenever an electric current flows in a gas, the "temperature" of the charge carriers, refered to the mass-average velocity, will be higher than the uncharged particles. This temperature depends on the loss of energy of the charge carrier when it suffers a collision with an uncharged particle; in Chapter V it was shown that this effect is most pronounced in light charge carriers, that is, electrons. As the electrons enter the generator, their temperature is changed in accordance with the electron energy equation as follows:

$$\frac{5}{2} n_e k u_e \frac{\partial T_e}{\partial x} = \underset{\sim}{j}_e \cdot \underset{\sim}{E}^* - \frac{3 m_e}{M} \delta n_e \nu_e k (T_e - T_g) - \dot{n}_e k T_I \tag{14.90}$$

where T_g is the gas temperature, n_e is the local ionization or deionization rate, and T_I is the ionization temperature equal to $e E_I/k$, where E_I is the ionization potential.

From (14.90), the relaxation length to change the electron temperature

$$x = \frac{5}{6\delta} \sqrt{\frac{M}{m_e}} \lambda_e \frac{u_e}{\langle c \rangle_M} \tag{14.91}$$

where λ_e is the electron mean-free path, and $\langle c \rangle_M$ is the mean thermal speed of the heavy particles. Since the electron velocity in the streamwise direction is about the same as the gas, the factor at $u_e/\langle c \rangle_M$ is approximately equal to the gas Mach number; thus, (14.91) becomes:

$$x \approx \sqrt{\frac{M}{m_e}} \frac{\mathcal{M}}{\delta} \lambda_e \tag{14.92}$$

If $\mathcal{M} \gtrsim \delta \gtrsim 1$, then (14.92) shows that the relaxation length is of the order of $10^2 - 10^3$ mean-free paths, which in an MHD generator is much shorter than the magnetic interaction length given by (14.26). If the asymptotic temperature is considerably higher than the gas temperature, then considerable additional ionization may occur, which makes $\dot{n}_e$ positive, and decreases the rate of increase of the electron temperature somewhat.

The asymptotic electron temperature is obtained by setting the first and second term on the right side of (14.90) equal to zero. This tacitly assumes that the relaxation length (14.92) is much less than the length over which the gas temperature or density changes appreciably, that is, the magnetic interaction length, Equation (14.26). The relaxation length for ionization is of the order of n_e/n of the interaction length; since n_e/n is of the order of 10^{-4} to 10^{-2}, the assumption appears to be valid. Note also that $\underset{\sim}{j}_e \cdot \underset{\sim}{E}^*$ is always positive, so that the electron temperature is always greater than the gas temperature.

To obtain the asymptotic electron temperature, the relation between j_e and E^* must be specified. Since this relation depends on the generator geometry, this will be analyzed for the three basic geometry shapes. Note that the electron conduction current is given by:

$$\underset{\sim}{j}_e = \frac{\sigma}{1 + \beta_e^2} \left[\underset{\sim}{E}^* - \frac{\beta_e}{B} \underset{\sim}{E}^* \times \underset{\sim}{B} \right] \tag{14.93}$$

where it has been assumed that $\underset{\sim}{E}^* \cdot \underset{\sim}{B} = 0$, and where $\sigma = n_e e^2/m_e \nu_e$. Thus,

$$\underset{\sim}{j}_e \cdot \underset{\sim}{E}^* = \frac{\sigma}{1 + \beta_e^2} \left| E^* \right|^2 \tag{14.94}$$

Thus, the electron heating depends only on the magnitude of the electric field.

(i) Continuous Electrodes

In this geometry, the only component of the electric field is $E_y^* = (K-1)\, U B$. The component of the electron current in this direction is

$j_{e_y} = \sigma E_y^*/(1 + \beta_e^2)$. Equating the sum of the first two terms on the right side of (14.90) to zero, substitution of E_y^* and j_{e_y}, and solving for the electron temperature, one obtains:

$$\frac{T_e}{T_g} = 1 + \frac{\gamma (1-K)^2 \beta_e^2 \mathcal{M}^2}{3\delta (1 + \beta_e^2)} \tag{14.95}$$

where $\mathcal{M}$ is the Mach number of the flow. Now, it is more convenient to express the electron temperature in terms of the stagnation temperature of the flow, given by:

$$\frac{T_o}{T_g} = 1 + \frac{\gamma-1}{2} \mathcal{M}^2 \tag{14.96}$$

The ratio of the electron temperature to the local stagnation temperature is therefore:

$$\frac{T_e}{T_o} = \frac{1 + \dfrac{\gamma (1-K)^2 \beta_e^2}{3\delta (1 + \beta_e^2)} \mathcal{M}^2}{1 + \frac{1}{2} (\gamma-1) \mathcal{M}^2} \tag{14.97}$$

In order for the electron temperature of the gas to exceed the local stagnation temperature, it is necessary for the coefficient of $\mathcal{M}^2$ in the numerator of (14.97) to exceed the coefficient of $\mathcal{M}^2$ in the denominator; that is, Ψ defined by:

$$\frac{2}{3\delta} \left(\frac{\gamma}{\gamma-1}\right) (1-K^2) \left(\frac{\beta_e^2}{1 + \beta_e^2}\right) \equiv \psi \tag{14.98}$$

must exceed unity. To make ψ large, it is necessary for β_e to be large and δ small. In addition, the generator should be close to short-circuited so that $K \tilde{\sim} 0$. Under these conditions, the maximum value of ψ is 5/3. Thus, if the Mach of the flow is large, $T_e/T_o \rightarrow 5/3$.

Although this electron temperature may cause additional ionization, it is not practical to operate an MHD generator at short circuit. Note also that δ must be small for appreciable electron heating.

From Chapter V, values of δ close to unity may be possible in monatomic gases at high electron densities. However, in combustion gases in which δ is 10^2 - 10^3, no appreciable electron heating will occur.

(ii) Segmented Electrodes

In the segmented electrode generator, the total Hall current is zero so that the electric field from (14.32) is given by:

$$\left.\begin{aligned} E_y^* &= -(1-K)\,UB \\ E_x^* &= -\frac{(1-K)\,\beta_e\,UB}{1+\beta_e\beta_I} \end{aligned}\right\} \qquad (14.99)$$

Substitution of (14.99) into (14.94) yields:

$$\underset{\sim}{j}_e \cdot \underset{\sim}{E}^* = \frac{\sigma(1-K)^2U^2B^2}{1+\beta_e^2}\left[\frac{1+\beta_e^2+2\beta_e\beta_I+\beta_e^2\beta_I^2}{(1+\beta_e\beta_I)^2}\right] \qquad (14.100)$$

In the numerator of the bracket, β_I may be neglected in comparison to β_e; substitution of (14.100) into (14.90) yields:

$$\frac{T_e}{T_g} = 1 + \frac{\gamma(1-K)^2\beta_e^2\mathcal{M}^2}{3\delta(1+\beta_e\beta_I)^2} \qquad (14.101)$$

for the asymptotic electron temperature; the ratio of the electron temperature to the local stagnation temperature is then:

$$\frac{T_e}{T_o} = \frac{1 + \dfrac{\gamma (1-K)^2 \beta_e^2 \mathcal{M}^2}{3\delta (1 + \beta_e \beta_I)^2}}{1 + \frac{1}{2} (\gamma-1) \mathcal{M}^2} \tag{14.102}$$

Comparison of (14.102) with the corresponding expression for continuous electrodes, (14.97), shows that the factor $\beta_e^2/(1 + \beta_e^2)$ which is always less than unity is replaced by $\beta_e^2/(1 + \beta_e \beta_I)$, which can be much greater than unity. In fact, as the magnetic field, i.e., β_e is increased, $\beta_e^2/(1+\beta_e\beta_I)$ has a maximum when $\beta_e = (\mu_e/\mu_I)^{1/2}$, which can be of the order of 10 - 20. The maximum value of the factor is therefore:

$$\left.\frac{\beta_e^2}{(1 + \beta_e \beta_I)^2}\right|_{max} = \frac{\beta_e^2{}_{max}}{4} = \frac{1}{4} \frac{\mu_e}{\mu_I} \tag{14.103}$$

which is of the order of 25 - 250. Thus, considerable electron heating is possible in a segmented-electrode generator. If the ionization follows the electron temperature, extremely high electrical conductivities may be obtained. For example, calculations have been made for a mixture of argon and 1% molar potassium for a stagnation temperature of 1500°K as a function of the local stagnation pressure and Mach number of the resulting current density, see Figure 14.14. The corresponding values of $\beta_e = \omega_e \tau_e$ are shown in Figure 14.15. The parameter is (1-K) UB, where U is related to the local Mach number by:

$$U = \mathcal{M} \sqrt{\gamma k T/M} = \frac{\mathcal{M} \sqrt{\gamma k T_o}}{\sqrt{1 + \frac{1}{2} (\gamma-1) \mathcal{M}^2}} \tag{14.104}$$

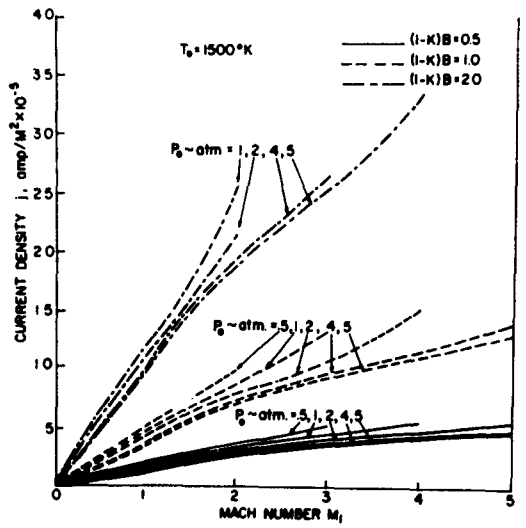

Figure 14. 14. Calculated Electron Current in a Segmented Electrode MHD Generator For Argon and 1% Potassium

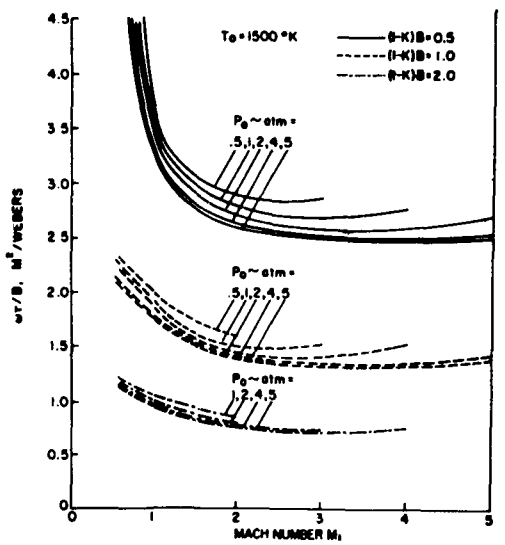

Figure 14. 15. Calculated $\omega_e \tau_e$ In a Segmented Electrode MHD Generator for Argon and 1% Potassium

and the local pressure is given by

$$\frac{p}{p_o} = \left(\frac{T}{T_o}\right)^{\frac{\gamma}{\gamma-1}} \tag{14.105}$$

when the temperature ratio is given by (14.96). In these calculations, the effect of ion slip was neglected; the perfect gas law was used, and the effect of the ionization energy on the energy equation was neglected. The electrical conductivity is obtained by dividing the current density by the transverse electric field (1-K) UB. The resulting electrical conductivity is several orders of magnitude greater than that of the equilibrium electrical conductivity at T_o. Note also that the electrical conductivity increases with increasing Mach number, which merely indicates that the coefficient of $\mathcal{M}^2$ in the numerator of (14.102) is greater than $(\gamma-1)/2$. Calculations at other stagnation temperatures indicate that the electrical conductivity is approximately proportional to the stagnation temperature. Thus, magnetically induced ionization may be of interest in closed cycle applications of MHD generators. As of the present time, however, magnetically induced ionization has not been demonstrated experimentally. Experiments using an electric field, however, have verified the basic theory.[8,9]

(iii) Hall Generator

For the Hall generator:

$$\left.\begin{aligned} E_y^* &= - UB \\ E_x^* &= \frac{\beta_e KUB}{1 + \beta_e \beta_I} \end{aligned}\right\} \tag{14.106}$$

For the Hall generator, the components of the electric field are given by:

Use of (14.106, 14.94, 14.90) yields the following expression for the electron temperature:

$$\frac{T_e}{T_g} = 1 + \frac{\gamma m^2 \beta_e^2}{3(1+\beta_e^2)} \left[\frac{K^2 \beta_e^2}{(1+\beta_e \beta_I)^2} + 1 \right] \qquad (14.107)$$

As the magnetic field is increased, the first factor $\beta_e^2/(1+\beta_e^2)$ rapidly reaches a maximum of unity. The factor in the bracket reaches a maximum when $\beta_e^2 = \mu_e/\mu_I$; thus, this value of β_e yields the maximum electron temperature. Note that this maximum is the same as that for the segmented electrode geometry. The maximum value coefficient of $\gamma m^2/3$ then $1 + \frac{1}{4} K^2 \beta_e^2$, which compares to $\frac{1}{4}(1-K)^2 \beta_e^2$ for the segmented electrode generator. Since in the Hall generator K is comparable to (1-K) in the segmented electrode generator, the maximum electron temperature is approximately the same in both generators.

14.4 POLYTROPIC EFFICIENCY OF MHD GENERATORS

The local efficiency which was defined in the previous chapter is not useful for thermodynamic cycles; the reason being that the previous definition was based on local conditions instead of stagnation conditions. The local efficiency was defined as

$$\eta_L = \frac{\underset{\sim}{E} \cdot \underset{\sim}{j}}{\underset{\sim}{v} \cdot \underset{\sim}{j} \times \underset{\sim}{B}} = \frac{-\underset{\sim}{E} \cdot \underset{\sim}{j}}{\underset{\sim}{j} \cdot (\underset{\sim}{v} \times \underset{\sim}{B})} = \frac{-\underset{\sim}{E} \cdot \underset{\sim}{j}}{-\underset{\sim}{E} \cdot \underset{\sim}{j} + \underset{\sim}{E}^* \cdot \underset{\sim}{j}} \qquad (14.108)$$

Since the power density is $-\underset{\sim}{E} \cdot \underset{\sim}{j}$ and the ohmic heating per unit volume is $\underset{\sim}{E}^* \cdot \underset{\sim}{j}$, this definition is the same as

$$\eta_L = \frac{\text{Power}}{\text{Power + Dissipation}}$$

The denominator of (14.108) is also equal to the ideal power output corresponding to zero dissipation for the same pressure drop due to Lorentz forces, that is, for the same current density. Thus, the ideal power is given by:

$$P_{Ideal} = (-\underset{\sim}{E} \cdot \underset{\sim}{j})_{Ideal} = -(\underset{\sim}{E}^* - \underset{\sim}{v} \times \underset{\sim}{B}) \cdot \underset{\sim}{j} \qquad (14.109)$$

For the same Lorentz force but zero ohmic dissipation, E* must be zero, which yields the denominator of (14.108). The local efficiency can also be represented on a Mollier diagram along the static line A-B, see Figure 14.16. Consider two axial stations 1 and 2 along an MHD generator which are a distance Δx apart. As the gas passes between these two stations, the total enthalpy per unit mass is changed by ΔH, which is also equal to the change in static enthalpy if the change in gas velocity is negligible, while the static pressure change is $p_1 - p_2$. The ideal change in static enthalpy between these two pressures is Δh_i. The local efficiency may therefore also be defined as:

$$\eta_L = \frac{\Delta H}{\Delta h_i} \qquad (14.110)$$

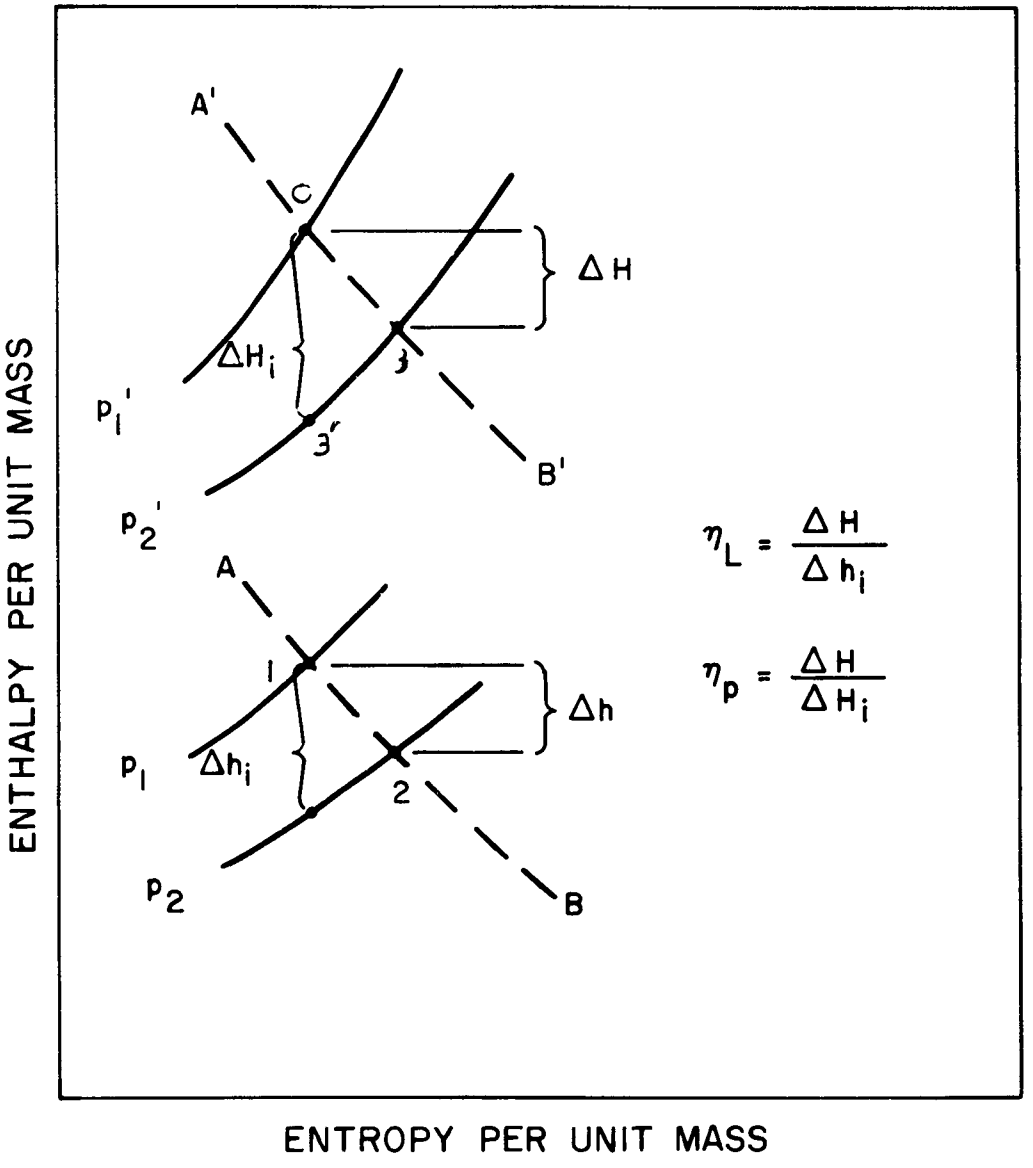

Figure 14.16. Relation between Local and Polytropic Efficiencies

However, the thermodynamicist is usually interested in the stagnation behavior of the gas, as along the line A'-B'. The reason for this is that the gas usually starts at a small Mach number in a combustor or heat exchanger, and after being accelerated in a nozzle and passing through the generator, is again brought almost to rest to recover the pressure or to pass the gas through a heat exchanger or some other low speed device. Thus, one is interested in the stagnation conditions of the gas in the generator. The local efficiency calculated on the basis of stagnation conditions is called the polytropic efficiency η_p, sometimes called the "stage" or "local adiabatic" efficiency. From Figure 14.16, $\eta_p = \Delta H/\Delta H_i$. Now, because of the spreading of the constant pressure lines with increasing enthalpy, $\Delta H_i > \Delta h_i$; hence, $\eta_p < \eta_L$.

A slightly different definition of the polytropic efficiency is:

$$\eta_p = \frac{d H_e}{d H_i} \tag{14.111}$$

where $d H_e$ is the increment in total enthalpy due to electric power generation, $-\underset{\sim}{E} \cdot \underset{\sim}{j}$, and $d H_i$ is the isentropic or ideal change in total enthalpy between the same increment in pressure. The difference in $d H_e$ and the actual change in total enthalpy $d H$ is due to heat transfer from the gas. In this definition, the heat transfer is charged as a loss against the generator, although this energy may be utilized elsewhere in the cycle. This definition, of course, is not an adiabatic efficiency. For the ideal or isentropic generator, there is zero heat transfer, the first law of thermodynamics yields:

$$d Q_i = 0 = d H_i - \frac{d p_S}{\rho_S} \tag{14.112}$$

where p_S and ρ_S are the stagnation pressure and density, respectively. Substitution of (14.112) into (14.111) and use of the ideal gas law for the stagnation density yields:

$$\eta_p = \frac{p_S}{RT_S} \frac{dH_e}{dp_S} = \frac{p_S}{RT_S} \frac{dH_e}{dH} \frac{dH}{dp_S} \tag{14.113}$$

The ratio dH_e/dH is the fraction of the total enthalpy which is converted into electrical energy; the remainder is heat transfer from the generator; let this fraction be $a = dH_e/dH$. Also $dH = C_p T_S$, and $C_p/R = \gamma/(\gamma-1)$ where γ is the ratio of specific heats. Then (14.113) may be written as:

$$\eta_p = \frac{a\gamma}{\gamma-1} \frac{d\ell n H}{d\ell n p_S} \tag{14.114}$$

Then (14.114) may be integrated to obtain:

$$\frac{H}{H_o} = \left(\frac{p_S}{p_{S_o}}\right)^{\left\langle \frac{\eta_p(\gamma-1)}{a\gamma} \right\rangle} \tag{14.115}$$

where the exponent of the stagnation pressure ratio is an average defined by the integration of (14.114) as follows:

$$\left\langle \frac{\eta_p(\gamma-1)}{a\gamma} \right\rangle = \frac{\int_{p_{S_o}}^{p_S} \frac{\eta_p(\gamma-1)}{a\gamma} d\ell n p_S}{\int_{p_{S_o}}^{p_S} d\ell n p_S} \tag{14.116}$$

Now, in the complete MHD generator, the stagnation enthalpy progresses from 1 to 3, see Figure 14.16, that is, from H_o to H_3. The ideal change in enthalpy

between the same stagnation pressures is given by $H_o - H_{3'}$. The overall generator efficiency is defined as:

$$\eta_g = \frac{a\,(H_o - H_3)}{H_o - H_{3'}} \tag{14.117}$$

since only the fraction a of $(H_o - H_3)$ is converted into electrical energy. The relation between $H_{3'}$ and H_o is obtained from (14.116) with $\eta_p = a = 1$:

$$\frac{H_{3'}}{H_o} = \left(\frac{p_{S_3}}{p_o}\right)^{\left\langle \frac{\gamma-1}{\gamma} \right\rangle} \tag{14.118}$$

while H_3 is obtained from (14.115) directly. The generator efficiency therefore becomes:

$$\eta_g = a\,\frac{\left[1 - \left(\frac{p_{S_3}}{p_{S_o}}\right)^{\left\langle \frac{\eta_p(\gamma-1)}{a\gamma} \right\rangle}\right]}{\left[1 - \left(\frac{p_{S_3}}{p_{S_o}}\right)^{\left\langle \frac{\gamma-1}{\gamma} \right\rangle}\right]} \tag{14.119}$$

For small pressure ratios across the generator, that is, for $p_{S_3}/p_{S_o} \tilde{\sim} 1$, the generator efficiency given by (14.119) becomes just η_p. But for large pressure ratios, the pressure ratio terms in the (14.119) become small, and the generator efficiency approaches a; if the pressure ratio is sufficiently large, the generator efficiency becomes independent of the polytropic efficiency. This effect is well

known in the design of steam turbines and is the reason for designing them for very large pressure ratios. The reason for the high efficiency is as follows: the dissipation in each stage, or at each section of the generator, appears as heat energy which is passed onto the next stage or section; the main effect of the dissipation being a loss of total pressure. But, if the pressure ratio of the machine is large enough, the loss of pressure is small, due to the flattening of the constant pressure lines at low pressure on the Mollier diagram, as shown in Figure 14.17. For moderate pressure ratios, η_g is equal to a $(H_o - H_2)/(H_o - H_{2'})$. For large pressure ratios, η_g is shown as a $(H_o - H_3)/(H_o - H_{3'})$. From Figure 14.17, it is seen that the generator efficiency is larger for the larger pressure ratio. Note that large pressure ratios imply large temperature ratios, since (14.119) can also be written as:

$$\eta_g \simeq \frac{a\left[1 - \left(\frac{T_{S_{3'}}}{T_{S_o}}\right)^{\frac{\eta_p}{a}}\right]}{1 - \frac{T_{S_{3'}}}{T_{S_o}}} \qquad (14.120)$$

with the use of (14.118).

However, in a MHD generator, in which combustion gases are used at pressures greater than one atmosphere, the lowest total temperature at which the gas still has sufficient electrical conductivity is about $4000^{o}R$; the highest possible flame temperature is about $8000^{o}R$. For these conditions, it is important that the polytropic efficiency be as high as possible because the generator efficiency, as calculated from (14.119) or (14.120), will be only slightly larger than η_p. The generator efficiency will be improved appreciably over the polytropic efficiency if the pressure ratio is very large, which requires some method for improving the electrical conductivity at low temperatures.

14.4a Polytropic Efficiency in Linear MHD Generators

In this section, the general expression is derived for the polytropic efficiency in linear MHD generators under steady flow conditions at a particular generator

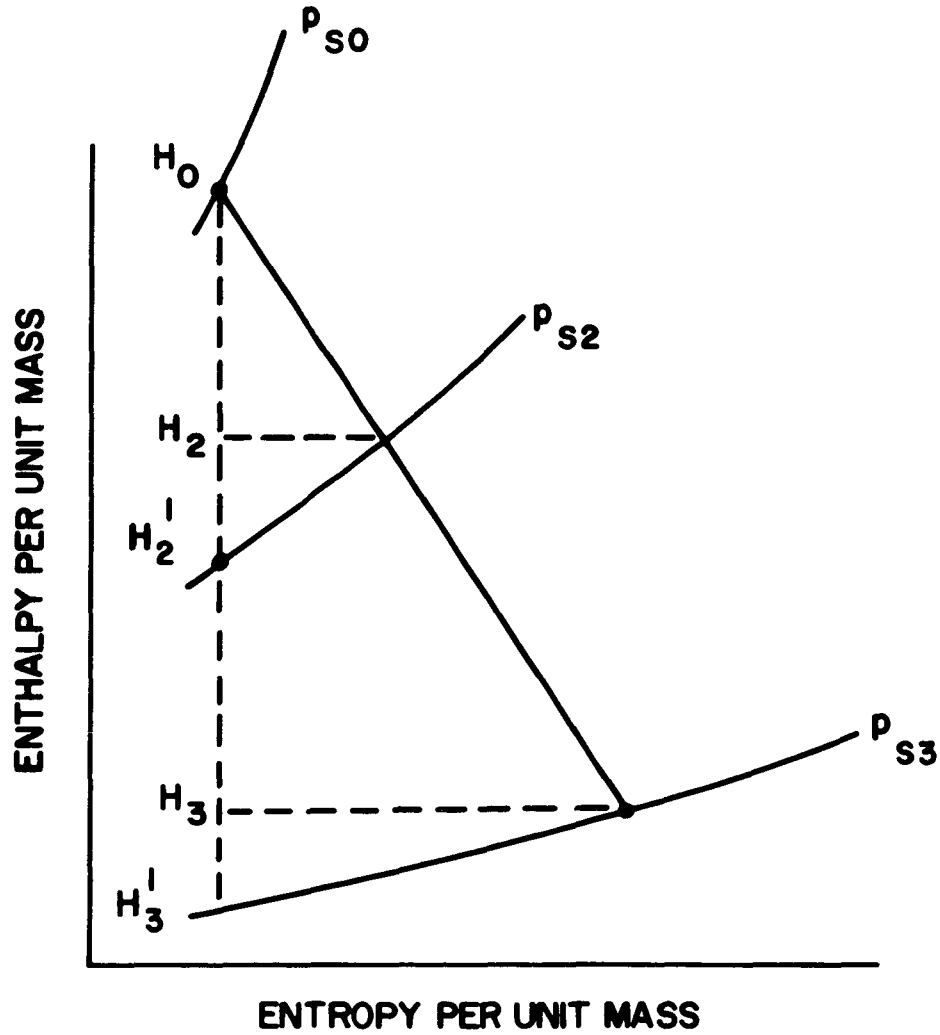

Figure 14.17. Effect of Large Stagnation Pressures on Generator Efficiencies

station x, where the flow velocity in the x-direction is u (x), and the transverse velocity components are negligible. As before, the local magnetic field is transverse to the generator in the z-direction. It is assumed that the magnetic Reynolds number is small so that perturbations of the imposed magnetic field may be neglected. If current is allowed to flow, then there will be a Lorentz force in the direction of the flow, and power generation per unit volume equal to $-\underset{\sim}{E} \cdot \underset{\sim}{j}$. In addition, there is a friction pressure drop $(dp/dx)_f$ which is negative, given as follows:

$$\left(\frac{dp}{dx}\right)_f = - \frac{\tau_W C}{A}$$

where τ_W is the average shear stress at the wall; C is the perimeter length of the cross-section, and A is the cross-sectional area; each of these will generally be a function of the generator station x. In general, a friction factor c_f is defined as follows:

$$\tau_W = \frac{1}{2} \rho u^2 c_f$$

In addition to the skin friction, there may also be heat transfer from the gases in the MHD generator to the walls; this is given by:

$$\left(\frac{\partial H}{\partial x}\right)_q = - q_W C/A$$

where q_W is the average heat transfer rate per unit area over the perimeter of the cross-section. The heat transfer rate is generally related to the film coefficient h as follows:

$$q_W = h (T_S - T_W)$$

where T_S is the local bulk gas stagnation temperature and T_W is the wall temperature; the film coefficient is usually made non-dimensional as follows:

$$S_t = \frac{h}{\rho u C_p}$$

where S_t is the local Stanton number. Now, if the Prandtl number of the gas, $C_p \mu / \kappa$ is close to unity, as is the case for most gases, if the degree of ionization is less than a few per cent, then as a general rule the Stanton number is equal to half the friction factor,* or:

$$S_t \simeq \frac{1}{2} c_f$$

The one-dimensional momentum and energy equations therefore become:

$$\rho u \frac{du}{dx} + \frac{dp}{dx} = \underset{\sim}{(j} \times \underset{\sim}{B)_x} + \left(\frac{dp}{dx}\right)_f = \frac{\underset{\sim}{(j} \times \underset{\sim}{B)_x}}{b} \qquad (14.121)$$

$$\rho u \frac{dH}{dx} = \underset{\sim}{E} \cdot \underset{\sim}{j} - \frac{q C}{A} = \frac{\underset{\sim}{E} \cdot \underset{\sim}{j}}{a} \qquad (14.122)$$

where b is the fraction of the pressure drop due to the Lorentz force:

$$b = \frac{\underset{\sim}{(j} \times \underset{\sim}{B)_x}}{\underset{\sim}{(j} \times \underset{\sim}{B)_x} + \left(\frac{dp}{dx}\right)} \qquad (14.123)$$

*The presence of a magnetic field may alter this relation, if the magnetic interaction parameter is much larger than unity.

and a is the fraction of the enthalpy drop which is due to electrical power generation as was previously defined. From (14.122),

$$\frac{dH_e}{dx} = \frac{\underset{\sim}{E} \cdot \underset{\sim}{j}}{\rho u} \tag{14.124}$$

and from (14.113), the polytropic efficiency is:

$$\eta_p = \frac{p_S}{R T_S} \frac{dH_e/dx}{dp_S/dx} = \frac{\underset{\sim}{E} \cdot \underset{\sim}{j}}{\rho u R T_S \, d(\ell n \, p_S)/dx} \tag{14.125}$$

To evaluate $d(\ell n \, p_S)/dx$, use is made of the following isentropic relation:

$$\frac{p_S}{p} = \left(\frac{T_S}{T}\right)^{\frac{\gamma}{\gamma-1}}$$

or

$$\ell n \, p_S = \ell n \, p + \frac{\gamma}{\gamma-1} \ell n \, T_S - \frac{\gamma}{\gamma-1} \ell n \, T \tag{a}$$

Differentiation with respect to x yields:

$$\frac{d(\ell n \, p_S)}{dx} = \frac{p'}{p} - \frac{\gamma}{\gamma-1} \frac{T'}{T} + \frac{\gamma}{\gamma-1} \frac{T'_S}{T_S} \tag{b}$$

where $(\;)' \equiv (d/dx)$. Next, substitute

$$H' = C_p T' + u u' \tag{c}$$

in the energy equation, and eliminate $\rho u u'$ between the energy equation and the momentum equation. The result is:

$$\frac{p'}{p} - \frac{\gamma}{\gamma-1}\frac{T'}{T} = \frac{1}{p}\left[\frac{(\underset{\sim}{j} \times \underset{\sim}{B})_x}{b} - \frac{\underset{\sim}{E} \cdot \underset{\sim}{j}}{u}\right] \tag{d}$$

also, from the energy equation,

$$T'_S = \frac{\underset{\sim}{E} \cdot \underset{\sim}{j}}{a\rho u C_p} \tag{e}$$

Substitution of (e,d) into (b), and then into (14.125) yields:

$$\eta_p = \frac{a}{\dfrac{\underset{\sim}{u} \cdot (\underset{\sim}{j} \times \underset{\sim}{B})}{\underset{\sim}{E} \cdot \underset{\sim}{j}} \cdot \dfrac{a}{b} \cdot \dfrac{T_S}{T} + 1 - \dfrac{T_S}{T}} \tag{f}$$

since $\underset{\sim}{u}(\underset{\sim}{j} \times \underset{\sim}{B}) \equiv \underset{\sim}{u} \cdot (\underset{\sim}{j} \times \underset{\sim}{B})$; hence, the first factor in the denominator is just the reciprocal of the previously defined "local" electrical efficiency η_L. Thus, the polytropic efficiency becomes:

$$\eta_p = \frac{a}{\dfrac{a\,T_S}{\eta_L\, b\, T} + 1 - \dfrac{T_S}{T}} \tag{14.126}$$

where T_S/T is the ratio of the local stagnation temperature to static temperature, which for a perfect gas is given by:

$$\frac{T_S}{T} = 1 + \frac{\gamma-1}{2}\mathcal{M}^2, \tag{14.127}$$

where $\mathcal{M}$ is the local Mach number. To proceed, expressions are required for a, b. Several possible cases will be examined in the next three sections: a = b = 1, corresponding to zero friction and zero heat transfer; a = 1, b < 1, corresponding to zero heat transfer but finite friction, and a < 1, b < 1, corresponding to both heat transfer and friction.

14.4b Polytropic Efficiency for Zero Friction and Zero Heat Transfer

For this case a = b = 1, and use of (14.127) in (14.126) yields:

$$\eta_p = \frac{\eta_L}{1 + \frac{\gamma-1}{2}\mathcal{M}^2(1-\eta_L)} \qquad (14.128)$$

Thus, for the polytropic efficiency to be close to the local efficiency η_L, either η_L must be close to unity or else $\frac{1}{2}(\gamma-1)\mathcal{M}^2$ must be small. Thus, the local efficiency η_L is identically equal to the polytropic efficiency of a subsonic, zero heat transfer, zero friction, flow. For combustion gases where $\gamma \approx 1.2, \mathcal{M} \approx 1$, and $\eta_L = 0.8$, the polytropic efficiency is only 2% less than η_L. But for gases in which $\gamma = 5/3, \mathcal{M} = 2$, and $\eta_L = 0.8$, the polytropic efficiency is almost 25% less than the local efficiency η_L.

14.4c Polytropic Efficiency With Friction But Zero Heat Transfer

With friction but zero pressure drop, a = 1, and from the definition of b,

$$\frac{1}{b} = 1 - \frac{\tau\, C/A}{(\underset{\sim}{j} \times \underset{\sim}{B})_x} \qquad (14.129)$$

To proceed further, an expression is needed for $(\underset{\sim}{j} \times \underset{\sim}{B})_x$, which requires that the geometry be specified. We will consider all three basic geometries. Actually, since the local efficiency is equal to K for both the continuous and segmented

electrode geometries, they may be considered as one case with an effective transverse electrical conductivity which is evaluated as follows:

Continuous Electrodes: $$\sigma_{eff} = \frac{\sigma}{(1 + \beta_e \beta_I)^2 + \beta_e^2}$$

Segmented Electrodes: $$\sigma_{eff} = \frac{\sigma}{1 + \beta_e \beta_I}$$

Since the local efficiency is different for the Hall generator, this will be considered separately.

(i) Continuous and Segmented Electrode Generators

For these two geometries, $(\underset{\sim}{j} \times \underset{\sim}{B})_x = (K-1)\, \sigma_{eff}\, u B^2$, so that the expression for b becomes:

$$\frac{1}{b} = 1 + \frac{c_f}{2\, I\, (1-K)} \qquad (14.130)$$

where I is the magnetic interaction parameter based on a length equal to A/C as follows:

$$I = \frac{\sigma_{eff}\, B^2 A}{\rho u C} \qquad (14.131)$$

Finally, a parameter Z may be defined as:

$$Z = \frac{c_f}{2I} \qquad (14.132)$$

so that b is given by:

$$\frac{1}{b} = 1 + \frac{Z}{1-K} \tag{14.133}$$

Substitution of (14.133) into the expression for the polytropic efficiency yields:

$$\eta_p = \frac{1}{\left[\frac{1-K+Z}{K(1-K)} - 1\right] \frac{T_S}{T} + 1} \tag{14.134}$$

Now, for any given value of Z and T_S/T, there is a value of K which minimizes the bracket in (14.134) and which therefore yields the highest polytropic efficiency. This value of $K = K_m$ is given by:

$$K_m = 1 + Z - \sqrt{Z + Z^2} \tag{14.135}$$

or alternatively,

$$Z = \frac{(1 - K_m)^2}{2K_m - 1} \tag{14.136}$$

The maximum polytropic efficiency is therefore:

$$\eta_{pm} = \frac{2K_m - 1}{1 + (1-K_m)(\gamma-1)\mathcal{M}^2} \tag{14.137}$$

For subsonic flows where the Mach number is negligible, $\eta_{pm} = 2 K_m - 1$; substitution of K_m in terms of η_{pm} into (14.136) then yields:

$$Z\Big|_{\mathcal{M} \ll 1} = \frac{(1-\eta_{pm})^2}{4\,\eta_{pm}} \tag{14.138}$$

which is identical to the expression for the maximum local efficiency of a Hall generator, given by (14.56) with Z replacing $1/\hat{\varepsilon}'_e{}^2$. This indicates that small values of Z are required to achieve high values of the polytropic efficiency. Now, I based on A/C will seldom be more than 0.1, while the friction factor f is generally inversely proportional to the Reynolds number raised to the power of 1/2 for laminar flows and 0.2 for turbulent flows.* The result is that very large flow Reynolds numbers are required to obtain high values of the polytropic efficiency; that is, Z must be small.

For Z much less than unity, and finite Mach number, the above expressions may be simplified as follows:

$$Z \ll 1: \qquad K_m \simeq 1 - \sqrt{Z} \tag{14.139a}$$

$$\eta_{pm} \simeq 1 - 2\sqrt{Z}\left(1 - \frac{\gamma-1}{2}\mathcal{M}^2\right) \tag{14.139b}$$

which clearly shows that the polytropic efficiency decreases with both increasing Z and Mach number.

In the preceding discussion, it was assumed that the Mach number was held constant. However, in an MHD generator, the mass flow rate is usually specified. It is therefore of interest to determine the manner in which η_{pm} changes with Mach number for a constant mass flow rate.

*It has been assumed here that the magnetic field does not affect the friction factor.

For simplicity, consider a square cross-section which has a characteristic dimension h, so that

$$A/C = \frac{1}{4} h, \text{ and } h = \sqrt{\dot{m}/\rho u}$$

where $\dot{m}$ is the total flow rate. Also, the skin friction factor c_f is inversely proportional to the Reynolds number to a power n:

$$c_f = G R_e^{-n} = G \left(\frac{\rho u h}{\mu}\right)^{-n} = \frac{G \mu^n}{\dot{m}^{n/2}} (\rho u)^{-n/2}$$

where n = 0.5 for laminar flow and 0.2 for turbulent flow, and G is a constant. Also,

$$\rho u = \frac{\gamma p_S}{a_S} \mathcal{M} \left(1 + \frac{\gamma - 1}{2} \mathcal{M}^2\right)^{\frac{\gamma + 1}{2(1-\gamma)}}$$

Thus,

$$\eta_{pm} = 1 - \frac{G^{1/2} \mu^{n/2} \left(\gamma p_S / a_S\right)^{\frac{3}{4} - \frac{n}{4}}}{\sqrt{2} \dot{m}^{(n+1)/4} B \sigma_{eff}^{1/2}} \times$$

$$\left(1 + \frac{\gamma - 1}{2} \mathcal{M}^2\right)^{\left(\frac{3}{4} - \frac{n}{4}\right)\left(\frac{\gamma+1}{2(1-\gamma)}\right) + 1} \mathcal{M}^{\frac{3}{2} - \frac{n}{2}} \qquad (14.140)$$

The terms which depend explicitly on Mach number increase with increasing Mach number, as is shown in Figure 14.18.

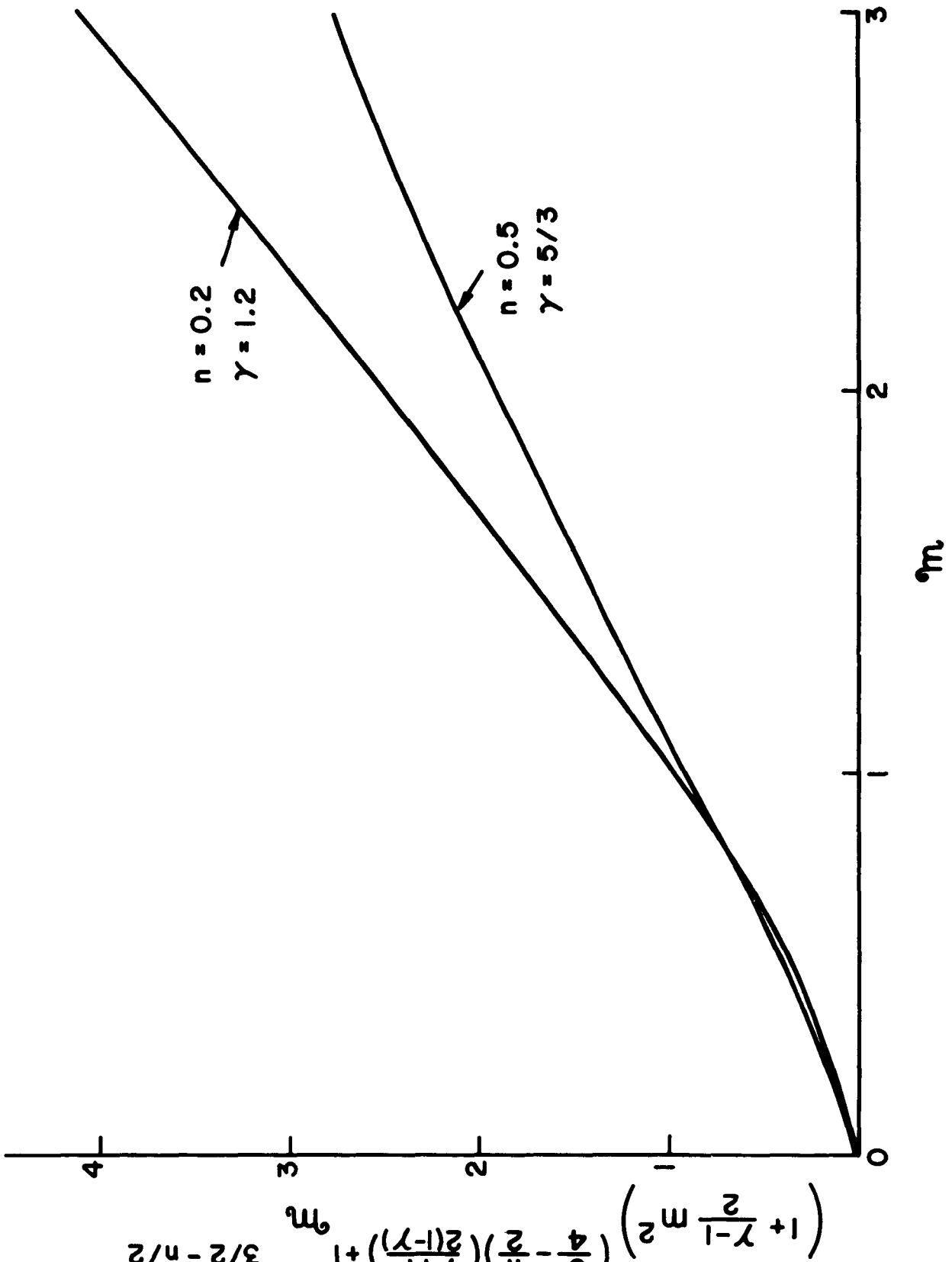
$\left(1+\frac{\gamma-1}{2}m^2\right)^{\left(\frac{3}{4}-\frac{n}{2}\right)\left(\frac{\gamma+1}{2(1-\gamma)}\right)+1}\eta_m^{3/2-n/2}$
m
n = 0.2
γ = 1.2
n = 0.5
γ = 5/3
0
1
2
3
4

Figure 14.18

If the effective electrical conductivity also decreases, then the maximum polytropic efficiency given by (14.140) will decrease with increasing Mach number. On the other hand, if the electrical conductivity increases with increasing Mach number, as for example is the case with magnetically induced ionization, then the effect of increasing Mach number on the polytropic efficiency is mitigated.

(ii) Hall Generator

From (14.44) and (14.123) the expression for b becomes:

$$\frac{1}{b} = 1 + \left(\frac{1 + \beta_e'^{\,2}}{1 + \beta_e'^{\,2} K} \right) Z \qquad (14.141)$$

so that the expression for the polytropic efficiency, (14.126) becomes:

$$\frac{1}{\eta_p} = 1 - \frac{T_S}{T} + \frac{1}{K(1-K)} \left[\frac{1+Z}{\beta_e'^{\,2}} (1+Z) + K + Z \right] \qquad (14.142)$$

This expression is essentially the same as that given by (14.128) in the absence of friction, except that in computing the local efficiency of the Hall generator, $\beta_e'^{\,2}$ should be divided by the factor $1 + Z + \beta_e'^{\,2} Z$

14.4d Polytropic Efficiency With Friction and Heat Transfer

For this case, the factor a defined as

$$a^{-1} = 1 - \frac{q_W \, C/A}{\underset{\sim}{E} \cdot \underset{\sim}{j}}$$

is now larger than unity. Use of $\underset{\sim}{E}\cdot\underset{\sim}{j} = \sigma_{eff} K(1-K) u^2 B^2$ for a crossed field generator, $u^2 = c_p(T_s - T)$, $q_w = h(T_s - T_w)$, $St = h/\rho u c_p$, $c_f = 2S_t$, and (14.131, 14.132) yields:

$$\frac{1}{a} = 1 + \frac{Z\left(1 - \frac{T_W}{T_S}\right)}{K(1-K)\left(1 - \frac{T}{T_S}\right)} \qquad (14.143)$$

where Z is defined by (14.132). Then, use of (14.133, 14.143) in (14.126) yields:

$$\frac{1}{\eta_p} = \frac{T_S}{KT} + 1 - \frac{T_S}{T} + \frac{Z}{K(1-K)}\left(\frac{T_W}{T}\right) \qquad (14.144)$$

The last term in the above expression represents the effect of skin friction and is identical to 14.134, except that T_W has replaced T_S in the last term. Thus, wall cooling, that is, $T_W < T_S$, leads to a reduction in the pressure drop due to friction. This, of course, is the well known effect in one-dimensional compressible flow, namely, that cooling increases the stagnation pressure.

14.5 END LOSSES IN LINEAR MHD GENERATORS

In addition to the friction losses described in Section 14.4, there may be electrical losses at the inlet and exit, caused by eddy currents which flow from the positive electrode to the negative electrode through the conducting gases in the region of the channel which is external to the main magnetic field, that is, upstream and downstream of the electrode region, see Figure 14.19. At present, only the simplest analyses of this problem have been made because of its complexity. The assumptions generally made are:

1. The average electron collision time τ_e is constant.
2. The presence of viscous boundary layers is neglected. The basis for this assumption is that the viscous Reynolds number will be large in MHD generators, so that the viscous boundary layer will be quite thin.
3. The gas velocity is a constant, taken as U in the downstream (x) direction. This assumption really contains two assumptions:
   a) The flow is essentially incompressible, that is, the Mach number is small.
   b) The induced Lorentz forces do not appreciably alter the velocity profile. This assumption is valid if the magnetic interaction parameter based on the channel width, $\sigma B^2 h/\rho U$, is small compared to unity.[10]
4. The magnetic field in the generator is equal to the imposed magnetic field. This assumption is valid if the magnetic Reynolds number $\sigma \mu_o U h$ is small, which is generally true in MHD generators.
5. The imposed magnetic field is in the transverse direction only of the magnitude is a function only of the longitudinal coordinate in the region near the ends of the magnetic field, that is, in the "shaded" region. This assumption violates Maxwells' equations, but the error is not serious if the pole face separation distance is sufficiently small; the results are qualitatively correct.

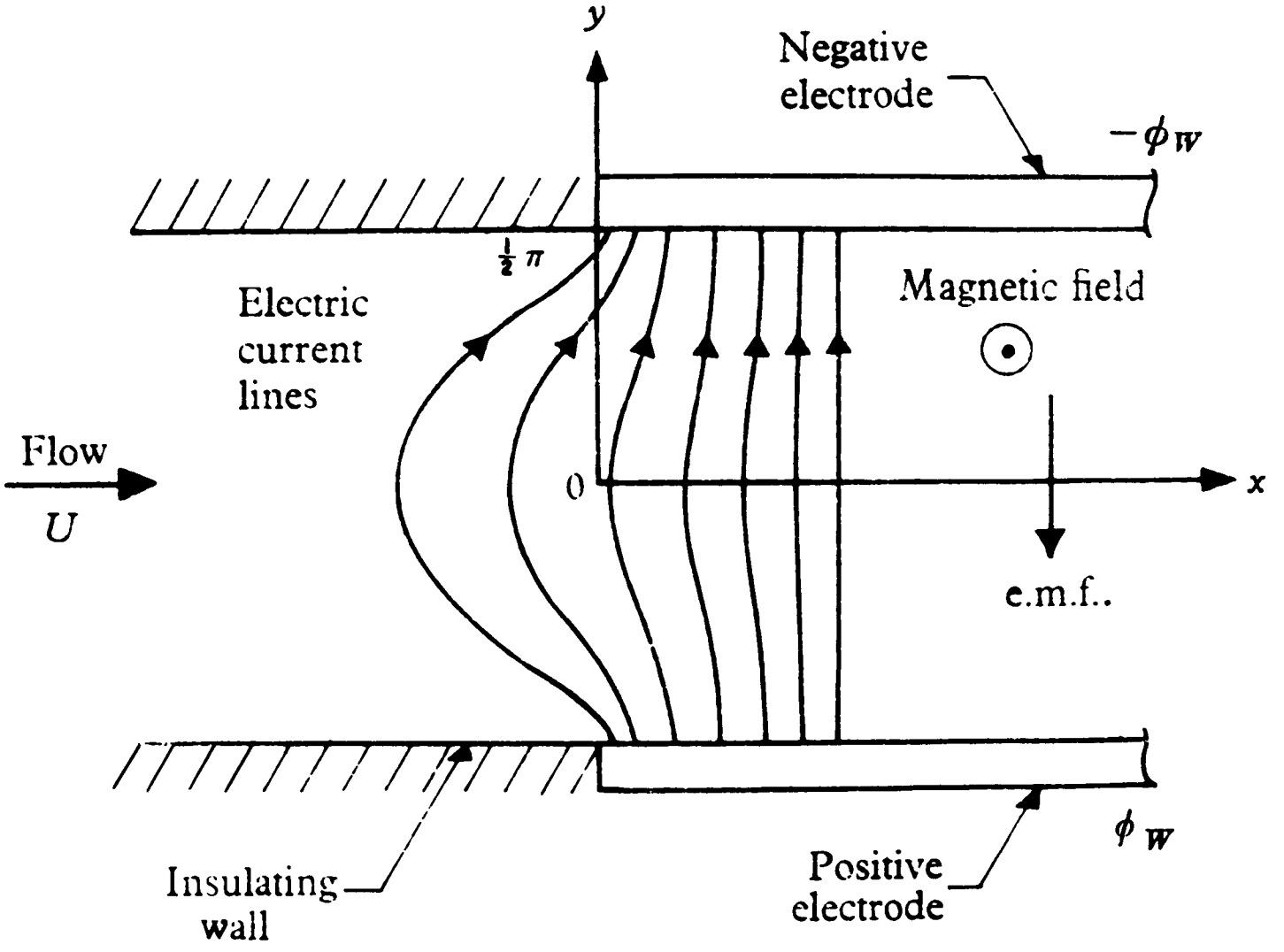

Figure 14.19. Electric Current Lines Due to Electric Fields in the Entrance Region of the Channel

6. The insulating sides are perfect electrical insulators and the electrodes and leads have zero electrical resistance.
7. With the above assumptions, the problem is two-dimensional in the plane normal to the magnetic field.
8. The flow, magnetic field and electric field are steady. The problem is then to calculate the electrical current distribution in the generator, the power generated, the pressure drop, and the overall efficiency of the generator.

14.5a Basic Equations

The basic equations are:

$$\underset{\sim}{\nabla} \times \underset{\sim}{E} = 0 \tag{14.145}$$

$$\underset{\sim}{\nabla} \cdot \underset{\sim}{j} = 0 \tag{14.146}$$

Since the flow is steady, $\underset{\sim}{E} = -\underset{\sim}{\nabla} \varphi$. Thus, from (14.145), the electric potential is continuous, while from (14.146), the electric current is continuous.

The boundary condition at the insulator is that the normal component of the electric current must be zero. In the geometry of Figure 14.19, this means that

$$j_Y(X, h) = j_Y(X, 0) = 0; \quad X < 0 \tag{14.147}$$

At the electrodes, the boundary conditions depend upon the type of electrodes which are used. If the electrodes are continuous, then they are equipotential. On the other hand, if the electrodes are segmented, then one may specify either (a) the current distribution along the electrodes, (b) the transverse voltage difference $\varphi(X, 0) - \varphi(X, h)$, or (c) the ratio of the voltage to the current, which is the same as specifying the distribution of external load resistance. In the ensuing sections, we will consider both continuous electrodes and segmented electrodes for generators which use the Faraday current.

In the generator, there usually exists an insulated inlet section, the electrode region, and an insulated outlet section; in principle all three regions should be analyzed simultaneously. However, it has been found that if the generator aspect ratio a, defined as the ratio of the electrode region to the generator width h, is greater than about 0.7, then the inlet and exit regions can be analyzed separately, and the results combined to yield the generator efficiency; that is, the exit region has no effect over the inlet region and vice versa.[11] In addition, if the velocity profile is constant, then the current distribution at the inlet and exit are similar; hence, only the inlet region is analyzed in this section. However, in order to calculate the generator efficiency, both the inlet and exit losses must be considered. Although in general, the MHD generator will have a diverging cross-section so that the inlet and exit losses will be different, for simplicity we will assume that the inlet and exit losses are identical; that is, we will consider the generator to have a constant cross-sectional area. Thus, it is assumed that the insulating region extends an infinite distance upstream of the electrode region ($X < 0$) while the electrodes extend infinitely downstream.

Finally, the physical dimensions are made non-dimensional as follows:

$$x = X\pi/h$$

$$y = Y\pi/h$$

so that the non-dimensional channel width is π.

14.5b Continuous Electrodes, Scalar Electrical Conductivity

With the electrical conductivity scalar, the current equation becomes:

$$\underset{\sim}{j} = \sigma(\underset{\sim}{E} + \underset{\sim}{v} \times \underset{\sim}{B}) \qquad (14.148)$$

so that (14.146) becomes:

$$\nabla^2 \varphi = 0 \qquad (14.149)$$

since $\underset{\sim}{v} = \underset{\sim}{i}\, U$ and $B_Z = B_Z(X)$. At the electrode at $Y = 0$, the potential may be taken as $+\phi_W$, while at the electrode at $Y = h$, the potential is taken as $-\phi_W$ so that the potential difference between the two electrodes is $2\phi_W$. Along the insulator at $X < 0$, the normal component of the current is zero so that (14.148) becomes

$$\left.\begin{aligned} &\frac{\partial \phi}{\partial Y}(X, 0) = \frac{\partial \phi}{\partial Y}(X, h) = -UB_Z(X) \\ &(X < 0) \end{aligned}\right\} \qquad (14.150)$$

We will consider three different variations of the magnetic field in the region upstream and downstream of the electrode region:

(i) $B_Z(X) = 0;\ X < 0$

(ii) $B_Z(X) = B_o \exp(X/\bar{X});\ X < 0$

(iii) $B_Z(X) = B_o;\ -X_o < X < 0$

$B_Z(X) = 0 \quad X < -X_o$

Case (i) corresponds to the magnetic field ending at the end of the electrode region. Case (ii) corresponds to an exponential decrease in the magnetic field beyond the electrode region with an e-folding length $\bar{X}$. Case (iii) corresponds to an extension of the magnetic field at constant magnitude B_o for a distance X_o upstream (or downstream) of the electrode region.

This is then a problem of solving Laplace's equation in an infinite strip. However, it is complicated by the boundary conditions: for $x > 0$, the value of the potential is specified at boundaries, while for $x < 0$, the normal gradient is specified. For this reason, solutions cannot be obtained analytically by means

of separation of variables. However, this problem may be solved by means of various techniques which utilize complex variables; the simplest method is to conformal map the strip so that the boundary on which the normal gradient is specified is perpendicular to the boundary on which the potential is specified. The simplest mapping which accomplishes this transformation is shown in Figure 14.20, and is given by:

$$Z = \ell n \sin Z' \tag{14.151}$$

where $Z = X + iy$ is the original complex plane and $Z' = X' + iy'$ is the transformed plane. In the Z' plane, Laplace's equation must be satisfied with respect to x', y'; the potential along the electrodes remains the same, but the normal gradient must be appropriately transformed. The three cases are considered next:

(i) Zero Extension to Magnetic Field

For zero magnetic field upstream of the electrodes, from (14.150) $(\partial \varphi / \partial y) = 0$ along the boundaries; hence, in the transformed plane $(\partial \varphi / \partial y') = 0$. The solution to Laplace's equation in the Z' plane is then obviously:

$$\varphi = \frac{2\varphi_W}{\pi} x' \tag{14.152}$$

Next, the total electrode current to some point X_1 can be calculated as follows:

$$J_y(X_1) = \int_0^{X_1} j_y \, dX = -\sigma \int_0^{X_1} \left[\left(\frac{\partial \varphi}{\partial Y} (0, X_1) - UB \right) \right] dX$$

where (14.148) has been used. The first term in the bracket can be made dimensionless, and the second term integrated as follows:

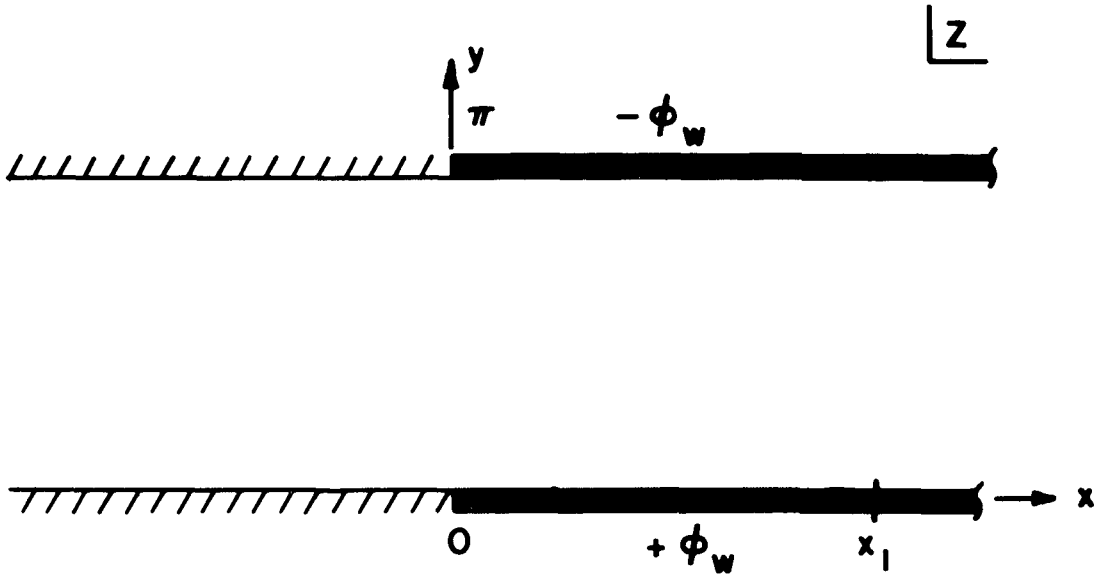

a. PHYSICAL PLANE

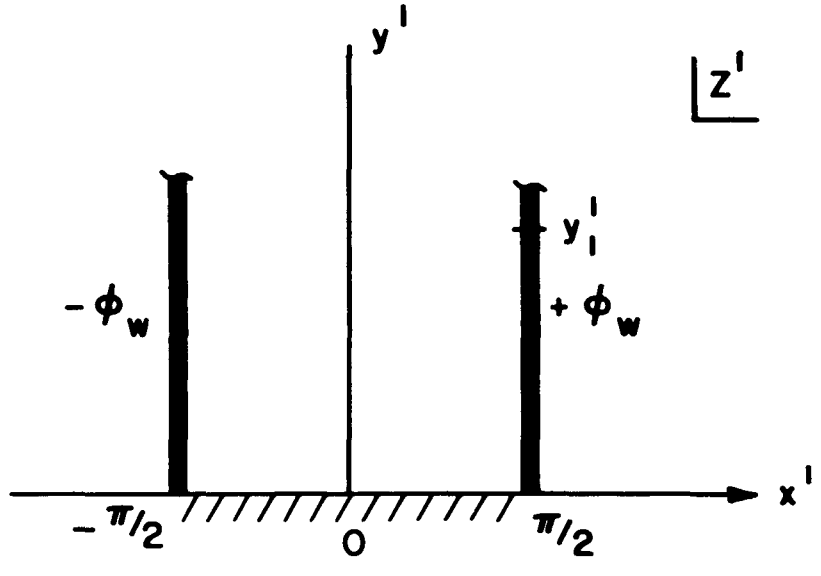

b. TRANSFORMED PLANE $Z = \text{Ln sin } Z'$

Figure 14.20. Conformal Mapping of End Losses

$$J_y(X_1) = -\sigma \int_0^{x_1} \frac{\partial \varphi}{\partial y}(0, x)\, dx - \sigma UBX_1$$

Now $(\partial\varphi/\partial y)\, dx = -(\partial\varphi/\partial x')\, dy'$ along the electrode, and from (14.152), $\partial\varphi/\partial x' = 2\phi_W/\pi$. Thus,

$$J_y(X_1) = 2\sigma \phi_W y'_1/\pi - \sigma UBX_1 \qquad (14.153)$$

Along the electrode $Z = x$ and $Z' = \pi/2 + i y'$, so that (14.151) becomes

$$x = \ell n \cosh y'$$

For large values of the argument, $\cosh y' \approx \frac{1}{2} \exp y'$ so that

$$x_1 \approx \ell n \left(\frac{1}{2} \exp y'_1\right) \approx y'_1 - \ell n\, 2$$

Substitution of y'_1 in terms of X'_1 into (14.153) then yields:

$$J_y(X_1) = \frac{2}{\pi} \sigma \varphi_W \left(\frac{X_1 \pi}{h} + \ell n\, 2\right) - \sigma UB X_1 \qquad (14.154)$$

Now, the definition of the load factor may be taken as:

$$K = 2\varphi_W/UBh$$

so that (14.154) becomes

$$J_y(X_1) = -\sigma UB X_1 (1-K) + K \sigma UBh \pi^{-1} \ell n\, 2 \qquad (14.155)$$

The first term in (14.155) is the "ideal" current, which would exist in the absence of end losses; the second term represents the current loss, due to the shunting effect of the conducting fluid upstream of the magnetic field. Note that this term is proportional to the voltage difference between the electrodes, that is, the load voltage. The generated power up to point X_1 is given by the product of the current $J_y(X_1)$ and the load voltage, KUBh. Thus, the second term in (14.155) also represents the power loss.

If the exit of the generator has the same dimensions as the inlet, a similar loss exists at the exit, thus, the total lost power P_L per unit height is:

$$P_L = 2 \cdot KUBh \cdot \sigma \pi^{-1} K U B h \ell n 2 \tag{14.156}$$

while the ideal power P_i for a generator of length L, width h, per unit height is:

$$P_i = \sigma K (1-K) U^2 B^2 h L \tag{14.157}$$

The actual power P_a is the difference of (14.157) and (14.156):

$$P_a = \sigma U^2 B^2 K h \left[(1-K) L - 2 \pi^{-1} h \ell n 2 \right] \tag{14.158}$$

To calculate the efficiency, the flow work W through the generator must be calculated:

$$W = \int_0^h \int_0^L \underset{\sim}{v} \cdot \underset{\sim}{j} \times \underset{\sim}{B} \, dY \, dX \tag{14.159}$$

The integration is taken over X to obtain the average flow work across the generator, while the integration over Y is taken only where the magnetic

field is non-zero. With $\underset{\sim}{v} = \underset{\sim}{i}\, U$, and B in the Z direction, the only component of current in (14.159) is j_y; thus,

$$W = -\sigma \int_0^L \int_0^h \left(\frac{\partial \varphi}{\partial Y} + UB \right) B \, dY \, dX \qquad (14.160)$$

Integration with respect to Y and then X and use of the definition of K yields:

$$W = -\sigma (1-K) U^2 B^2 L h \qquad (14.161)$$

which is identical to the expression which one obtains if the end regions are ignored. The efficiency is then given by

$$\eta = -\frac{P_a}{W} = K \left[1 - \frac{Ka^*}{1-K} \right] \qquad (14.162a)$$

from (14.158, 14.161), and where a* is a modification of the aspect ratio,

$$a^* = \frac{2}{\pi} \frac{h}{L} \ell n\, 2 \qquad (14.162b)$$

Note that as the generator becomes very long, that is, as $a^* \longrightarrow 0$, then the expression for the efficiency becomes identical to the "local" efficiency K. Also, K = 0 still corresponds to short circuit, but open-circuit conditions correspond to the bracket in (14.162a) equal to zero, e.g., when

$$K_{o.c.} = \frac{1}{1 + a^*} \qquad (14.163)$$

Thus, the larger the value of a*, the smaller the open-circuit voltage. However, when the voltage is equal to the open-circuit voltage, the efficiency is equal to zero, rather than equal to K. The efficiency is therefore

greater than zero only for $0 \leq K < (1 + a^*)^{-1}$. A typical efficiency curve is shown in Figure 14.21 for an aspect ratio L/h = 1. Note that the maximum efficiency is only 0.29, corresponding to a loading factor of 0.45. As the aspect ratio L/h increases, a* decreases, and both the maximum efficiency and loading factor at maximum efficiency increase . For any given aspect ratio, the maximum efficiency is obtained by equating to zero the derivative of (14.162a). The maximum efficiency is then given by:

$$\eta_m = \frac{\sqrt{\frac{1}{a^*} + 1} - 1}{\sqrt{\frac{1}{a^*} + 1} + 1} \qquad (14.164)$$

This maximum efficiency is shown in Figure 14.22. It is seen that large aspect ratios are required to obtain efficiencies greater than 0.6.

For a given aspect ratio, the efficiency can be improved by the insertion of insulating vanes at the inlet and exit parallel to the flow but external to the magnetic field region. For example, a single inlet vane and exit vane placed in midstream will double the apparent aspect ratio; two equally spaced vanes will triple the apparent aspect ratio, etc.

Another method of improving the efficiency is to extend the magnetic field. Actually, most magnetic fields decrease exponentially away from the pole faces. Hence, this type of "shading" is considered next.

(ii) Exponential "Shading" of Magnetic Field

To solve this case, it is convenient to introduce the complex potential

$$\Phi(z) = \varphi + i\,\psi \qquad (14.165)$$

such that φ, ψ obey the Cauchy-Riemann conditions; furthermore, the equation for ψ is also

$$\nabla^2 \psi = 0 \qquad (14.166)$$

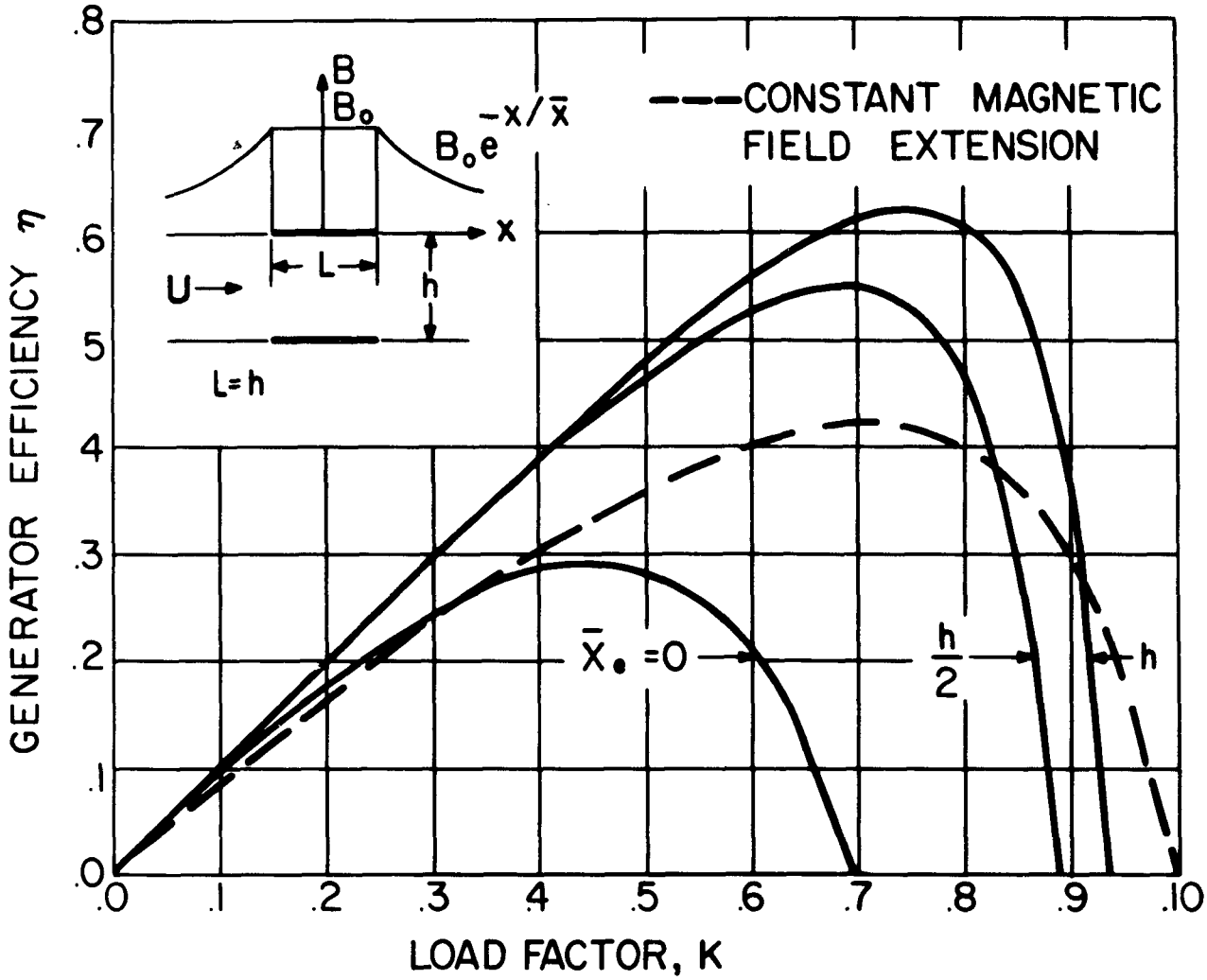

Figure 14.21. Generator Efficiency, For Channel Length Equal to Channel Width

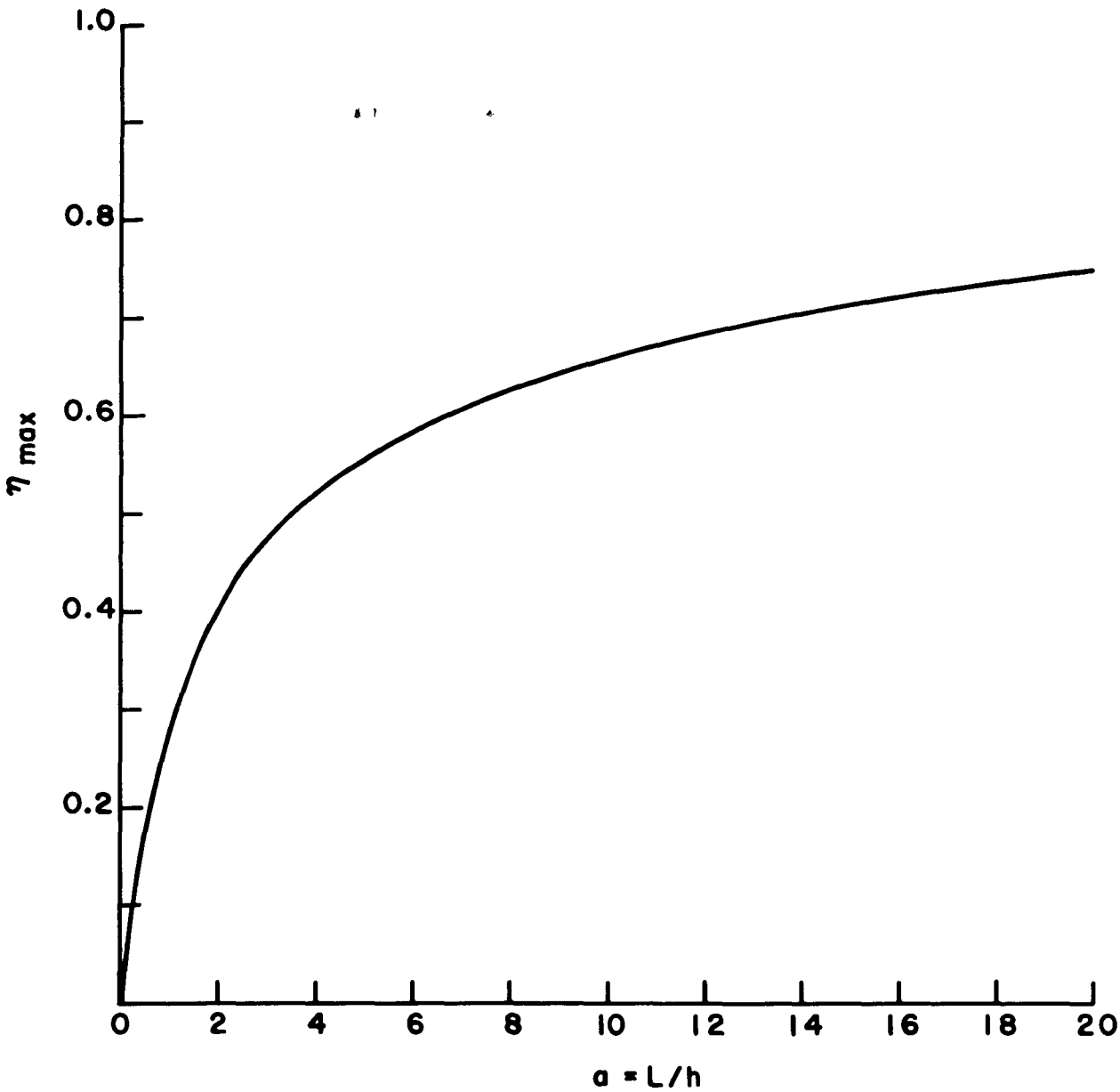

Figure 14.22. Maximum Efficiency Considering End Losses - Zero Extension to the Magnetic Field

Thus, ψ is a "stream function" for the potential. Also, the contribution to the current caused by the potential gradient j_ϕ is given by $\underset{\sim}{j}_\varphi = -\nabla \varphi$, or:

$$j_{\varphi_x} = -\frac{\sigma \pi}{h} \operatorname{Re} \frac{d\Phi}{dz}$$

$$j_{\varphi_y} = \frac{\sigma \pi}{h} \operatorname{Im} \frac{d\Phi}{dz}$$

or:

$$\bar{j}_\varphi = j_{\varphi_x} - i\, j_{\varphi_y} = -\frac{\sigma \pi}{h} \frac{d\Phi}{dz} \tag{14.167}$$

Thus, between any two points z_1 and z_2, the total current between these two points $\bar{J}_\varphi$ is:

$$\bar{J}_\varphi = -\sigma \left[\Phi(z_1) + \Phi(z_2)\right] \tag{14.168}$$

In particular, if z_1 and z_2 are points on the same equipotential, then:

$$\bar{J}_\varphi = -i\sigma \left[\psi(z_1) - \psi(z_2)\right]$$

or

$$\left.\begin{aligned} J_{\varphi_x} &= \sigma \operatorname{Im} \left[\psi(z_1) - \psi(z_2)\right] \\ J_{\varphi_y} &= \sigma \operatorname{Re} \left[\psi(z_1) - \psi(z_2)\right] \end{aligned}\right\} \tag{14.169}$$

Now, for this case,

$$B = B_o e^{-x/\overline{x}} ; \quad x < 0 \tag{14.170}$$

so that along the insulator, for j_y to be zero:

$$\frac{\partial \varphi}{\partial y} = - \frac{h}{\pi} U B_o e^{\gamma x} \tag{14.171}$$

where

$$\gamma = h/\pi \overline{X}$$

In the z' plane, along y' = 0,

$$\frac{\partial \varphi}{\partial y'} = \frac{\partial \varphi}{\partial y} \frac{dz}{dz'} = - \frac{\partial \psi}{\partial x'} \tag{14.172}$$

Use of (14.151) and (14.171) in (14.172) and integration with respect to x' yields:

$$\psi = \frac{h U B_o}{\gamma \pi} \sin \gamma x' \tag{14.173}$$

Now, ψ must obey Laplace's equation in the transformed plane; thus, the solution may be written as:

$$\psi = \frac{2 \varphi_W y'}{\pi} + \sum_{n=0}^{\infty} b_n \cos 2n x' e^{-2n y'} \tag{14.174}$$

The first term above satisfies the boundary condition at the electrodes; it is in fact the solution obtained in case (i). The second term represents the Fourier series solution to Laplaces equation. Only the cosine series is used because the sine series does not satisfy the boundary conditions along the electrodes. The cosine series thus represents the additional current due to the shading of the magnetic field; this will be designated as ψ^+. Now, from (14.169), the additional current to the electrode between ($\pi/2$, 0) and some point ($\pi/2$, y_1) where $y_1 \gg 1$ is:

$$J^+(y_1) = \sigma \left[\psi^+\left(\frac{\pi}{2}, y_1\right) - \psi^+\left(\frac{\pi}{2}, 0\right)\right] \tag{14.175}$$

From (14.174), the first term in the above bracket is just the first term in the Fourier series, b_o. This is obtained by solving for the Fourier coefficients along $y' = 0$ from (14.173, 14.174):

$$\psi^+ = \frac{h\,U B_o}{\pi\gamma} \sin^{\gamma} x' = \sum b_n \cos 2n x' e^{-2ny'}$$

from which

$$\lim_{y_1' \to \infty} \psi^+\left(\frac{\pi}{2}, y_1\right) \equiv b_o = \frac{2\,h\,U B_o}{\pi^2 \gamma} \int_0^{\pi/2} \sin^{\gamma} x'\, dx'$$

$$= \frac{h\,U B_o}{\pi\gamma} \left[\frac{1}{\sqrt{\pi}} \frac{\Gamma\left(\frac{\gamma+1}{2}\right)}{\Gamma\left(\frac{\gamma}{2}+1\right)}\right] \tag{14.176}$$

where Γ is the gamma-function.

From (14.173),

$$\psi^+\left(\frac{\pi}{2}, 0\right) = \frac{h\,U B_o}{\pi\gamma} \tag{14.177}$$

Substitution of (14.176, 14.177) into (14.175) yields the additional electrode current:

$$J^+ (Y_1 \longrightarrow \infty) = - \frac{\sigma U B_o h}{\pi \gamma} \left[1 - \frac{1}{\sqrt{\pi}} \frac{\Gamma\left(\frac{\gamma+1}{2}\right)}{\Gamma\left(\frac{\gamma}{2}+1\right)} \right] \qquad (14.178)$$

The additional power at the inlet is given by $2 \varphi_W J^+$. If the configuration at the exit is identical to that at the inlet, an equal amount of additional power will be generated at the exit due to the shading of the magnetic field.

To calculate the efficiency, the flow work is calculated in a manner analogous to (14.160):[11]

$$W = \sigma U^2 B_o^2 h^2 \left\{ \frac{2}{\pi \gamma} \left[1 - \frac{1}{\sqrt{\pi}} \frac{\Gamma\left(\frac{\gamma+1}{2}\right)}{\Gamma\left(\frac{\gamma}{2}+1\right)} \right] - (1-K)\, L/h \right.$$

$$\left. + \frac{16}{\pi^3} \sum_{n=2,4,6}^{\infty} n A_n^2 - \frac{1}{\gamma \pi} \right\} \qquad (14.179)$$

where:

$$A_n = \frac{\pi (-1)^{n/2}}{2^{\gamma+1} \gamma} \frac{\Gamma(\gamma+1)}{\Gamma\left(\frac{\gamma}{2}+1+\frac{n}{2}\right) \Gamma\left(\frac{\gamma}{2}+1-\frac{n}{2}\right)}$$

The efficiency is obtained by dividing the total power by the flow work given by (14.179); this is shown in Figure 14.21 for two different e-folding lengths of the magnetic field, $\frac{1}{2}$ h and h. It is seen that considerable improvement in the efficiency is obtained by slight shading of the magnetic field.

(iii) Constant Magnitude Extension of the Magnetic Field

The magnetic field may also be extended at constant magnitude[12]; the efficiency for an extension equal to ten channel widths is shown as the dashed line in Figure 14.21. It is apparent that the effectiveness of this type extension is poor in comparison to the exponentially shaded field. This is due to the sudden termination of the magnetic field at a point where the channel is an insulator. Thus, almost the full open-circuit voltage is developed there. This leads to a maximum eddy current loss of power at this point, since this loss is essentially proportional to the voltage difference across the channel.

14.5c Effect of Tensor Conductivity

In general, the electric current vector can be separated out into two parts: one due to the stationary potential gradient $\nabla \varphi$, and the other due to the induced field $\underset{\sim}{v} \times \underset{\sim}{B}$ as follows:

$$\underset{\sim}{j} = \underset{\sim}{j}_{\varphi} + \underset{\sim}{j}_{B} \tag{14.180}$$

This procedure has already been utilized in the preceding section, see (14.167). Since the values of $\underset{\sim}{v}$ and $\underset{\sim}{B}$ are assumed, the induced current is obtained easily, but to obtain the current due to the potential gradient requires the solution to the potential problem. The boundary conditions for the potential problem are usually either a specified potential or normal current. When the electrical conductivity is scalar, the normal current boundary condition becomes a normal gradient of the potential. When the potential or the normal potential gradients are specified on the boundaries, the problem is well posed.

However, when the electrical conductivity is tensor, the specification of the normal current does not lead to a normal gradient of the potential. For example, consider the velocity in x direction only, and the magnetic field in the z direction only. Then the current components become:

$$
\left.
\begin{aligned}
j_{B_x} &= \frac{\sigma \beta_e UB}{1+\beta_e^2} \quad ; \quad j_{B_y} = -\frac{\sigma UB}{1+\beta_e^2} \\
j_{\varphi_x} &= \frac{\sigma}{1+\beta_e^2}\left[-\frac{\partial \varphi}{\partial X} + \beta_e \frac{\partial \varphi}{\partial Y}\right] \\
j_{\varphi_y} &= \frac{\sigma}{1+\beta_e^2}\left[-\frac{\partial \varphi}{\partial Y} - \beta_e \frac{\partial \varphi}{\partial X}\right]
\end{aligned}
\right\} \qquad (14.181)
$$

Thus, if j_{φ_y} is specified as zero on a boundary, then $(\partial \varphi / \partial Y) = -\beta_e (\partial \varphi / \partial X)$. Thus, the equipotential lines have a slope of β_e^{-1} with respect to the x-axis. This type boundary condition is neither Dirichelet nor Neuman, and therefore requires special treatment. To solve this type of problem, one may conformal map the original region such that the equipotential lines are straight and equally spaced in the transformed plane. The boundaries along which the potential lines are sloped are then mapped at the appropriate angle to the equipotential lines. Using this technique, the potential map for the continuous electrodes have been calculated[6] when the electrical conductivity upstream of the electrode region is zero. The resulting equipotential and current flow lines are shown in Figure 14.23, for $\omega_e \tau_e = 1$. The potential and current due to the induced electric field UB have been omitted. It is seen that there is a current concentration at the upper left-hand corner of the electrode. There is no effect of the distortion at the inlet on the efficiency; however, the total power is reduced somewhat by the end effect.

Using this same technique, the potential field and current has been obtained when the magnetic field and electrical conductivity are extended infinitely upstream of the electrodes[13] and when the electrodes are skewed with respect to one another.[14]

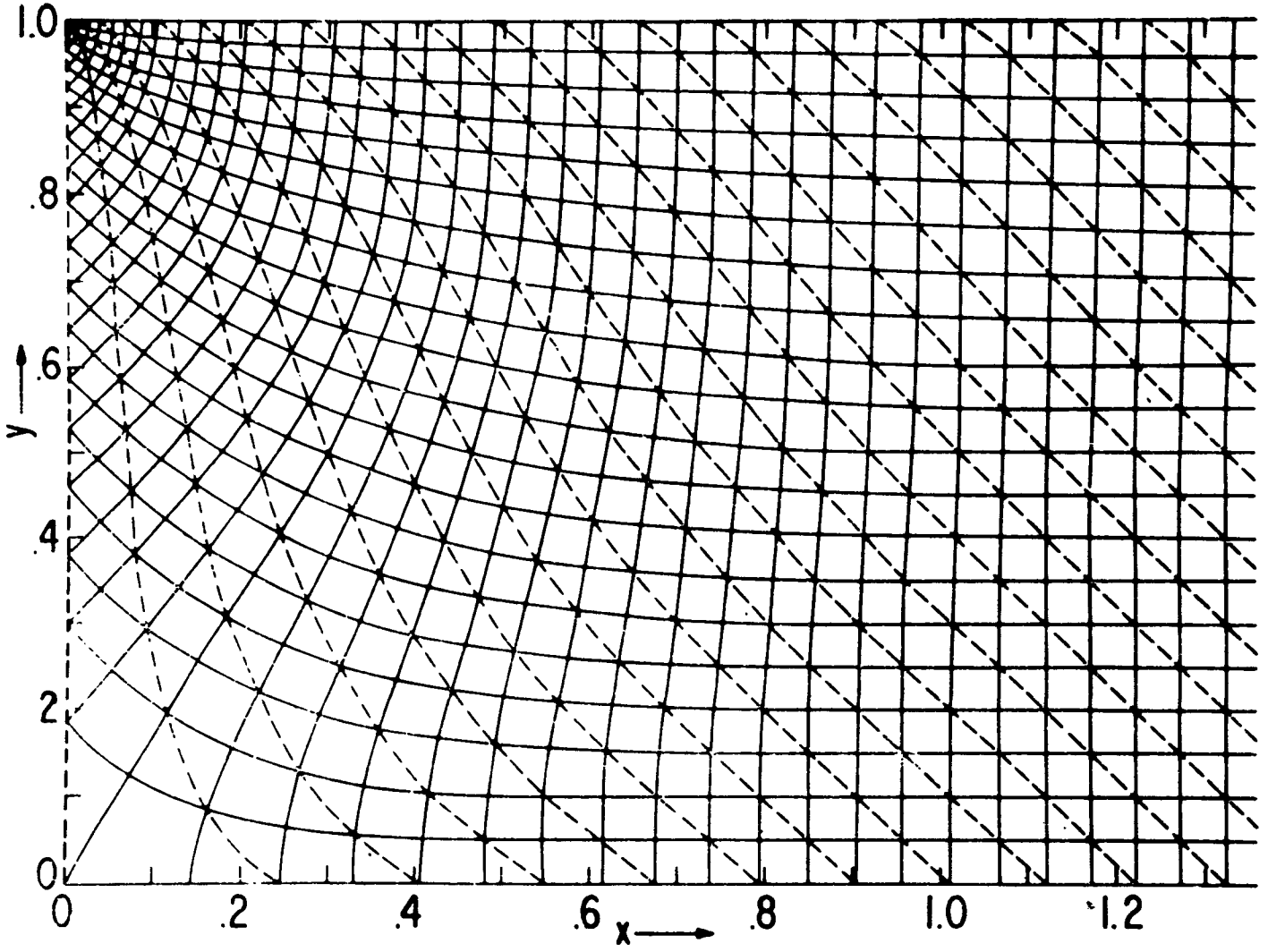

Figure 14.23. Potential Mesh (Solid Lines) and Current Flow (Dashed Lines) For $\omega_e \tau_e = 1$, And $\sigma = 0$ For $x < 0$. The Current and Potential Lines Due to UB Have Been Omitted.

For values of $\omega_e \tau_e$ in excess of unity, the mapping technique has also been used to determine the current flow in the vicinity of segmented electrodes,[6] when the electrode length in the direction of flow is equal to the length of insulation between electrodes. The calculated current distributions are shown in Figure 14.24. It is seen that there is a concentration of current in the downstream portion of the electrode; and also, the distortion of the current lines extends into the stream only a distance equal to the electrode length.

If the electrode pitch distance were infinitely small, the effect transverse conductivity would be equal to the scalar electron conductivity, in the absence of ion slip; the effect of finite size electrodes and insulators decreases the effective transverse conductivity. The theoretical reduction[15] is shown in Figure 14.25 for $\omega_e \tau_e = 1$, where it is seen that increasing pitch distances decrease the effective transverse conductivity. In addition, increasing values $\omega_e \tau_e$ also decreases the effective transverse conductivity as shown in Figure 14.26. Also, increasing the electrode width as compared to the electrode pitch is deleterious.[16] Finally, it has been shown that the viscous boundary layer along the electrode surface has no effect on these results, and also, finite size electrodes do not effect the efficiency,[15] neglecting end losses.

The effect of end losses on efficiency with segmented electrodes has also been investigated theoretically.[17] The maximum efficiency is shown in Figure 14.27 for various aspect ratios, where it has been assumed that the electrode pitch distance is infinitely small. In the vicinity of the inlet or exit, one may specify either (i) the current to each electrode, (ii) the transverse potential difference, or (iii) a relation between the electrode current and potential difference. To investigate the effect of these different conditions, calculations were made for $\omega_e \tau_e = 0$ for (i) constant electrode current and (ii) constant interelectrode potential. It can be seen that the efficiency for case (i) is greater than (ii). Also, it can be shown that the results for case (iii) will be between (i) and (ii); hence, only the "constant current" case was calculated for finite $\omega_e \tau_e$. It is seen that increasing $\omega_e \tau_e$ increases the efficiency slightly as does extending the magnetic field. It therefore appears that the

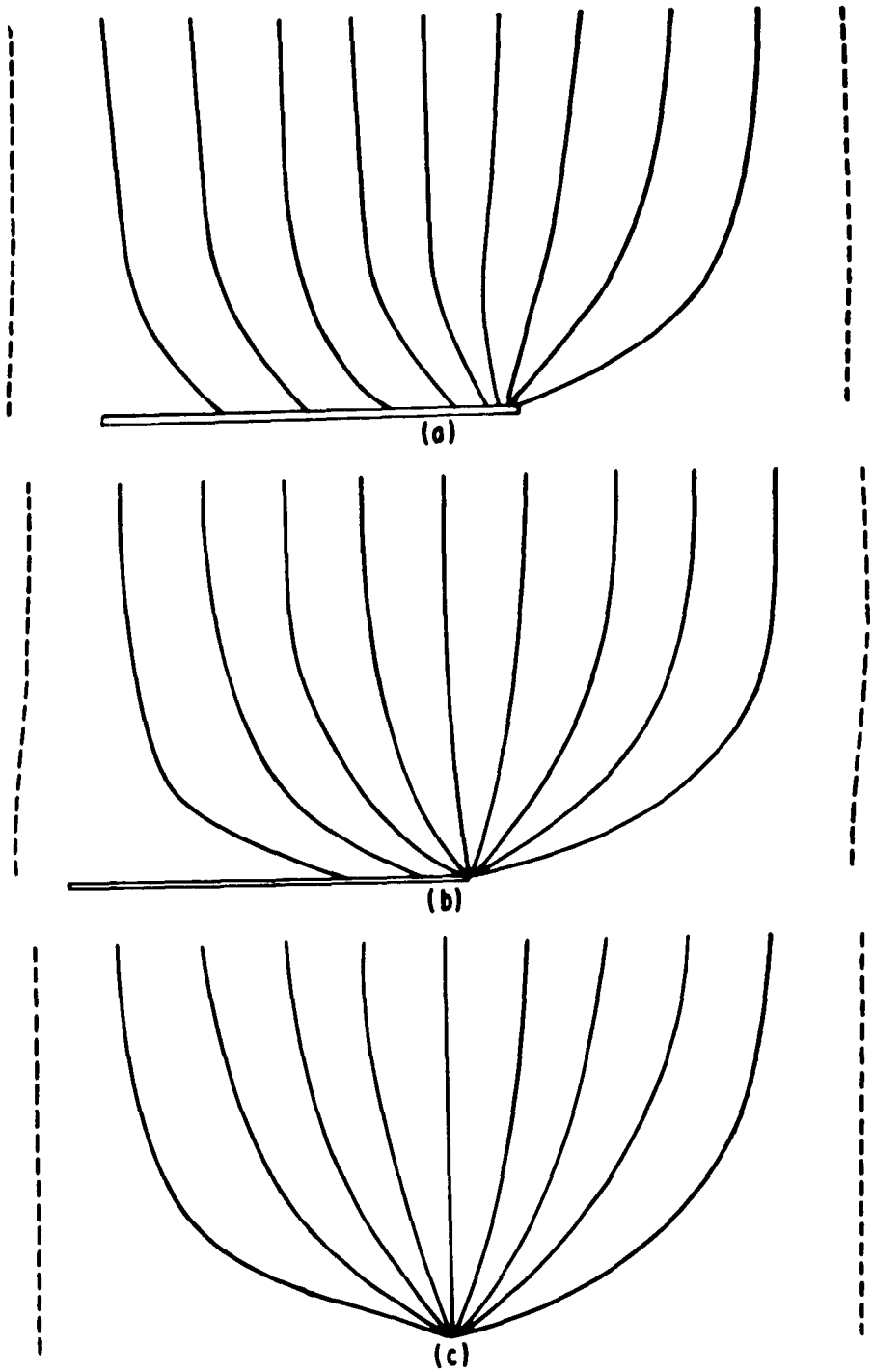

Figure 14.24. Current Flow Lines. (a) Segmented Electrodes with $\omega\tau = 1$. (b) Segmented Electrodes With $\omega\tau = 3$; Note That Most of the Current Flows Into the Right Hand Corner of the Electrode. (c) Infinitely Thin Electrode; This Case is Independent of $\omega\tau$. The Dashed Lines in the Figure Represent Current Dividing Lines Between Adjacent Electrodes.

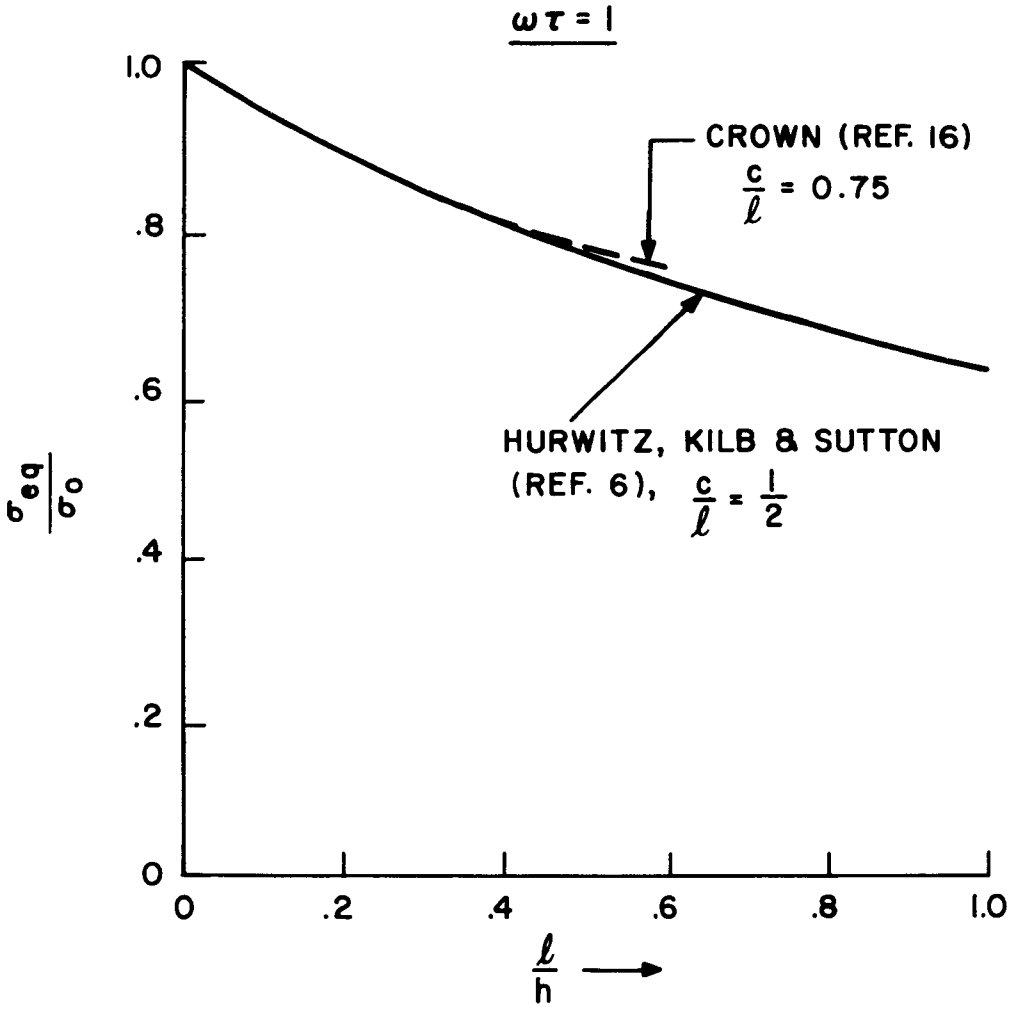

Figure 14.25. Effect of Electrode Pitch on Effective Transverse Electrical Conductivity for $\omega_e \tau_e = 1$

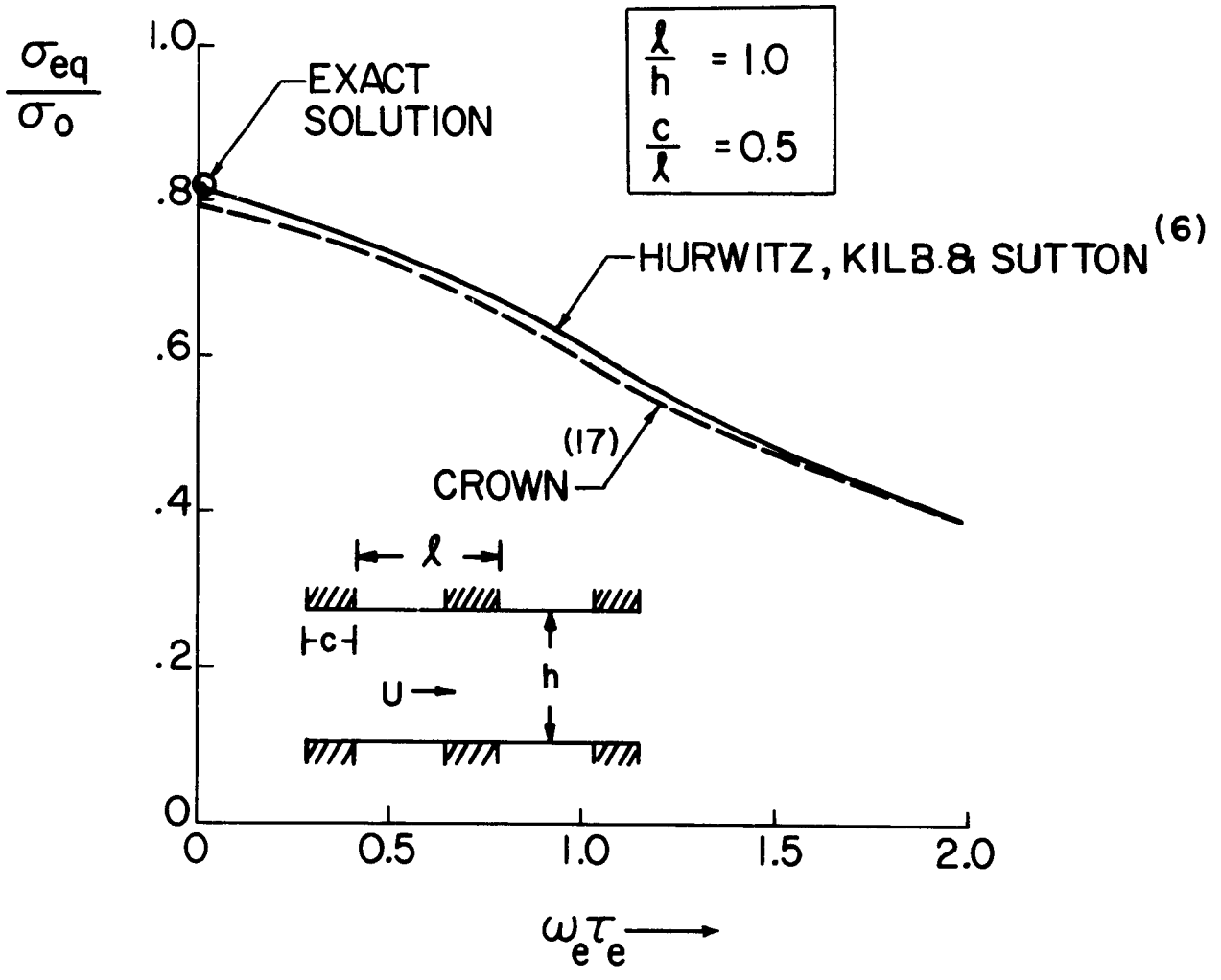

Figure 14.26. Effect of $\omega_e\tau_e$ On Effective Transverse Electrical Conductivity For Segmented Electrodes

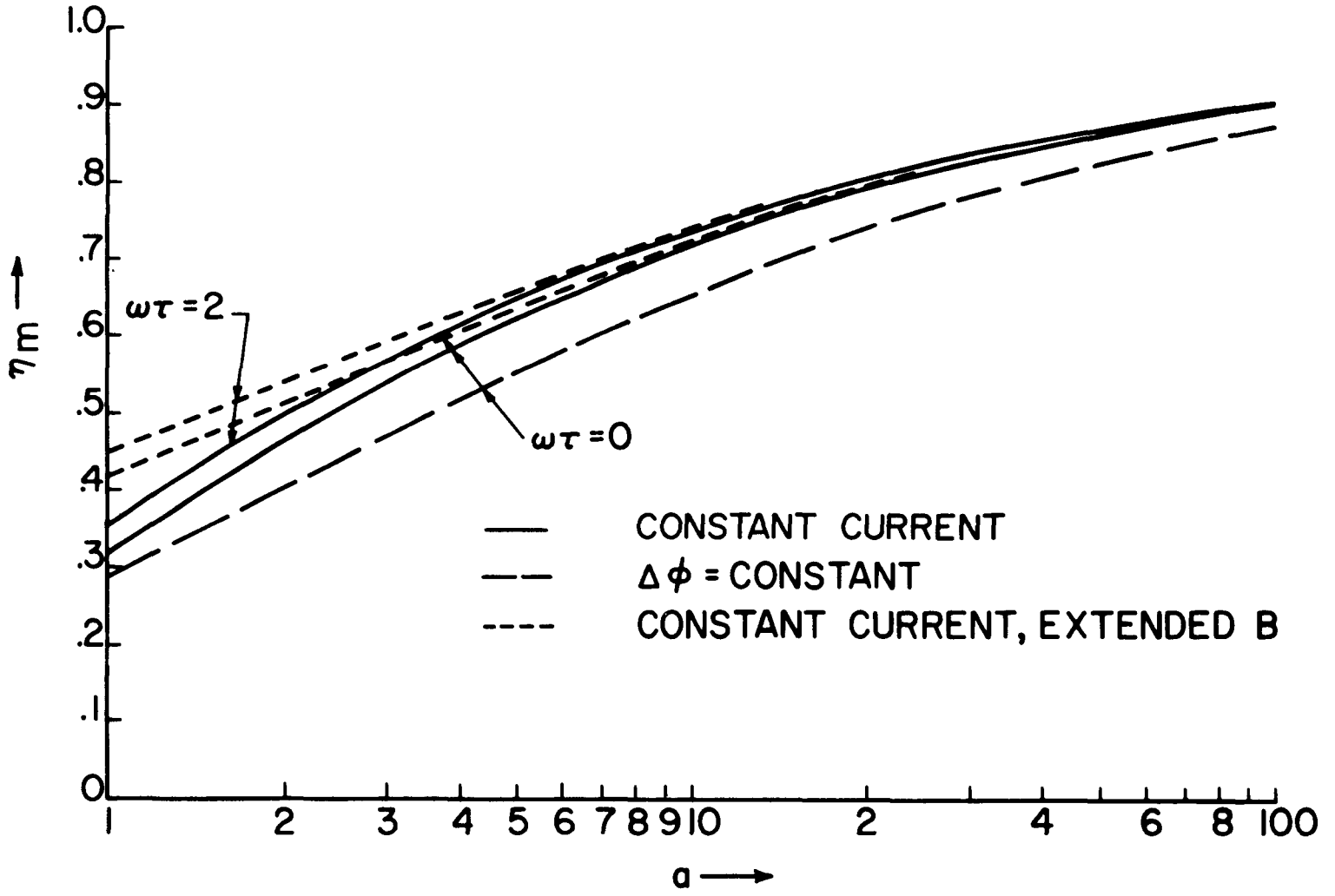

Figure 14.27. Maximum Generator Efficiency

generator efficiency for segmented electrodes and finite values of $\omega_e \tau_e$ is greater than for continuous electrodes.

The influence of tensor conductivity on end losses has also been calculated for the boundary condition at the electrode that $j_x = 0$. Although this is not as realistic as those used above, the resulting field distribution and conclusions are essentially the same.[18]

14.6 COMPRESSIBLE FLOW IN FARADAY CURRENT MHD GENERATORS[19,20]

In any magnetohydrodynamic generator which uses an ionized gas, the effect of compressibility must be included if there is a large pressure drop through the generator. Thus, the results of the previous sections may be regarded only as "local" analysis over a short section of the generator, in which the change in properties is small. As the temperature and pressure change in the generator, so will the degree of ionization or composition and hence the gas is not perfect, and the analysis of the flow may require numerical integration.[21,22] However, if the degree of ionization is small ($< 0.1\%$), then the total amount of ionization energy is small compared to the gas energy, and the compressibility factor is also close to unity. Under these conditions, one may assume that the gas is perfect.

The effects of friction and heat transfer may also be neglected if the Z factor (14.132) is small; which implies "large" generator dimensions. Finally, if the interaction parameter (14.131) is small compared to unity, which is generally correct, then the properties of the ionized gas change "slowly" in the flow direction. With this assumption, one may use the assumption of quasi-one dimensional flow; that is, the transverse flow velocities in the channel are small; and the axial flow velocity, magnetic field, electric field, and electrical conductivity do not vary across the cross section of the generator. The assumption concerning the magnetic field is valid when the magnetic Reynolds number is small. If x is the direction of flow and u is the mass averaged gas velocity in that direction, then the appropriate equations are as follows:

Continuity

$$\rho u A = \text{constant} = \dot{m} \tag{14.182}$$

Momentum

$$\rho u \frac{du}{dx} + \frac{dp}{dx} = \underset{\sim}{i} \cdot (\underset{\sim}{j} \times \underset{\sim}{B}) \tag{14.183}$$

Energy

$$\rho u \frac{d}{dx}\left(h + \frac{u^2}{2}\right) = \underset{\sim}{E} \cdot \underset{\sim}{j} \tag{14.184}$$

State

$$p = \rho RT = nkT \tag{14.185}$$

Caloric

$$dh = C_p dT \tag{14.186}$$

where A(x) is the cross-sectional area, C_p is the specific heat at constant volume assumed constant, and R is the gas constant,

$$R = k/<m> \tag{14.187}$$

when $<m>$ is the average mass of the particles:

$$<m> = \sum_s \frac{n_s}{n} m_s \tag{14.188}$$

In addition to these equations, it is necessary to specify Ohm's law, and the manner in which the conductivity, or the factors which enter the expression for the conductivity, vary with temperature, pressure, etc. These equations (14.182) - (14.186) have been used to analyze the compressible flow in Faraday type generators; that is, for continuous or segmented electrodes. At present, compressible analyses have been not performed for the Hall type geometry. The Hall geometry generally requires an additional equation for conservation of current in the downstream direction,

$$j_x A = \text{constant} \tag{14.189}$$

In general, it is also necessary to specify the manner in which the transverse magnetic field varies in the downstream direction. For convenience it will be assumed that the magnetic field is constant: methods for including the variation of the magnetic field will be indicated. Also, the electric field must be specified; in general the electric field will be taken as a fraction of the transverse induced electric field uB. Even with the magnetic field and electric field specified, equations (14.182) - (14.186) are not determinate: there is one more unknown than there are equations. It is therefore necessary to specify one of the variables to solve these equations.* In the following sections, solutions will be presented for various variables such as velocity, Mach number, temperature, pressure, and area specified constant. The paths which are taken by keeping these variables constant are shown in Figure 14.28.

14.6a Constant Velocity Generator

With the axial velocity held constant, the electrical energy is extracted from only the thermal energy of the gas. Actually, this may be regarded as a two-stage process, since the Faraday induction removes electrical energy only from the kinetic energy of the flow. However, the gas is then accelerated to restore the velocity, but in the process of acceleration the static temperature decreases. The momentum and energy equations become, respectively:

$$\frac{dp}{dx} = (\underset{\sim}{j} \times \underset{\sim}{B}) \cdot \underset{\sim}{i} \qquad \text{(a)}$$

$$\rho u C_p \frac{dT}{dx} = \underset{\sim}{E} \cdot \underset{\sim}{j} \qquad \text{(b)}$$

*There is a school of thought which asserts that even when the magnetic Reynolds number is small, one must include Maxwell's equation $j_x = \mu_o \frac{\partial B_z}{\partial x}$. However, it is physically more plausible that the current in the gas causes an x-component of the magnetic field and that $(\partial B_z/\partial x)$ may be neglected.[23]

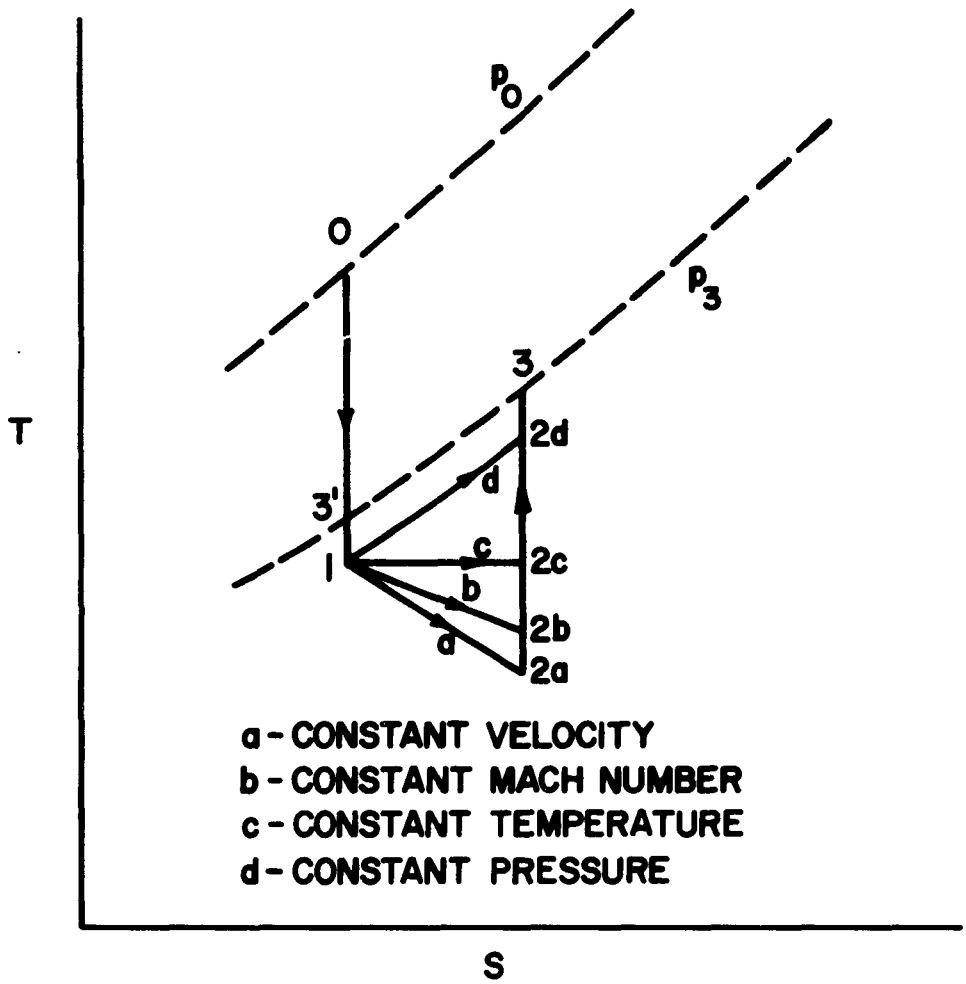

Figure 14.28. Paths on a Mollier Diagram For Various Linear MHD Generators. Point 0 = Stagnation Conditions Upstream of Generator; 1 = Generator Inlet; 2 = Generator Exhaust; 3 = Stagnation Conditions Corresponding to Generator Exhaust.

The first integral of equations (a), (b) is obtained by division of (a) by (b) and integration as follows:

$$\frac{\gamma - 1}{\gamma} \quad \frac{d \ell n\, p}{d \ell n\, T} = \frac{1}{\eta_L} = \frac{1}{K} \tag{c}$$

where use has been made (14.108), and the fact that in a Faraday type generator, the local efficiency is equal to the loading factor, whether the electrodes are continuous or segmented. Since the generator is expected to have a certain overall efficiency, it is desirable to have the polytropic efficiency approximately constant; hence, the loading factor K will be chosen constant. This also insures that every section of the generator will be generating electrical power. With K and γ constant, equation (c) may be integrated immediately.

$$\frac{T(x)}{T_1} = \left[\frac{p(x)}{p_1}\right]^{\frac{\eta_L (\gamma - 1)}{\gamma}} \tag{14.190}$$

Equation (14.190) may be compared to the usual isentropic expression:

$$\frac{T}{T_1} = \left(\frac{p}{p_1}\right)^{\frac{\gamma - 1}{\gamma}} \tag{d}$$

Since η_L is always less than unity, (14.190) shows that for the same pressure ratio, the temperature decrease is always <u>less</u> than isentropic. This is a direct result of the ohmic heating of the gas.

The entropy change may be calculated from:

$$\Delta S = C_p \ell n \frac{T}{T_1} - R \ell n \frac{p}{p_1} \tag{e}$$

Substitution of (14.190) in (e) yields:

$$\frac{\Delta S}{C_p} = \frac{1 - K}{K} \ell n \frac{T_1}{T} \tag{f}$$

which shows the rapid increase in entropy of the gas with decreasing K. This is also due to the increased ohmic heating associated with the increased electrical current density. Equation (f) may also be rearranged as follows:

$$\frac{T}{T_1} = \exp \left\{ - \frac{K \Delta S}{(1 - K) C_p} \right\} \tag{g}$$

To obtain the variation of the gas properties in the downstream direction, it is necessary to integrate either equation (a) or (b), making use of the generalized Ohm's law for a Faraday type generator:

$$\left.\begin{aligned} E &= KuB \\ j &= \sigma_{eff} (E - uB) = - \sigma_{eff} uB (1 - K) \end{aligned}\right\} \tag{14.191}$$

where the magnetic field B is taken in the Z-direction, the electric field E is in the y-direction and σ_{eff} is given in Section 14.4b. For example, substitution of (14.191) into (a) yields:

$$\frac{dp}{dx} = - (1 - K) \sigma_{eff} uB^2 \tag{14.192}$$

Now σ_{eff} is generally not a constant, but depends upon temperature, pressure, and possibly the recombination rate. If σ_{eff} is purely a "state" variable, then it may be expressed in terms of pressure alone by the use of (14.185, 14.190); and (14.192) may be integrated directly. Also, if B varies in a prescribed manner with x, this variation may also be included in (14.192), and the integration

performed. A different method of handling the variation of conductivity and magnetic field is to use a transformed variable ξ, defined as follows:

$$d\xi = \frac{\sigma_{eff} B^2}{(\sigma_{eff} B^2)_1} dx \tag{14.193}$$

where the subscript 1 refers to conditions at the generator inlet. Then (14.192) becomes:

$$\frac{dp}{d\xi} = -(1 - K)(\sigma_{eff} B^2)_1 u$$

which may be integrated immediately to:

$$p_1 - p(\xi) = (1 - K)(\sigma_{eff} B^2)_1 u\xi \tag{14.194}$$

Now with the use of (14.185, 14.190), ρ, T, and consequently σ_{eff} may be obtained as a function of ξ. The variation of ξ with x is then obtained by integration of (14.194) as follows:

$$\int_0^{\xi} \left[\sigma_{eff}(\xi)\right]^{-1} d\xi = \sigma_{eff_1}^{-1} \int_0^{x} (B/B_1)^2 dx \tag{14.195}$$

The variations of B and σ_{eff} may therefore be regarded as a "scaling" of the length parameter x; that is, the value of ξ which is required to obtain a given pressure drop is equal to the length x required to obtain the same pressure drop in a generator in which the magnetic field and effective conductivity remain constant. Decreases in either the magnetic field or conductivity increase the length x required to obtain the same pressure drop.

In spite of the variable conductivity or magnetic fields, (14.19) may be used to define an "interaction length" L, which is the length in units of ξ for which the exhaust pressure is much smaller than the inlet pressure p_1, and hence may be neglected. Thus,

$$L = \frac{p_1}{(1 - K)\,(\sigma_{eff} B^2)_1\, u} \tag{14.196}$$

The interaction length is therefore a measure of the length of the MHD generator which is required to obtain a large pressure drop; that is, an appreciable temperature drop of the gas. Note that L is different than the magnetic interaction parameter I which was defined in order to compare the magnitude of the Lorentz force to the friction pressure drop.

(i) Optimum Inlet Mach Number, Constant Velocity Generator

Now if L as calculated from (14.196) is large compared to the transverse dimension of the generator, then it may be desirable to change the inlet conditions to decrease the generator length: the most convenient method for accomplishing this being to change the inlet Mach number, e.g., the inlet static temperature. The interaction length L is a minimum when the derivative of $p_1/(\sigma_{eff}\, u)_1$ is set to zero. For example, we may consider a segmented electrode generator with thermal ionization. Neglecting electron-ion collisions, and letting the collision cross sections be constant, the scalar electrical conductivity is:

$$\sigma = \frac{\sqrt{\pi} e^2\, T^{3/4} \quad \exp(-E_i/2kT)}{\sqrt{8m_e}\, \langle Q \rangle p^{1/2} \quad (n_s/n)^{1/2}} \tag{14.197}$$

where it is assumed that the degree of ionization of the seed material S is small. The gas velocity u is given by:

$$u = \sqrt{2C_p (T_o - T_1)} \tag{14.198}$$

The inlet static pressure is given by:

$$\frac{p_1}{p_o} = \left(\frac{T_1}{T_o}\right)^{\frac{\gamma}{\gamma - 1}} \tag{14.199}$$

Substitution of (14.197-199) into (14.196), differentiation with respect to T_1, and equating the resulting expression to zero yields the following expression for T_1 for which L is a minimum:

$$\frac{T_1}{T_o} = \frac{\beta_1 + \alpha_1 \pm \sqrt{\beta_1^2 - 2\beta_i\alpha_i + \alpha_i^2 + \frac{4}{3}\alpha_i}}{2(\beta_i - \frac{1}{3})} \tag{14.200}$$

where

$$\beta_1 = \frac{\gamma}{\gamma - 1} - \frac{1}{2} \tag{a}$$

$$\alpha_1 = \frac{E_i}{3kT_o} \tag{b}$$

The results of applying (14.200) is shown in table 14.3, for two typical gases: combustion gases, for which $\gamma \approx 1.20$, and inert gases, for which $\gamma = 5/3$. These results indicate that the minimum length is obtained for combustion gases when the flow is supersonic, while for inert gases, subsonic. It is to be expected that the optimum Mach number is less for inert gases than for combustion gases because the temperature of the former decreases more rapidly than the latter as the gas velocity increases.

For magnetically induced ionization, as the Mach number is increased, the conductivity increases up until ion slip begins to decrease the electron temperature, hence (14.200) may not be used in this case. Also, (14.200)

is not a useful criteria if the pressure drop due to Lorentz forces is small compared to p_1; or if the interaction length is already sufficiently small. In this case, one may wish to optimize the power density $K(1 - K)\sigma u^2 B^2$. Then, for thermal ionization, constant collision cross section, and small ionization, the optimum inlet static temperature T_1 is given by:

$$\frac{T_1}{T_o} = \frac{\beta_2 + \alpha_2 \pm \sqrt{(\beta_2 + \alpha_2)^2 - 4(\beta_2 - 1)\alpha_2}}{2(\beta_2 - 1)} \qquad (14.201)$$

where

$$\beta_2 = \frac{\gamma}{2(\gamma - 1)} - \frac{3}{4}; \quad \alpha_2 = \frac{E_i}{2kT_o}$$

The results of (14.201) are also shown in Table 14.3. Note that the optimum inlet Mach number for combustion gases is now subsonic, while the optimum Mach number for the inert gas is increased only slightly.

TABLE 14.3. COMPARISON OF OPTIMUM INLET MACH NUMBERS

$E_i = 3.87$ ev
$T_o = 3150^oK$

		Basis: Length	Basis: Power Density
Gas:	γ	$\mathcal{M}_1$	$\mathcal{M}_1$
Combustion	1.2	1.36	0.81
Inert	1.67	0.55	0.60

(ii) Effect of Variable Conductivity

To illustrate the direct integration technique with variable conductivity, consider a thermally ionized gas whose electrical conductivity is given by (14.197), which may be represented as follows:

$$\frac{\sigma}{\sigma_1} = \left(\frac{T}{T_1}\right)^{3/4} \left(\frac{p_1}{p}\right)^{1/2} e^{\frac{E_i}{2kT_1}\left(1 - \frac{T_1}{T}\right)} \tag{14.202}$$

It is convenient to use an expression as complicated as that given by (14.202); to simplify the analysis, let:

$$\frac{\sigma}{\sigma_1} = \left(\frac{T}{T_1}\right)^{\omega} \left(\frac{p_1}{p}\right)^{\nu} \tag{14.203}$$

where ω, ν are exponents which are obtained by matching with (14.202), that is:

$$\nu = \frac{1}{2}$$

$$\omega = \frac{3}{4} + \frac{\frac{E_i}{2kT_1}\left(1 - \frac{T_1}{T}\right)}{\ell n\,(T/T_1)} \tag{14.204}$$

Although ω varies with temperature, the variation is small, and the temperature T in (14.204) may be chosen at some average value. With the variation of conductivity given by (14.203), either the momentum equation (14.192) or the energy equation may be integrated; to illustrate this, consider the energy equation (for constant velocity):[24]

$$\rho u C_p \frac{dT}{dx} = -K(1 - K)\,\sigma\, uB^2 \tag{14.205}$$

law, (14.185),

Use of the perfect gas, (14.190), and (14.203), (14.205) reduces to:

$$\left(\frac{T}{T_1}\right)^{\alpha - 1} \quad \frac{d}{dx}\left(\frac{T}{T_1}\right) = -\frac{1}{x^*} \tag{14.206}$$

where

$$\alpha = \omega - \left(\frac{\gamma}{\gamma - 1}\right)\left(\frac{\nu + 1}{K}\right)$$

$$x^* = \frac{\gamma p_1}{(\gamma - 1)\, T_1\, K(1 - K)\, \sigma_1\, B^2}$$

Equation (14.206) then integrates immediately to:

$$\frac{T}{T_1} = \left\{ 1 + \frac{\alpha x}{x^*} \right\}^{-1/\alpha}, \tag{14.207}$$

and with the use of (14.190) the corresponding pressure ratio is obtained.

To illustrate the use of the scaling law, we may integrate (14.195) with constant magnetic field. From (14.194), (14.190), and (14.203), the conductivity as a function of ξ is given by:

$$\frac{\sigma}{\sigma_1} = \left(1 - \frac{\sigma_1 (1 - K)\, uB^2\, \xi}{p_1}\right)^{\frac{\omega(\gamma - 1)}{\gamma} K - \nu}; \tag{14.208}$$

integration of (14.195) then yields:

$$\left(1 - \frac{\sigma_1 (1 - K)\, uB^2\, \xi}{p_1}\right)^{\nu + 1 - \omega K \left(\frac{\gamma - 1}{\gamma}\right)} =$$

$$1 - \frac{\sigma_1 (1 - K)\, uB^2}{p_1} \left[\nu + 1 - \omega K \left(\frac{\gamma - 1}{\gamma}\right)\right] x \qquad (14.209)$$

which is the required scaling relationship. Successive substitution of (14.209) into (14.194) and (14.190) then yields the same relation (14.207) as obtained by direct integration.

Other examples of direct integration are given in reference 20, which includes the effects of electron-ion collisions, and the Hall reduction in conductivity. The resulting expressions are generally more complex than (14.207). The constant velocity case with thermal ionization and constant collision cross section was first integrated by Brocher.[24]

(iii) Generator Efficiency

The overall generator adiabatic efficiency is defined as

$$\eta = \frac{T_o - T_3}{T_o - T_3'} = \frac{1 - \frac{T_3}{T_o}}{1 - \frac{T_3'}{T_o}} \qquad (14.210)$$

where it is assumed that the specific heat of the gas is constant, see Figure 14.28. Now,

$$\frac{T_3}{T_o} = \frac{T_3}{T_2} \frac{T_2}{T_1} \frac{T_1}{T_o} \qquad (a)$$

The path 0-1 occurs in the nozzle, and is close to isentropic. The path 2-3 occurs in the diffusor; this is actually not isentropic since all diffusors have an entropy loss. However, for the present purposes this path will be considered isentropic; the effect of diffusor losses is given in ref. 37 . Thus, for paths 0-1 and 2-3, the temperatures are related to the pressures by the isentropic expressions so that (a) becomes:

$$\frac{T_3}{T_o} = \left(\frac{p_3}{p_2}\right)^{\frac{\gamma - 1}{\gamma}} \frac{T_2}{T_1} \left(\frac{p_1}{p_o}\right)^{\frac{\gamma - 1}{\gamma}} \tag{b}$$

If K is constant for the entire generator, the relation given by (14.190) may be used as follows:

$$\frac{T_2}{T_1} = \left(\frac{p_2}{p_1}\right)^{K(\gamma - 1)/\gamma} \tag{c}$$

Substitution of (c) into (b) yields:

$$\frac{T_3}{T_o} = \left[\left(\frac{p_1}{p_2}\right)^{1 - K} \frac{p_3}{p_o}\right]^{\frac{\gamma - 1}{\gamma}} \tag{d}$$

Next, it is necessary to express the static pressure ratio across the generator, p_2/p_1, in terms of the desired stagnation pressure ratio p_3/p_o. We may write

$$\frac{p_3}{p_o} = \frac{p_3}{p_2} \cdot \frac{p_2}{p_1} \cdot \frac{p_1}{p_o} \tag{e}$$

The first and last pressure ratios are given by the following isentropic relations:

$$\frac{p_1}{p_o} = \frac{1}{\left[1 + \frac{\gamma - 1}{2}\mathcal{M}_1^2\right]^{\gamma/\gamma - 1}} \tag{f}$$

$$\frac{p_3}{p_2} = \left[1 + \frac{\gamma - 1}{2}\mathcal{M}_2^2\right]^{\frac{\gamma}{\gamma - 1}} \tag{g}$$

Also,

$$\mathcal{M}_2^2 = \frac{u^2}{\gamma RT_2} = \frac{u^2}{\gamma RT_1} \cdot \frac{T_1}{T_2} = \mathcal{M}_1^2 \left(\frac{p_1}{p_2}\right)^{\frac{K(\gamma - 1)}{\gamma}} \tag{h}$$

Substitution of (f, g, h) into (e) yields:

$$\frac{p_3}{p_o} = \left(\frac{p_2}{p_1}\right) \left[\frac{1 + \frac{\gamma - 1}{2}\mathcal{M}_1^2 \left(\frac{p_1}{p_2}\right)^{\frac{K(\gamma - 1)}{\gamma}}}{1 + \frac{\gamma - 1}{2}\mathcal{M}_1^2}\right]^{\frac{\gamma}{\gamma - 1}} \tag{14.211}$$

Unfortunately this is an implicity relation for p_2/p_1 in terms of the desired stagnation pressure ratio. Thus for specified values of $\gamma, \mathcal{M}_1$, and K, (14.211) must be solved numerically to obtain (p_2/p_1). The alternative, of course, is to choose (p_2/p_1) and solve for p_3/p_o.

Finally, T_3'/T_o is given by the isentropic relation:

$$\frac{T_3'}{T_o} = \left(\frac{p_3}{p_o}\right)^{\frac{\gamma-1}{\gamma}} \qquad (14.212)$$

overall adiabatic

With the use of (14.210, 14.212) in (14.209), the efficiency becomes:

$$\eta = \frac{1 - \left[\left(\frac{p_1}{p_2}\right)^{1-K} \frac{p_3}{p_o}\right]^{\frac{\gamma-1}{\gamma}}}{1 - \left(\frac{p_3}{p_o}\right)^{\frac{\gamma-1}{\gamma}}} \qquad (14.213)$$

where (p_1/p_2) is related to p_3/p_o by (14.211). When K becomes very close to unity, $\eta \longrightarrow 1$ as expected. However, with K less than unity, the efficiency may still become close to unity if the pressure ratio p_3/p_o is sufficiently large. This is the familiar, internal reheat of turbomachinery - in the case of MHD generator, the ohmic heating is passed downstream and is available for conversion into electrical power. This effect may also be attributed to the "spreading" of the pressure lines on the temperature-entropy diagram: At very low pressures, a large entropy change causes only a small change in temperature. The various efficiencies are shown in Figures 14.29, 14.30. In Figure 14.29 the value of $\frac{\gamma-1}{\gamma}\mathcal{M}_1^2 << 1$, and the local efficiency η_L and polytropic efficiency η_p are both equal to the loading factor K. But as the pressure ratio p_3/p_o is increased, the generator efficiency becomes greater than K.

The situation is not nearly as favorable for large values of the Mach number; in Figure 14.30 the various efficiencies are shown for $1/2\ (\gamma-1)\mathcal{M}_1^2 = 1$. The polytropic efficiency is now much less than

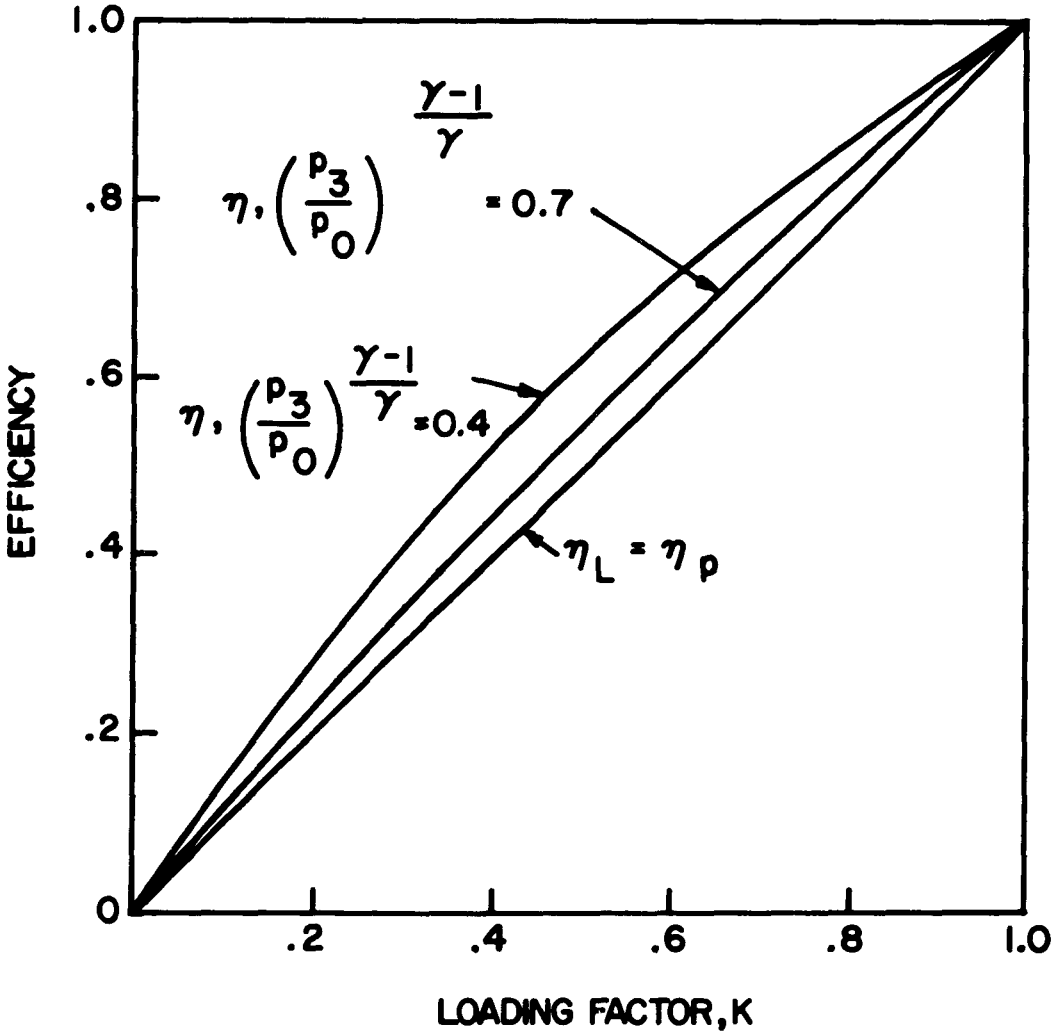

Figure 14.29. Frictionless Adiabatic Efficiency, Crossed-Field MHD Generator, Constant Velocity, $M_1 << 1$.

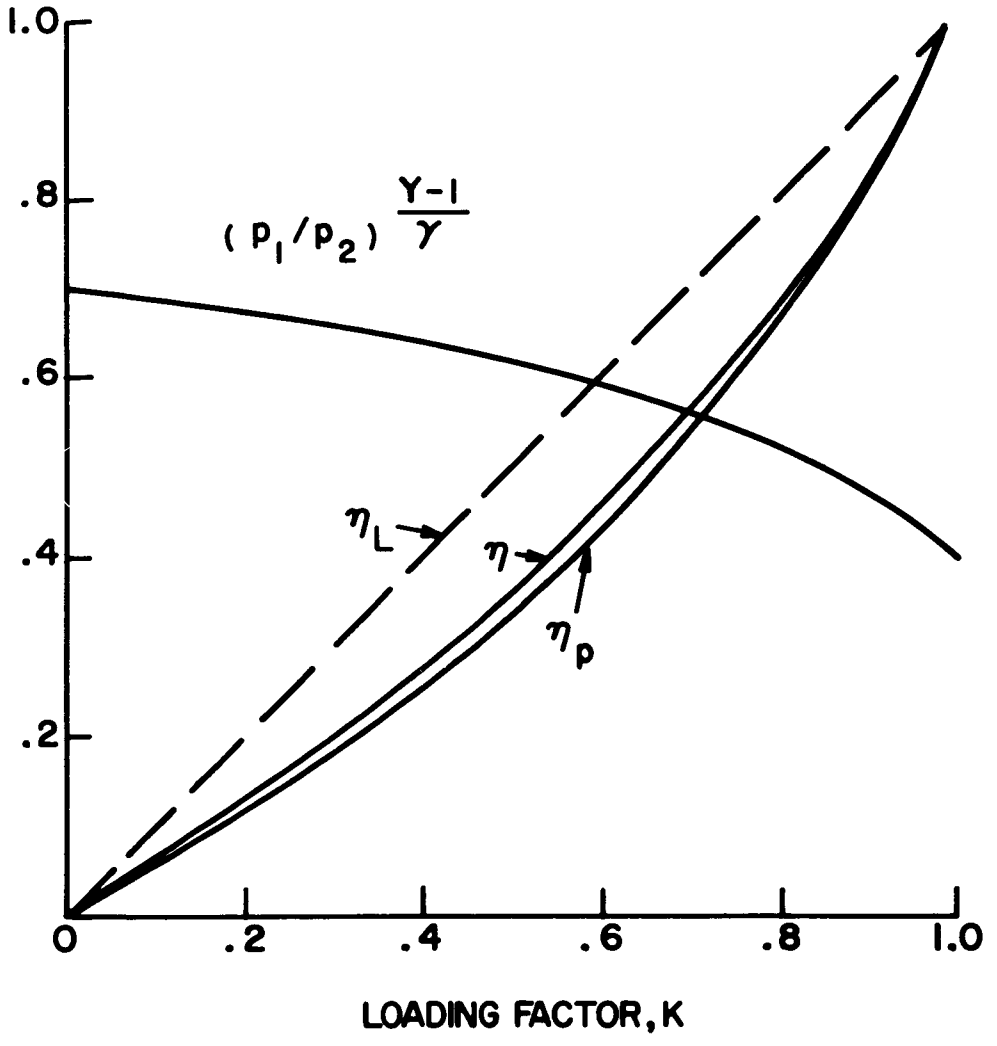

Figure 14.30. Frictionless Adiabatic Efficiency, Crossed-Field MHD Generator, Constant Velocity, $\frac{\gamma-1}{2} M_1^2 = 1$, $(P_3/P_o)^{\gamma-1/\gamma} = 0.7$

the loading factor; and the overall generator efficiency is only slightly better than the polytropic efficiency.

The variation of the cross-sectional area is obtained from the continuity equation; thus

$$\frac{A(x)}{A_1} = \frac{\rho_i}{\rho(x)} = \frac{p_1}{p(x)} \cdot \frac{T(x)}{T_1}$$

$$= \left[\frac{p(x)}{p_1}\right]^{\frac{K(\gamma-1)}{\gamma} - 1} \qquad (14.214)$$

Generally, the smaller the inlet Mach number and the larger the value of γ, the smaller the area increase.[19] For continuous electrodes, each of which is maintained at the same potential, the interelectrode spacing h must remain constant, since u and K are both constant. This means that all of the area increase must be in the direction of the magnetic field.

Another disadvantage of the constant velocity generator is that the local Mach number at the exit is higher than at the inlet, due to the decrease in static temperature. This increases the problem of pressure recovery in the exit diffusor, especially if the exit Mach number is near or greater than unity. For this reason it is desirable to consider other flows in which the exit Mach number is equal to, or less than, the inlet Mach number.

14.6b Constant Mach Number Generator

If the Mach number of the gas flow in the generator is kept constant, then as electrical power is extracted from the flow, both the gas velocity and static temperature of the gas will decrease. For this case, the momentum and energy equations become:

$$\rho u u' + p' = -(1 - K)\,\sigma_{eff_1}\, uB^2 \qquad (a)$$

$$\rho u \left(C_p T' + uu'\right) = -\sigma K (1 - K) \sigma_{eff_1} u^2 B^2 \tag{b}$$

where ' indicates $d/d\xi$. The local Mach number is defined as:

$$\mathcal{M}^2 = \frac{u^2}{\gamma RT} \tag{c}$$

Since the Mach number is taken constant, (c) may be differentiated with respect to x, which yields:

$$uu' = \frac{1}{2} \mathcal{M}^2 \gamma RT' \tag{d}$$

Substitution of (d) into (a) and (b); then division of (a) by (b), and rearrangement yields:

$$\frac{p'}{p} = \frac{T'}{T} \frac{\gamma}{K} \left[\frac{1}{\gamma - 1} + \frac{\mathcal{M}^2}{2} (1 - K)\right]$$

which can be immediately integrated to obtain the following first integral of (a, b):

$$\frac{p}{p'} = \left(\frac{T}{T_1}\right)^{\frac{\gamma}{\gamma - 1} \frac{1}{K}} \left[1 + \frac{1}{2} (1 - K) (\gamma - 1) \mathcal{M}^2\right] \tag{14.215}$$

Since the polytropic efficiency is given by:

$$\eta_p = \frac{K}{1 + \frac{1}{2} (1 - K) (\gamma - 1) \mathcal{M}^2},$$

then (14.215) can be rewritten simply as:

$$\frac{p}{p'} = \left(\frac{T}{T_1}\right)^{\frac{\gamma}{(\gamma-1)\,\eta_p}} \tag{14.216}$$

Since both the Mach number and loading factor K have been assumed constant for this generator, then η_p is also constant.

To obtain the variation of temperature or pressure in the direction of flow, (14.216) is substituted into (a) and integrated, which yields:

$$\frac{1 + \frac{1}{2}\,\eta_p\,(\gamma-1)\,\mathcal{M}^2}{1 - \frac{1}{2}\,\eta_p\,\frac{\gamma-1}{\gamma}} \left[1 - \left(\frac{T}{T_1}\right)^{\frac{\gamma}{(\gamma-1)}\,\eta_p - \frac{1}{2}}\right]$$

$$= \frac{(1-K)\,\sigma_{eff_1}\,B^2\,u_1\,\xi}{p_1} \tag{12.217}$$

Equation (14.217) gives the length in units of ξ; however, (a) can be integrated directly for the case of variable conductivity of the form given in (14.203), since the pressure can be expressed in terms of the temperature by means of (14.216).

Because the Mach number is constant, the stagnation temperature ratio is equal to the static temperature ratio. Thus, the overall adiabatic efficiency (neglecting friction) is given by the following expression:

$$\eta = \frac{1 - \left(\frac{p_3}{p_o}\right)^{\eta_p\,(\gamma-1)/\gamma}}{1 - \left(\frac{p_3}{p_o}\right)^{(\gamma-1)/\gamma}} \tag{14.218}$$

which is identical to that for the constant velocity generator when $\frac{1}{2}(\gamma - 1)\mathcal{M}^2 << 1$. In fact, for moderate pressure ratios the performance of the constant Mach number generator is identical to the constant velocity generator, even for low supersonic Mach numbers.

14.6c. Constant Temperature Generator

In the constant temperature linear MHD generator, all of the electrical energy is extracted from the kinetic energy of the flow. The maximum energy is extracted when the exhaust velocity is very small; the fraction of energy removed from the gas is then:

$$\frac{T_o - T_1}{T_o} = \frac{\frac{\gamma - 1}{2}\mathcal{M}_1^2}{1 + \frac{\gamma - 1}{2}\mathcal{M}_1^2} \qquad \text{(a)}$$

Thus, to obtain an appreciable energy extraction from the flow, the flow Mach number at the inlet should be greater than unity, depending on the value of γ. The constant temperature generator has, however, the advantage that the exit Mach number is always less than the inlet Mach number, thus reducing the diffusor losses. In fact, the theory indicates a throatless transition from supersonic to subsonic flow may be possible, although this has not yet been proven.

The quasi one-dimensional equations for constant temperature flow are:

Momentum

$$\frac{p}{RT} uu' + p' = -\sigma_{eff}(1 - K) uB^2 \qquad \text{(a)}$$

Energy

$$\frac{p}{RT} uu' = -\sigma_{eff} K(1 - K) uB^2 \qquad \text{(b)}$$

Subtraction of (b) from (a) yields:

$$p' = -\sigma_{eff}(1-K)^2 uB^2, \tag{c}$$

then division of (b) by (c) yields:

$$\frac{pu}{RT}\frac{du/dx}{dp/dx} = \frac{K}{1-K} \tag{d}$$

which may then be integrated to obtain the first integral by noting that $(du/dx)/(dp/dx) = (du/dp)$. The result is

$$\frac{p}{p_1} = e^{-\frac{1-K}{2KRT_1}(u_1^2 - u^2)} \tag{14.219}$$

To determine the variation of velocity with ξ, the energy equation (b) may be integrated by use of $\rho = p/RT_1$, and substitution of (14.219). The resulting expression is

$$\left[\frac{2\gamma}{K(1-K)}\right]^{\frac{1}{2}} \mathcal{M}_1 \exp\left[(K-1)\gamma\mathcal{M}_1^2/2K\right] \int_{\frac{1-K}{2K}\gamma\mathcal{M}_2^2}^{\frac{1-K}{2K}\gamma\mathcal{M}_1^2} e^{+\zeta^2}\, d\zeta$$

$$= (1-K)\sigma_{eff} u_1 B^2 \xi/p_1 \tag{14.220}$$

If the electrical conductivity varies in a manner given by (14.203), the integration may be easily performed to obtain the variation of the velocity with the physical length.[25]

The adiabatic efficiency is given by

$$\eta = \frac{\frac{u_1^2}{2} - \frac{u_2^2}{2}}{C_p(T_o - T_3')} = \frac{\frac{\gamma-1}{2}\mathcal{M}_1^2}{1 + \frac{\gamma-1}{2}\mathcal{M}_1^2} \cdot \frac{1 - (u_2^2/u_1^2)}{1 - (p_3/p_o)^{\gamma-1/\gamma}} \tag{14.221}$$

Now the stagnation pressure ratio is given by:

$$\frac{p_3}{p_o} = \frac{p_3}{p_2} \cdot \frac{p_2}{p_1} \cdot \frac{p_1}{p_o} \tag{e}$$

The first and last factors in (e) are given by the isentropic relations, so that (e) becomes

$$\frac{p_3}{p_o} = \frac{p_2}{p_1} \left(\frac{1 + \frac{\gamma-1}{2}\mathcal{M}_2^2}{1 + \frac{\gamma-1}{2}\mathcal{M}_1^2} \right)^{\frac{\gamma}{\gamma-1}} \tag{f}$$

Use of (14.219) for p_2/p_1 and $\mathcal{M}_2^2 = (u_2^2/u_1^2)\mathcal{M}_1^2$ in (f), the stagnation pressure ratio is given by:

$$\frac{p_3}{p_o} = e^{-\frac{(1-K)}{2K}\gamma\mathcal{M}_1^2\left(1 - \frac{u_2^2}{u_1^2}\right)} \left(\frac{1 + \frac{\gamma-1}{2}\mathcal{M}_1^2 \frac{u_2^2}{u_1^2}}{1 + \frac{\gamma-1}{2}\mathcal{M}_1^2} \right)^{\frac{\gamma}{\gamma-1}} \tag{14.222}$$

Thus, with the inlet Mach number and stagnation pressure ratio chosen, (14.222) is used to obtain the velocity ratio u_2/u_1, which is then substituted into (14.221) to obtain the efficiency. Figure 14.31 shows the results of such a calculation, for

$$(p_3/p_o)^{\frac{\gamma-1}{\gamma}} = 0.5 \text{ and } \frac{1}{2}(\gamma-1)\mathcal{M}_1^2 = 1,$$

so that the isentropic velocity ratio, u_2/u_1 for K = 1, is zero according to (14.222). Note that the efficiencies are quite close to K.

The variation of efficiency for K = 0.9 with stagnation pressure ratio is shown in Figure 14.32. It may be seen that large pressure ratios decrease the efficiency markedly. This is due to the high inlet Mach number associated with large pressure ratios, which causes a large decrease in the polytropic efficiency. Thus, the constant temperature magnetohydrodynamic generator is not suitable for very large pressure ratios.

14.6d Constant Pressure Generator

As can be seen from the temperature-entropy diagram, Figure 14.28, if the local static pressure is kept constant, the local static temperature will increase. Thus, only a part of the initial kinetic energy is converted into electrical energy; the remainder is converted back into thermal energy of the gas. This may be of some advantage if the gas is thermally ionized since the electrical conductivity will increase in the downstream direction. Also, by converting the kinetic energy back into thermal energy, the generator acts as a diffusor.

For this generator, the momentum and energy equations become respectively:

$$\rho uu' = -\sigma_{eff}(1-K)uB^2 \qquad \text{(a)}$$

$$\rho(C_p T' + uu') = -\sigma_{eff}K(1-K)uB^2 \qquad \text{(b)}$$

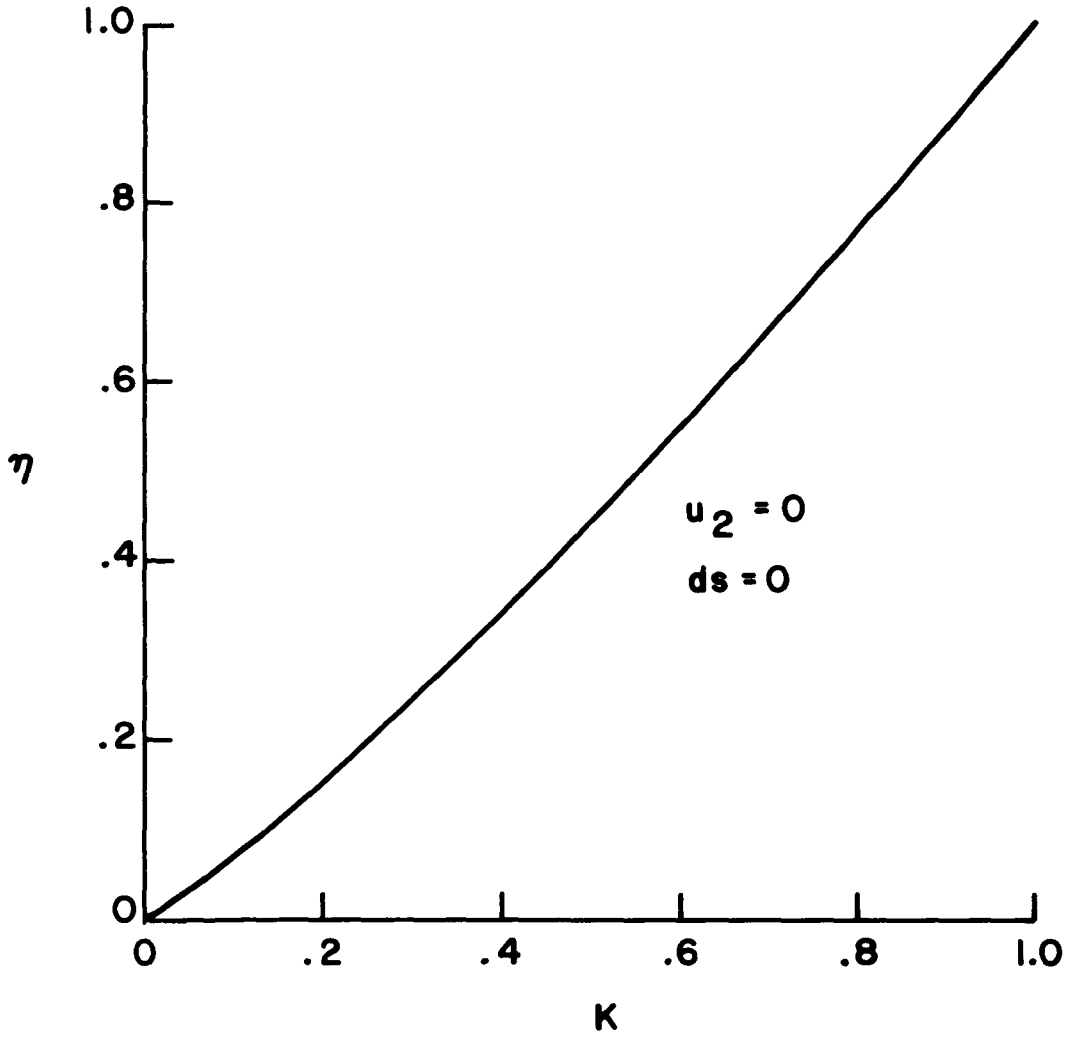

Figure 14.31. Variation of Generator Efficiency with Loading Factor, Constant Temperature Generator, For $(p_3/p_1)^{\gamma-1/\gamma} = 0.5$, $1/2\ (\gamma-1)\ M_1^2 = 1$.

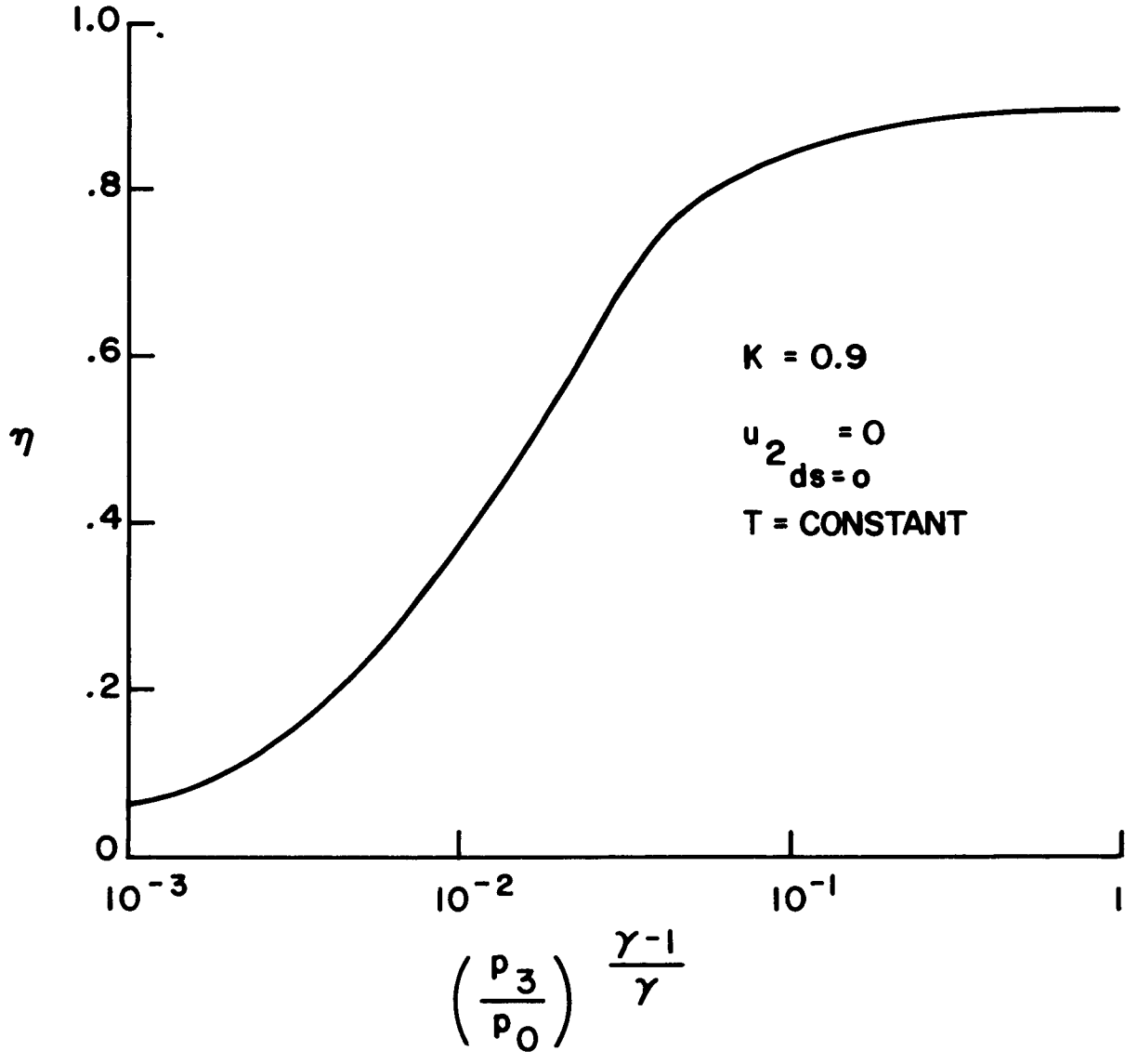

Figure 14.32. Variation of Constant Temperature Generator Efficiency with Pressure Ratio for K = 0.9.

Subtraction of (a) from (b) yields:

$$\rho C_p T' = \sigma_{eff} (1-K)^2 uB^2 \qquad \text{(c)}$$

and division of (a) by (c) yields:

$$\frac{u\, du/dx}{C_p dT/dx} = -\frac{1}{1-K} \qquad \text{(d)}$$

which may be integrated immediately to obtain the following first integral:

$$\frac{1}{2}(u^2 - u_1^2) = -(1-K)^{-1} C_p (T - T_1) \qquad (14.223)$$

To obtain the variation of velocity with distance, use the perfect gas law to eliminate the density from equation (c), and then eliminate temperature with the use of (14.223), as follows:

$$\frac{d(u/u_1)}{m^2 - \left(\frac{u}{u_1}\right)^2} = -\frac{(\gamma-1)}{2\gamma p_1} \sigma_{eff_1} (1-K)^2 B^2 u_1 \, d\xi \qquad \text{(e)}$$

where:

$$m^2 = 1 + \frac{2}{(1-K)(\gamma-1)\mathcal{M}_1^2}$$

Integration of (e) then yields:

$$\frac{1}{m}\left\{\tanh^{-1}\frac{1}{m} - \tanh^{-1}\frac{u/u_1}{m}\right\} = -\frac{(\gamma-1)}{2\gamma p_1} \sigma_{eff_1} (1-K)^2 u_1 \xi$$

(14.224)

The physical length can also be obtained for variable electrical conductivity by expressing (e) in terms of temperature instead of velocity, since the conductivity will also depend only on temperature because the pressure is constant.[25] The adiabatic efficiency (neglecting friction) is given by:

$$\eta = \frac{T_o - T_3}{T_o - T_3'} = \frac{1 - \frac{T_3}{T_o}}{1 - \left(\frac{p_3}{p_o}\right)^{\frac{\gamma-1}{\gamma}}} \tag{f}$$

Now,

$$\frac{p_3}{p_o} = \frac{p_3}{p_2} \cdot \frac{p_1}{p_o} = \left(\frac{1 + \frac{\gamma-1}{2}\mathcal{M}_2^2}{1 + \frac{\gamma-1}{2}\mathcal{M}_1^2}\right)^{\frac{\gamma}{\gamma-1}}, \tag{g}$$

since $p_1 = p_2$. Rearrangement of (g) yields $\mathcal{M}_2$ in terms of the stagnation pressure tatio:

$$\mathcal{M}_2^2 = \frac{\left(\frac{p_3}{p_o}\right)^{\frac{\gamma-1}{\gamma}} \left(1 + \frac{\gamma-1}{2}\mathcal{M}_1^2\right) - 1}{\frac{1}{2}(\gamma - 1)} \tag{h}$$

The temperature ratio can be expressed in terms of the Mach number as follows:

$$\frac{T_3}{T_o} = \frac{T_3}{T_2}\,\frac{T_2}{T_1}\,\frac{T_1}{T_o} = \frac{1 + \frac{\gamma-1}{2}\mathcal{M}_2^2}{1 + \frac{\gamma-1}{2}\mathcal{M}_1^2} \cdot \frac{T_2}{T_1} \tag{i}$$

From (14.223),

$$\frac{T_2}{T_1} = 1 + \frac{(1-K)(\gamma-1)}{2}\mathcal{M}_1^2\left(1 - \frac{\mathcal{M}_2^2}{\mathcal{M}_1^2}\frac{T_2}{T_1}\right) \tag{j}$$

Equation (j) may be solved for T_2/T_1 as follows:

$$\frac{T_2}{T_1} = \frac{1 + \frac{(1-K)(\gamma-1)}{2}\mathcal{M}_1^2}{1 + \frac{(1-K)(\gamma-1)}{2}\mathcal{M}_2^2} \tag{k}$$

Substitution of (k) into (i), and substitution of $\mathcal{M}_2^2$ from (h) yields:

$$\frac{T_3}{T_o} = \left(\frac{p_3}{p_o}\right)^{\frac{\gamma-1}{\gamma}} \frac{1 + (1-K)\frac{\gamma-1}{2}\mathcal{M}_1^2}{K + (1-K)\left[1 + \frac{\gamma-1}{2}\mathcal{M}_1^2\right]\left(\frac{p_3}{p_o}\right)^{\frac{\gamma-1}{\gamma}}} \tag{14.225}$$

Substitution of (14.225) into f yields the desired expression for efficiency, in terms of $\mathcal{M}_1$, γ, K, and the stagnation pressure ratio p_3/p_o.

14.6e Constant Cross-Sectional Area

For the purposes of performing experiments on magnetohydrodynamic electrical power generation, the most convenient channel configuration is a straight, rectangular duct of constant width and height, and hence constant area. The performance will then depend on whether the electrodes are continuous or segmented. If continuous, the voltage difference between the two electrodes will be constant, and hence the electric field will be a constant. This causes

the loading factor K to vary along the length of the generator, so that the local conversion efficiency varies. In fact, it is possible to have one part of the duct acting as a generator while some other part is acting as an accelerator.

On the other hand, if the electrodes are segmented, then the voltage difference between pairs of electrodes need not be constant, and can be made proportional to the local velocity by setting the ratio of the external load resistance per unit length to the internal resistance of the generator per unit length equal to some constant.

For either configuration, the flow Mach number tends toward $\mathcal{M} \approx 1$. If the flow was initially subsonic, the temperature decreases while the velocity increases. Thus, additional thermal energy is converted into kinetic energy which is not recoverable in the generator. If the flow was initially supersonic, the velocity will decrease and temperature will increase, so that some thermal energy cannot be converted. For these reasons, the constant cross-sectional area generator does not appear to be practical. In fact, in multiple stage gas or steam turbines the flow cross-sectional area is always increased in the downstream direction in order to limit the axial velocity. It is found that for all of the previous cases in this chapter, the cross-sectional area increases in the downstream direction also. However, because the constant cross section generator is simpler to design and construct than the others, the theory is included here.

The basic equations are:

Conservation:

$$\rho u = \rho_1 u_1 \tag{a}$$

Momentum

$$\rho u \frac{du}{dx} + \frac{dp}{dx} = \sigma_{eff} B (E - uB) \tag{b}$$

Energy

$$\rho u \frac{d}{dx}\left[C_p T + \frac{1}{2} u^2\right] = \sigma_{eff} E (E - uB) \qquad (c)$$

where E is the constant transverse electric field, taken equal to its value at the inlet. It is convenient to reference this value of the electric field to the inlet velocity u_1 as follows:

$$E = K_1 u_1 B$$

Thus K_1 is a constant for the generator. This definition is different than the one used in previous sections, where the electric field was referenced to the local velocity. It is also convenient to let $C_p T = \left[\gamma/(\gamma-1)\right] (p/\rho)$, and to make the equations non-dimensional by letting

$$\left.\begin{aligned} U &= u/u_1 \\ P &= p/\rho_1 u_1^2 \\ X &= x/h \\ I &= \frac{\sigma_{eff} B^2 h}{\rho_1 u_1} \end{aligned}\right\} \qquad (d)$$

Then equations (b, c) become:

$$\frac{dU}{dX} + \frac{dP}{dX} = I (K_1 - U) \qquad (14.226)$$

$$\frac{d}{dX}\left[\frac{\gamma}{\gamma - 1} PU + \frac{1}{2} U^2\right] = K_1 I(K_1 - U) \qquad (14.227)$$

Equations (14.226, 14.227) have been integrated[26,27] by first eliminating I(K - U) between them:

$$\frac{d}{dX}\left[\frac{\gamma}{\gamma-1}PU+\frac{1}{2}U^2\right]=K_1\frac{dU}{dX}+\frac{dP}{dX}K_1$$

This is integrated immediately as follows:

$$\frac{\gamma}{\gamma-1}PU+\frac{1}{2}U^2=K_1U+PK_1+\text{constant} \qquad \text{(e)}$$

At the inlet, U = 1, and $P = P_1/\rho_1 u_1^2 = (\gamma M_1^2)^{-1}$; which allows the constant in (e) to be evaluated. Rearrangement of (e) then yields the following first integral:

$$P=\frac{\frac{1}{2}U^2-K_1U+\left[1+\frac{1}{\gamma M_1^2}\right]K_1-\left[\frac{1}{2}+\frac{1}{(\gamma-1)M_1^2}\right]}{K_1-\frac{\gamma}{\gamma-1}U} \qquad (14.228)$$

To obtain the variation of velocity with distance, the left side of (14.227) is expanded, and (14.226) and (14.228) are used to eliminate (dP/dX) and P, respectively. Rearrangement yields:

$$\left\{\frac{K_1}{1-\frac{U}{K_1}}-\frac{K_1}{1-\frac{\gamma}{\gamma-1}\frac{U}{K_1}}+\frac{\gamma}{\gamma-1}\left[\frac{(\gamma-1)^2(\delta-\frac{K_1}{2})}{1-\frac{U}{K_1}}\right.\right.$$

$$\left.\left.+\frac{\delta+(\gamma-1)^2\left[\frac{K_1}{2}-\delta\right]-\frac{U}{2}-\gamma^2\left[\frac{1}{2}-\frac{\delta}{K_1}\right]U}{\left[1-\left(\frac{\gamma}{\gamma-1}\right)\frac{U}{K_1}\right]^2}\right]\right\}\frac{dU}{dX}=K_1^2 I \qquad \text{(f)}$$

where:

$$\delta = 1 + \frac{1}{\gamma \mathcal{M}_1^2} - \left[\frac{1}{2} + \frac{1}{(\gamma-1)\mathcal{M}_1^2}\right] K_1^{-1} \qquad \text{(g)}$$

If the effective conductivity is assumed to be constant, then the interaction parameter I is also constant, and (f) can be integrated to become:

$$\left\{-K^2 + \frac{\gamma(\gamma-1)}{2} K^2 - \gamma(\gamma-1) K\delta\right\} \ell n \left[\frac{1 - \frac{U}{K_1}}{1 - \frac{1}{K_1}}\right]$$

$$+ \left\{-K_1^2 \frac{(\gamma-1)^2}{2\gamma} (\gamma+1) + K_1 \delta \gamma(\gamma-1)\right\} \ell n \left[\frac{1 - \frac{\gamma}{\gamma-1} \cdot \frac{U}{K_1}}{1 - \frac{\gamma}{(\gamma-1)K_1}}\right]$$

$$+ \frac{\left[\frac{\gamma^2}{\gamma-1}\delta - \frac{K_1}{2}(\gamma+1)\right]\left[U-1\right]}{\left[1 + \frac{\gamma}{\gamma-1} \cdot \frac{U}{K_1}\right]\left[1 - \frac{\gamma}{(\gamma-1)K_1}\right]} = K_1^2 \, IX \qquad (14.229)$$

The length required to reach $\mathcal{M}_2 = 1$ has been calculated in reference 27 and is shown in Figure 14.33. It is seen that the higher the initial load factor K_1 or the lower the inlet Mach number, the longer the generator length.

Also, high loading factors or low inlet Mach number lead to the largest electrical energy extraction from the flow, as is shown in Figure 14.34. On the other hand, the largest average power density is obtained when $K_1 \approx 0.5$, for any subsonic inlet Mach number.[27]

For the second case, in which segmented electrodes are used so that the local transverse electric field is a fixed fraction of the local value of uB, the corresponding first integral is given by:[20]

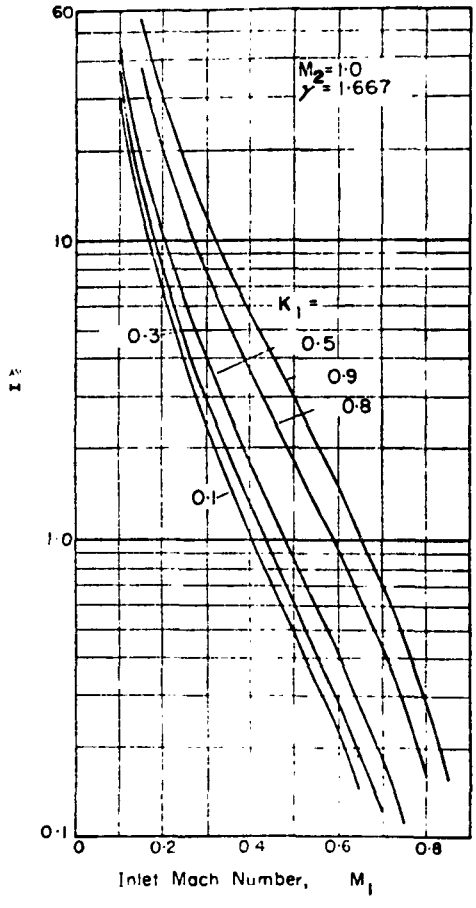

Figure 14.33. Length to Reach Mach 1·0 at Outlet (From Ref. 27)

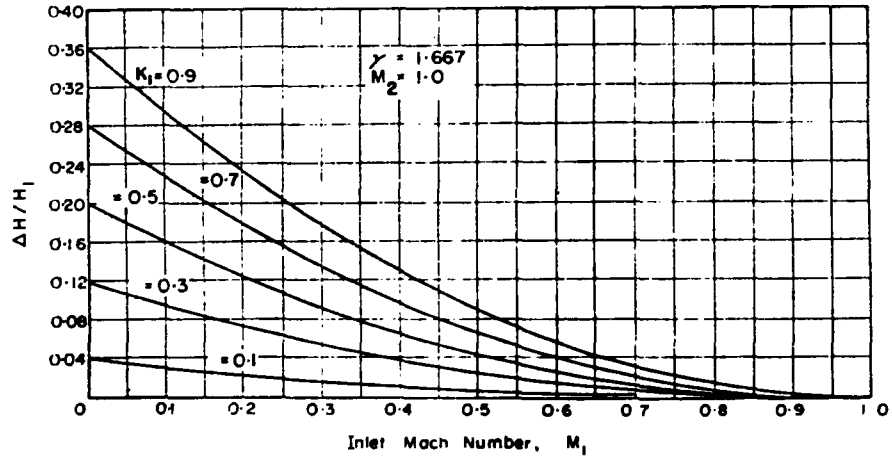

Figure 14.34. Energy Extraction as a Function of Inlet Mach Number (From Ref. 27)

$$\frac{p}{p_1} = \gamma \mathcal{M}_1^2 \left\{ \frac{K-1}{\frac{2\gamma}{\gamma-1} - K} \left(\frac{u}{u_1}\right) + \left[\frac{1}{\gamma \mathcal{M}_1^2} + \frac{1-K}{\frac{2\gamma}{\gamma-1} - K}\right] \left(\frac{u}{u_1}\right)^{-\frac{1}{1-\frac{K(\gamma-1)}{\gamma}}} \right\} \quad (14.230)$$

and the variation with length is given by:

$$\frac{(1-K)\,\sigma_{eff_1} B^2 \xi}{\rho_1 u_1} = \frac{2\gamma - (\gamma-1)}{2\gamma - K(\gamma-1)} \ln \frac{u}{u_1} + \frac{\gamma}{2\gamma - K(\gamma-1)} \left[\frac{1}{\gamma \mathcal{M}_1^2} + \frac{1-K}{\frac{2\gamma}{\gamma-1} - K} \left(1 - \frac{u_1}{u}\right)^{\frac{2\gamma - K(\gamma-1)}{\gamma - K(\gamma-1)}} \right] \quad (14.231)$$

14.7 ALTERNATING CURRENT POWER GENERATION

For many applications it is desirable to have the output power of the MHD generator as alternating current rather than direct current; in addition, if ac induction generators could be made, the electrode problem would be eliminated. However, there are two problems associated with induction generators: first, it appears that they would have a poor power factor; and second, if the power factor could be increased, the power density in the generator would be reduced.

The first effect, of poor power factor, can be estimated from the following simple argument: The simplest method of generating ac power is to alternate the imposed magnetic field at some frequency f. Now the magnetic field energy per unit volume is $B^2/2\mu_o$; thus, the rate of circulation of magnetic field energy per unit volume, P_B, is:

$$P_B \approx \frac{fB^2}{2\mu_o} \tag{a}$$

while the generated electrical power per unit volume is approximately:

$$P \approx \frac{\sigma u^2 B^2}{2} K(1-K) \tag{b}$$

Thus, the ratio of the circulating magnetic field power to the generated power is

$$\frac{P_B}{P} \approx \frac{f}{\mu_o \sigma u^2 K(1-K)} \tag{c}$$

Next, a characteristic length L may be defined as the distance the gas will move during one period:

$$L = \frac{u}{f} \tag{d}$$

so that (c) becomes:

$$\frac{P_B}{P} = \frac{1}{K(1-K)\,\mu_o\, u\sigma\, L} = \frac{1}{K(1-K)\,R_m} \qquad \text{(e)}$$

where R_m is the magnetic Reynolds number. This ratio may be estimated with some typical values: With σ = 100 Mho/Meter, u = 10^3 M/sec, and f = 60 cycles/sec, $R_m \simeq 2$. The maximum value of K(1 - K) is 0.25. Thus, the ratio of circulating magnetic power to generated power is about 2, which means that the power factor is poor. In addition, the circuit used for circulating the current for the magnetic field must have a low ohmic resistance; otherwise this circuit will consume all of the generated power.

14.7a Induction MHD Generator

The electrodeless induction-type MHD generator operates by means of a traveling, alternating magnetic field, which induces currents in the gas. In turn, this induced current creates an induced magnetic field which cuts the field windings of the magnet. If the gas velocity is greater than the velocity of the traveling magnetic field, the induced currents will be in such a direction that the Lorentz force retards the flow; and in addition, there will be power output from the field windings.

A very simplified analysis of the induction generator to illustrate its performance, see Figure 14.35, more detailed analyses have been made. It is assumed that the generator channel is infinite in the y-direction. The field coils are also in the y-direction, and are so excited that the z-component of the magnetic field is approximately sinusoidal and moving in the downstream direction x with velocity u_B. The gas is assumed to have a constant scalar conductivity, to be incompressible, and moving in the downstream direction with constant velocity u. Also, it is assumed that the induced current loops close at $y = \pm \infty$. In practice, this may be accomplished by the use of an annular geometry.

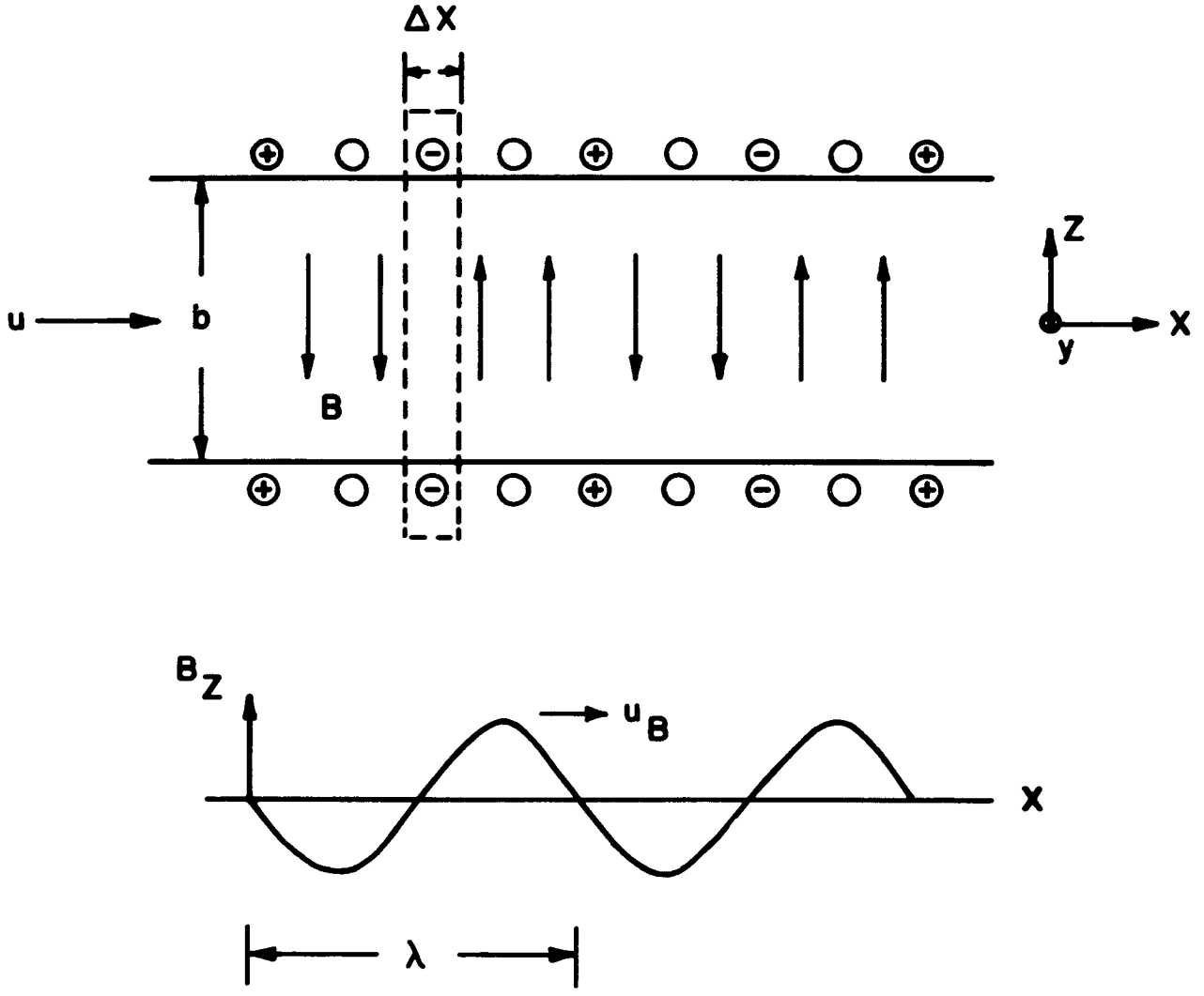

Figure 14.35. Schematic Diagram of Travelling Magnetic Field Induction Generator

In the absence of a conducting fluid in the generator, the imposed magnetic field B_o is given by:

$$B_{z_o} = \text{Re}\, B_o^* \; e^{\frac{i2\pi}{\lambda}(x - u_B t)} \tag{a}$$

where λ is the wavelength of the magnetic field. In the presence of a conducting fluid there will also be an induced magnetic field B_{z_i}, caused by the currents in the fluid which may be represented by:

$$B_{z_i} = \text{Re}\, B_i^* \; e^{\frac{i2\pi}{\lambda}(x - u_B t)} \tag{b}$$

such that

$$\nabla \times \underset{\sim}{B}_i = \mu_o \underset{\sim}{j}_i \tag{c}$$

where $\underset{\sim}{j}_i$ is the induced current in the fluid. It is assumed that the variation of the magnetic field is only in the x-direction, and the current is only in the y-direction. Then (c) becomes:

$$\frac{\partial B_{z_i}}{\partial x} = -\mu_o j_{y_i} \tag{d}$$

Use of (b) for B_{z_i} yields:

$$\frac{i2\pi}{\lambda} B_{z_i} = -\mu_o j_{y_i} \tag{e}$$

The induced current may also be obtained from Ohms Law. First, the electric field in the y-direction is obtained from Maxwell's equation:

$$\frac{\partial E_y}{\partial x} = - \frac{\partial B_z}{\partial t} \tag{f}$$

Let

$$E_y = E_o^* \; e^{\frac{i2\pi}{\lambda}(x - u_B t)} \tag{g}$$

$$B_z = B_{z_o} + B_{z_i} = B_z^* \; e^{\frac{i2\pi}{\lambda}(x - u_B t)} \tag{h}$$

Substitution of (g), (h) into (f) yields:

$$E_y = u_B B_z \tag{i}$$

Ohms law then yields:

$$j_{y_i} = \sigma (E_y - uB_z)$$

$$= \sigma (u_B - u) B_z$$

$$= - (1 - S) \sigma u (B_{z_i} + B_{z_o}) \tag{j}$$

where S is the slip, $S = u_B/u$. Equating the two expressions for the induced current (e) and (j), one may solve for the induced magnetic field:

$$B_{z_i} = \frac{B_{z_o}}{\frac{i}{R_m} - 1} \tag{k}$$

where R_m is a magnetic Reynolds number defined by:

$$R_m = \mu_o \sigma u \lambda (1 - S)/2\pi \tag{l}$$

The total magnetic field is given by:

$$B_z = B_{z_i} + B_{z_o} = \frac{B_{z_o}}{1 + iR_m} \tag{m}$$

and, from (i):

$$E_y = \frac{u_B B_{z_o}}{1 + iR_m} \tag{n}$$

Now the current in the field windings may be related to B_{z_o} by means of Stokes theorem for the area enclosed by the dashed line in fig. 14.35:

$$\left[B_{z_o}(x) - B_{z_o}(x + \Delta x)\right] b = 2\mu_o J_y \Delta x \tag{o}$$

where J_y is the field current per unit length in the x-direction on each side of the generator. Equation (o) may be written as:

$$-\frac{\partial B_{z_o}}{\partial x} = \frac{2\mu_o J_y}{b} \tag{p}$$

Thus,

$$J_y = -\frac{i\,2\pi b}{2\mu_o \lambda} B_{z_o} \tag{r}$$

Now the complex power per unit length and width delivered to the upper or lower field windings is given by $P^* = \frac{1}{2} \tilde{E}_y J_y$, where $\tilde{E}_y$ is the complex conjugate of E_y. Thus, the total power per unit volume is:

$$P^* = \frac{1}{2} \tilde{E}_y J_y = \frac{\pi B_o^2 u_B \sigma}{\mu_o \lambda} \left[\frac{R_m - i}{1 + R_m^2} \right] \qquad (14.232)$$

where equations (n, r) have been used. The real power is given by the real part of (14.232) while the reactive power is given by the imaginery part of (14.232). Equation (14.232) thus clearly illustrates that the reactive power is larger than the actual power when $R_m < 1$. To increase the power factor, R_m must be increased, but then the power density will decrease for $R_m > 1$. Equation (14.232) may also be compared to the direct current generator by substitution of (l) for R_m in the numerator:

$$\text{Re } P^* = \frac{1}{2} \frac{S(1 - S) \sigma u^2 B_o^2}{1 + R_m^2}$$

Thus, the slip velocity S replaces the load factor K. The factor of $\frac{1}{2}$ is caused by the sinusoidal variation of power output, as is usually associated with alternating current power. Equation (14.232) clearly shows that increasing the magnetic Reynolds number will decrease the power density. However, it is unlikely that magnetic Reynolds numbers in excess of unity can be achieved, so that the main problem is the power factor. From (14.232), it is seen that the phase angle between the voltage and current is given by $\theta = \tan^{-1} R_m - 1$; more detailed analyses have verified this poor power factor.[28]

14.8 MHD POWER CYCLE ANALYSIS

In the previous sections, methods were presented for calculating the performance and efficiency of various magnetohydrodynamic electric power generators. These methods allow for the calculation of the decrease in total enthalpy in the generator, the pressure drop, and the equivalent turbine efficiency. In the present section, it is assumed that this performance can be calculated, and it is now desired to determine the overall efficiency of a generator system.

There are three general types of MHD generator systems. In the simplest system, liquid or solid fuel and liquid oxidizer are burned, seed added, and the resulting gas mixture passed through the generator with no further recovery of the remaining thermal energy or seed material in the exhaust gases. Such a system is feasible only for small or short duration generators. Since the amount of energy required to pump the liquid (or solid) fuel and oxidizer is small, all of the generated electrical power is available for the load except that required to energize the magnet, if it is an electromagnet. This system will be discussed further in section 14.8a.

For the generation of bulk power, fossil fuel must be used for economic reasons, and the oxidizer must be air, although some enrichment with additional oxygen may be possible. In order for the combustion temperature to be high enough for thermal ionization, preheating of the incoming air is necessary. The exhaust temperature of the gas from the generator is determined by the decrease in the ionization of the gas; but because combustion gases must be thermally ionized, the exhaust temperature is still very high. For economic operation further extraction of this energy is necessary, which may be accomplished by using the exhaust gases to generate steam power. These systems are described further in Section 14.8b.

Finally, the gas which passes through the generator may be in a completely closed cycle; that is, the gas (or vapor) is heated in a heat exchanger, expanded through a nozzle, passed through the generator, cooled, and

recompressed (or pumped) back through the heat exchanger. For such a cycle, the maximum temperature of the gas is set by the allowable working temperature of the materials in the heat exchanger. At the present state of development of refractory materials, it is highly unlikely that sufficiently high temperatures can be sustained over long periods of time to permit thermal ionization; thus, some form of non-thermal ionization is necessary.

At present, the main use for such closed cycles appears to be for vehicle power. The most interesting potential application for such cycles is for the generation of electrical power in space where the heat rejction must be by radiation. This is described in Section 14.8.c.

14.8a Simple Open Cycle

In the simple open cycle fuel and oxidizer, without preheating, are burned, and "seed" material is added. The combustion products are accelerated by a nozzle and passed into the generator and exhausted into the atmosphere. Since seeded combustion gases are not sufficiently conducting below about $4000^{o}F$ at a pressure of one atmosphere, the flame temperature must exceed $4000^{o}F$ in order to extract any electrical power. Since the temperature of most flames with air is below $4000^{o}F$, it is necessary to use either pure oxygen or a chemical oxidizer. Even if pure oxygen is used the flame temperature with ordinary hydrocarbons is not especially high due to dissociation of the products of combustion, see Table 14.4.

The overall efficiency for this type open cycle generator can be expressed in terms of the enthalpy difference between the flame temperature and ambient:

$$\eta_t = \frac{\text{Net work/unit mass of gas}}{H_o - h_a}$$

where H_o is the total enthalpy of the products of combustion at the combustor pressure, and h_a is the sensible enthalpy of the same gas if cooled to ambient

pressure and temperature. The net work is the difference between the generator inlet total enthalpy and the exit total enthalpy, less any heat transfer, and power for auxiliary equipment. Thus,

$$\eta_t = \frac{H_o - h_2 - u_2^2/2 - Q - P_{aux}}{H_o - h_a}$$

The thermal efficiency is therefore limited by the minimum temperature T_{min} at which there is sufficient ionization, and by the exhaust velocity. If the exhaust velocity is reduced by adjusting the cross-sectional area, then additional energy can be extracted from the gas before T_{min} is reached; however, decreasing the gas velocity generally increases the generator length. For this reason, it is desirable to use the higher flame temperatures.

TABLE 14.4. FLAME TEMPERATURES OF FUELS BURNED WITH LIQUID OXYGEN AT 20 ATM. PRESSURE

Fuel	Flame Temperature, ^oF
*Ethyl Alcohol	5250
*Kerosene	5570
*Hydrogen	~ 5400
*Methane	5040
Cyanogen	~ 8200

*From Rocket Propulsion Elements by G. P. Sutton, 2nd Edition, John Wiley and Sons, Inc., 1956, N. Y.

Also listed in Table 14.4 is the flame temperature with Cyanogen, C_2N_2. The high flame temperature results not so much from a larger heat of combustion, but from the fact that the products of combustion do not dissociate as in hydrocarbon flames; that is:

$$C_2N_2 + O_2 \longrightarrow 2\,CO + N_2$$

Detailed calculations of the performance of an oxy-cyanogen generator[22] indicate that over 36% of the input chemical energy can be converted into terminal power. This is to be compared to about 15% for hydrocarbon fuels. With an initial total pressure of one atmosphere, K = 0.5, $\mathcal{M}_1 = 0.9$, and segmented electrodes, only 10 cm. of length is required to obtain the overall efficiency. The magnetic field was 2 webers/M^2 at the inlet and 0.45 at the exit. Because of this short length, it is necessary to have a small cross-sectional area in order to have quasi-one dimensional flow. For an inlet area of 1 cm^2, the exit area is 63 cm^2, and the total generated power was 10.87 kilowatt. No magnet power was required because it was assumed that the magnetic field was supplied by a permanent magnet. For larger total powers, larger inlet cross sections are required, and the length must be increased, but this can be easily accomplished by reducing the magnetic field.

In these calculations, it was assumed that the seed material was 10% pure cesium. Because of the high cost of cesium, this system is attractive only for small units and short duty cycles. A cheaper source of cesium is pollucite ore which contains 27% cesium. Certain potassium compounds such as the hydroxide or carbonate are also relatively inexpensive. The halides are generally not as suitable for seed materials due to the formation of negative chlorine atoms which decrease the electron density.

(i) Magnet Power

A fraction of the output power may be used to energize an electromagnetic, instead of using a permanent magnet. To determine the conditions which must be met for self-energizing the field coil, we may examine the equation for the field current to the electromagnet, I:

$$L \frac{dI}{dt} + IR = huB \qquad (a)$$

where R is the sum of the internal and external resistance. If it is assumed that the magnet power is obtained from some fraction α of the total length of generator ℓ, then

$$R \approx \frac{h}{\sigma b \alpha \ell} + \frac{2N\ell}{\sigma_W A_W} \tag{b}$$

where σ and σ_W are the gas and wire electrical conductivities, respectively, N is the number of turns of the field coil, h is the transverse distance between electrodes, and b is the transverse distance in the direction of the magnetic field, see Figure 14.36.

The magnetic field for an air core and iron core magnets are given by respectively:

Air Core

$$B \approx \frac{\mu_o N I}{\mathcal{L}} \tag{c}$$

Iron Core

$$B \approx \frac{\mu_o N I}{b'} \tag{d}$$

where $\mathcal{L}$ is the average length of the flux path for the air core magnet, and b' is the iron magnet gap. Combining (a - d), it is seen that the requirement for self-exitation which is $dI/dt > 0$, becomes:

Air Core

$$\frac{\mathcal{L}}{\sigma \mu_o u b \ell \alpha N} + \frac{2\ell \mathcal{L}}{\sigma_W \mu_o A_W u h} < 1 \tag{e}$$

Iron Core

$$\frac{b'}{\sigma \mu_o u b \ell \alpha N} + \frac{2\ell b'}{\sigma_W \mu_o A_W u h} < 1 \tag{f}$$

AIR CORE MAGNET

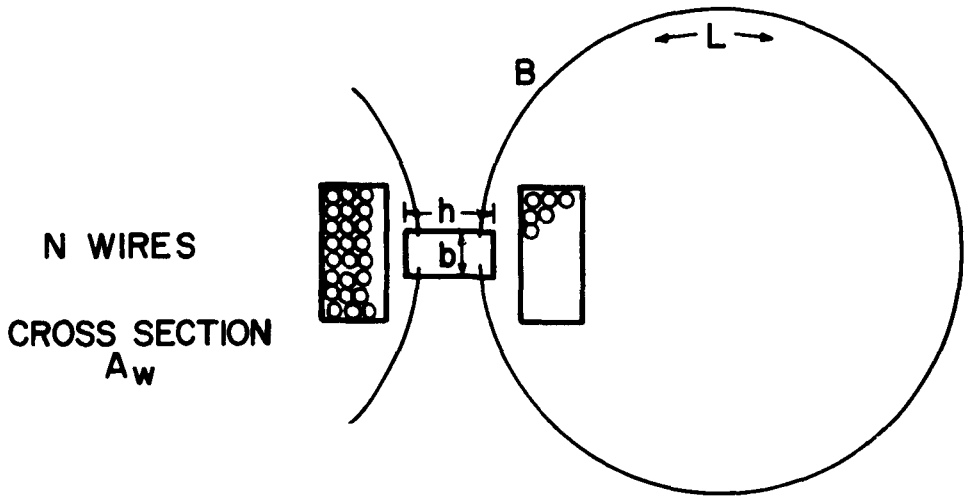

IRON CORE MAGNET

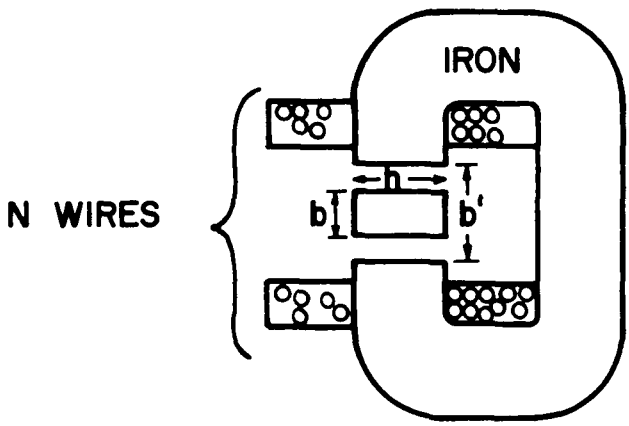

Figure 14. 36. Schematic Diagram for Magnet Analysis

Let us consider the air core magnet first. Equation (e) may be written as

$$\frac{1}{R_m'} + \frac{1}{R_m''} < 1 \qquad (g)$$

where R_m' and R_m'' are modified magnetic Reynolds numbers defined by:*

$$R_m' = (\sigma \mu_o u \ell)(\alpha N)(b/\mathcal{L}) \qquad (h)$$

$$R_m'' = \left(\frac{\sigma_W \mu_o u A_W}{2\ell}\right)\left(\frac{h}{\mathcal{L}}\right) \qquad (i)$$

Now, the value of the desired magnetic field affects both (h and i), because increasing the magnetic field decreases the length of the generator. It is easily shown that the left side of (g) is a minimum with respect to ℓ when $R_m' = R_m''$. Equating (i), (h) and solving for ℓ, one obtains

$$\ell = \sqrt{\frac{\sigma_W A_W h}{2\alpha N b}} \qquad (j)$$

while from (g),

$$R_m' > 2 \qquad (k)$$

Substitution of (h, j) into (k), and rearrangement yields:

Air Core

$$A_W N > \frac{4}{\sigma_W \sigma \mu_o^2 u^2 \alpha \left(\frac{b}{\mathcal{L}}\right)\left(\frac{h}{\mathcal{L}}\right)} \qquad (l)$$

*It is assumed that ion slip is negligible, and that the electrodes are segmented.

The left side of (l) is just the total cross-sectional area of the wire, bh is just the average cross-sectional area of the channel, while $\mathcal{L}^2$ is the average area enclosed by the magnetic flux path. The larger the cross-sectional area of the channel, the larger $\mathcal{L}^2$ will be. Hence, the ratio $(bh/\mathcal{L}^2)$ is approximately a constant, and is independent of the cross-sectional area of the generator.

We may next determine the effect of generator size on the required total cross section of wire, for a given gas velocity, and fraction of power directed to the magnet α. Since the right side of (l) is a constant, independent of cross-sectional area, the total cross section of wire is also constant. Thus, the dimensions of the field windings are independent of the generator power output, e.g., generator cross-sectional area. Thus, air-core magnets favor large generators. For example, let $\sigma_W = 10^8$ Mhos/M; $u = 10^3$M/sec, $\alpha = 10^{-1}$, $(bh/\mathcal{L}^2) = 10^{-2}$. For hydrocarbon-oxygen flames, $\sigma \approx 30$ Mho/M, and (l) predicts a minimum wire cross section of 0.8 Meters^2. This large cross-sectional area of wire makes it impractical to build generators with small duct cross-sectional areas. For example, if we set an arbitrary limit that the cross-sectional area of the generator duct must be at least $(0.01\ A_W N$, then the minimum duct cross-sectional area is 80 cm^2.

On the other hand, if cyanogen-oxygen is used, with a conductivity of about ten times larger, the minimum wire cross-sectional area is about 800 cm^2, which makes it possible to have a minimum duct area of about 8 cm^2.

A similar analysis can be made for iron core magnets. Then (l) is replaced by

$$A_W N > \frac{b'^2}{\sigma_W \sigma \mu_o^2 u^2 \alpha\ bh} \qquad \text{(m)}$$

The minimum wire cross-sectional area is now much smaller, since, for $b \sim h$, b' is only slightly larger than b; let us assume that $b' = 2b = 2h$, then the minimum wire area is reduced from the previous example by a factor of 25, which becomes 320 cm^2 for hydrocarbons, and 32 cm^2 for cyanogen. The cross-sectional area of the iron, on the other hand, is directly proportional to the generator cross-sectional area, except for very small sizes in which case sufficient space must be allowed for the field coil windings. Thus, the weight of an iron core magnet is approximately directly proportional to the generator output, except for very small sizes. This is in contrast to the cross section of the wire, which is almost independent of generator size.

(ii) Wall Losses

The two principal wall losses are skin friction and heat transfer. Skin friction increases the required pressure ratio across the generator. If the fuel and oxidizer are both liquid, the increased pressure ratio does not appreciably affect the net power output because the pumping energy for liquids is small. On the other hand, if the increased pressure ratio is obtained by increasing the inlet pressure, then for thermal ionization, the electrical conductivity will decrease and the generator length will increase.

The other major wall loss is heat transfer, if it is necessary to cool the walls. Heat removal reduces the enthalpy available for conversion into electricity before reaching the minimum temperature at which the gas is sufficiently ionized.

14.8b Open Cycle with Recovery

The previous open cycle is clearly unsuited for economic operation for three reasons: the seed material is not recovered; chemical oxidizers are expensive; and finally, the thermal energy of the exhaust gases is not recovered. For the economic generation of power, for example bulk power, these three problems must be considered.

The cheapest available oxidizer is obviously air, although power is required to compress it to the required combustion pressure. In addition, common fossil fuels must be used if the fuel cost is to be minimized. Now, it is impossible to burn fossil fuels, such as natural gas, oil, or coal, and achieve sufficiently high combustion temperatures to ionize the seed material. Hence, preheating of the inlet air is required to increase the combustion temperature; that is, a regenerative cycle is required,[29] see Figures 14.37, 14.38.

To design such a cycle it is first necessary to select the generator exhaust velocity u_2, exhaust stagnation pressure p_3 and exhaust temperature T_2. The exhaust pressure should be high enough to allow the gas to pass through the regenerator and any other heat-recovery equipment. The exhaust static temperature should be high enough so that there is sufficient thermal ionization of the seed material. From the Mollier diagram for the combustion products and seed material, and the diffusor losses, T_3 may be determined next. It is not necessary to select the allowable temperature drop $\Delta T = T_3 - T_7$ through the regenerator. The smaller the value of ΔT, the larger will be the physical size of the regenerator and vice versa. From the formulas of Section 14.6, the generator may be designed, but since the combustion pressure has not yet been selected, this must be done parametrically for various combustion pressures, p_o'. The results may be plotted as line 0' - 3.

Next, for an air preheat temperature T_7, the flame temperature, including the seed material, may be calculated for various values of the combustion pressure p_o'. Some typical calculations are shown in Figure 14.39.

The calculated combustion temperatures may be plotted as T_o'' as a function of p_o'. The intersection of the 0' line and the 0'' line gives the desired combustion temperature and pressure. The compressor pressure p_6 is then selected, allowing for the required pressure drop through the cold side of the regenerator. From standard compressor formulas, T_6 is then calculated with T_5, p_5 selected at ambient. Finally, the regenerator hot-side exhaust temperature is calculated from:

$$\dot{m}_6 (h_7 - h_6) = \dot{m}_3 (h_3 - h_4)$$

The difference between $\dot{m}_3$ and $\dot{m}_6$ is the mass flow rate of fuel plus seed material

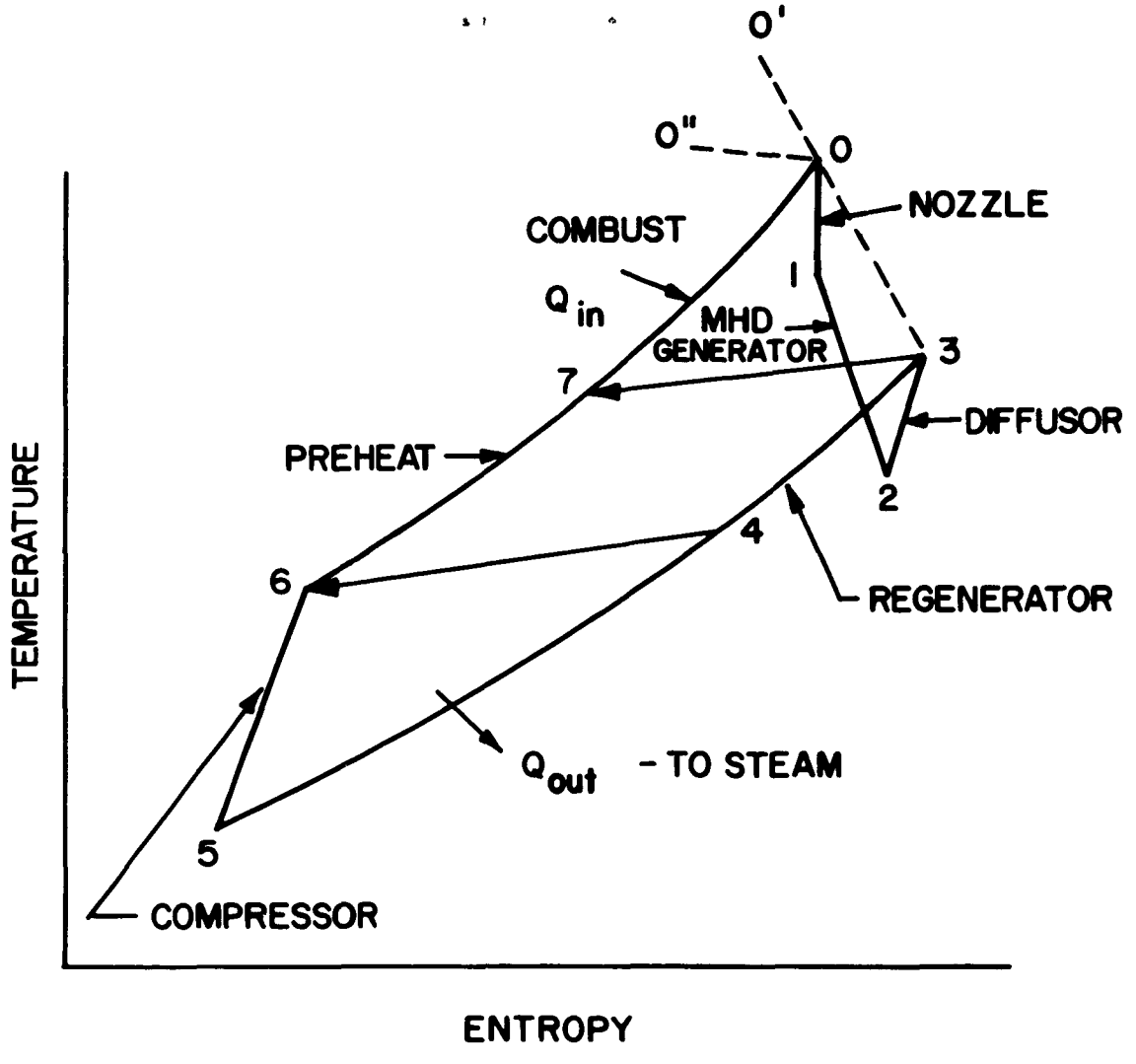

Figure 14.37. Regenerative Cycle, Temperature - Entropy Diagram

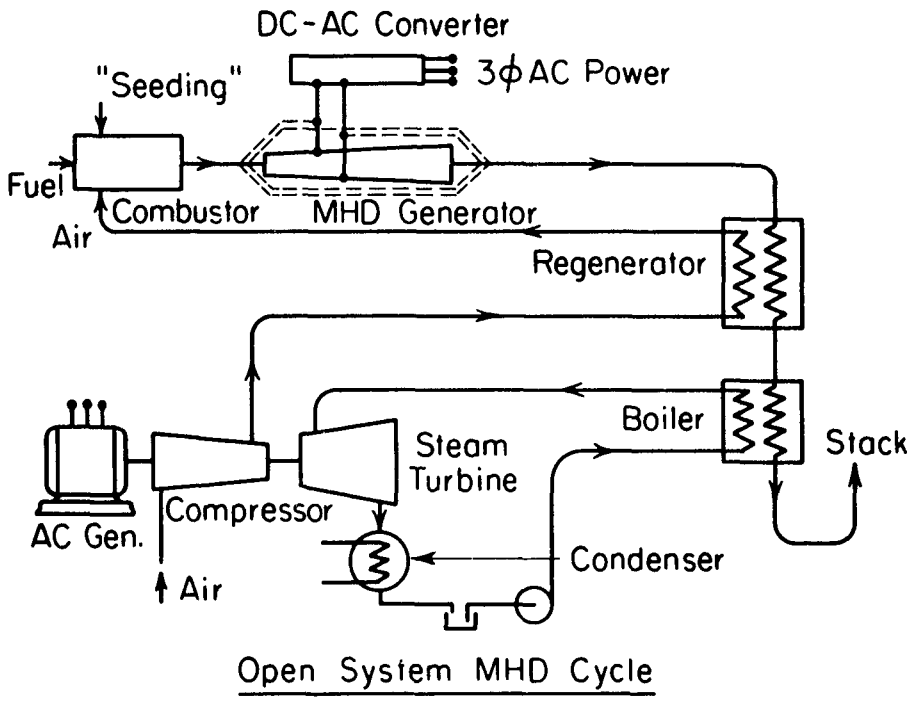

Figure 14.38. Regenerative Cycle, Flow Schematic (After S. Way)

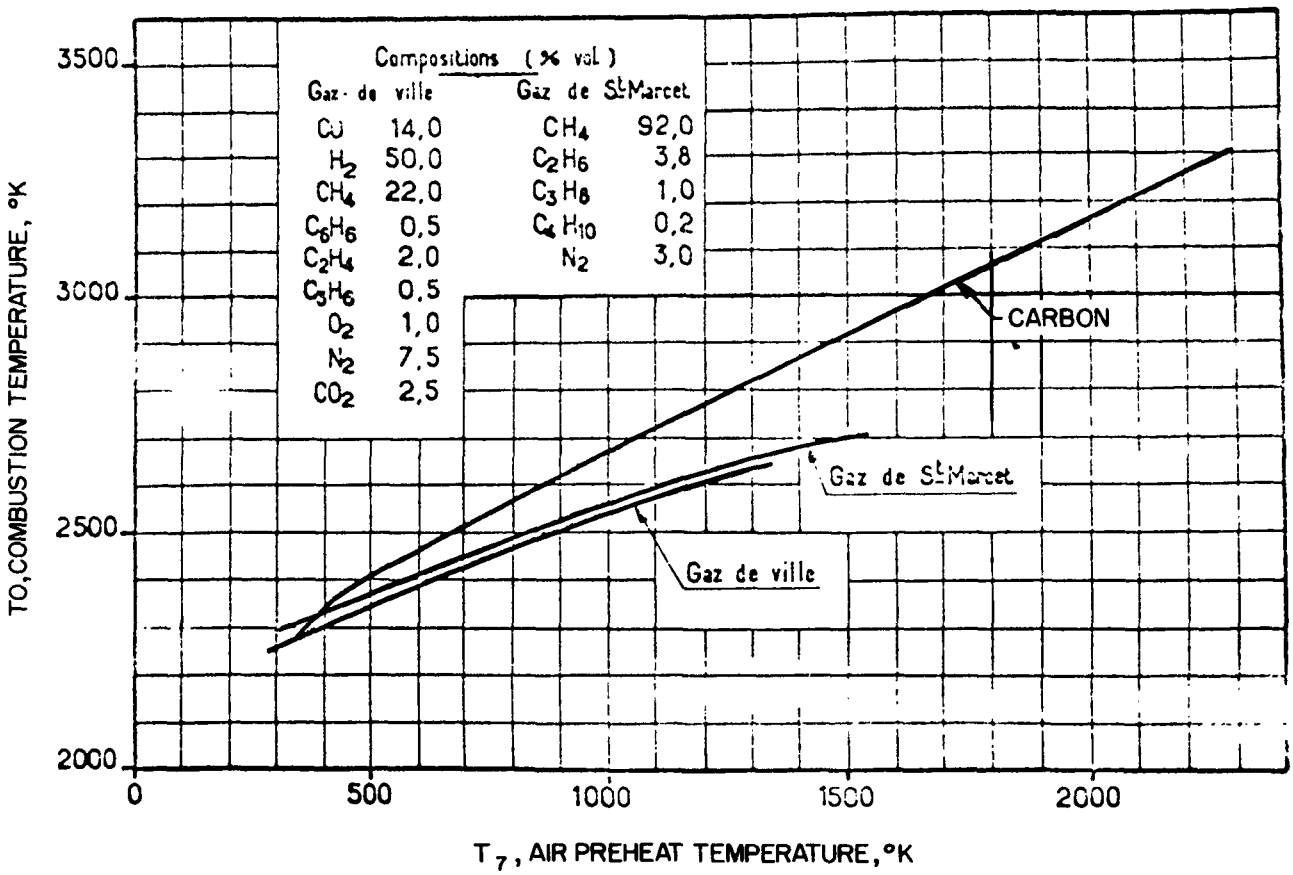

Figure 14.39. Dependence of Combustion Temperature on Air Preheat Temperature

Carbon - 9.7 atm. pressure, J. Fabre and J. Pericart, "Quelques études preliminaires en vue de la Génération Magnétohydrodynamique de l'energie Electrique", presented at Societe Hydrotechnique de France, 17 March 1961

Gases - 1.0 atm., G. Ribaud and N. Nauson, Applications des constantes et données thermodynamiques des mélanges gazeux aux températures élevées. Publications Scientifiques et Techniques du Ministére de l'air, No. 341 (1958)

Now, because the specific heat of combustion gas is larger than that for air, the regenerator hot-side exit temperature T_4 will normally be considerably higher than the regenerator cold-side inlet temperature, and additional energy can be recovered from the exhaust gases, by producing steam and using a steam turbine. It is possible to couple the turbine directly to the air compressor, and to use any remaining shaft power to generate electrical power. The net power output is then the direct current generated in the MHD generator, plus any remaining steam power, less the magnet power and auxiliary power. The dc power is essentially $\dot{m}_3 (h_o - h_3)$, less any energy lost by heat transfer. (It is possible, of course, to use the MHD generator coolant as the steam cycle feed water heater.) With these types of calculations, overall thermal efficiencies as high as 56% have been calculated.[29]

Several problems in the cycle are evident. First, for combustion products and about 1%molar potassium seeding, T_2 is about 4000°F, and the regenerator walls will then be close to this temperature. At the present time, economic materials which will withstand this temperature for long periods of time are not known (although some show promise for future development).[5] To reduce the regenerator surface temperature, several possibilities have been explored. First, T_7 can be reduced, which will help lower the regenerator surface temperature. However, this reduces the combustion temperature and the power generated in the MHD generator. An alternate to this is to cool the gases from temperature T_3 by use of a steam superheater, before passing the gas into the regenerator.[30] This also reduces the combustion temperature T_o.

A different solution is to reduce T_7, as explained above, but to obtain the same combustion temperature by enriching the inlet air with oxygen.[31] Although this alleviates the regenerator materials problems, for a given mass flow of combustion products, additional fuel is required to burn the additional oxygen, which reduces the thermal efficiency somewhat; in addition, additional investment in oxygen separation equipment, and additional auxiliary power is required.

A more novel remedy which has been suggested is to use molten ash as the regenerator,[32] which is similar in concept to the "rotating regenerator"

under development for gas turbines. The exhaust gases from the MHD generator are used to heat ash until molten; the molten ash is then sprayed through the compressed air in a counter flow arrangement. The ash solidifies as granules, and is mechanically recirculated to the exhaust gas heater.

A more practical method of reducing the regenerator temperature is to use pollucite as the seed, in order to utilize the lower ionization potential of cesium, and to use the higher field strengths that may become available through the development of high field superconductors. The latter also has the advantage that the magnetic field itself consumes no power; the only power consumed by the magnet system is that required to recondense liquid helium to keep the windings superconducting. With these two modifications, it has been estimated that a reduction in temperature of as much as 700°C can be expected.[33]

Figure 14.39 also shows that for a given amount of preheat, the combustion temperature varies with fuel. Although this is caused in part by the larger specific heat of the combustion products containing water vapor, it is important to select a fuel which yields the largest enthalpy change $h_3 - h_o$, for a given MHD generator exhaust temperature T_2 and preheat temperature T_7. In addition, the cost of the fuel should be considered. On these two bases, coal seems to be the best fuel for economic operation of an MHD generator. On the other hand, the high ash content of coal causes additional difficulties. Although it is possible to remove as much as 90% of the ash in a "cyclone" burner, the remaining ash becomes mixed with the seed material, which may be a potassium compound or pollucite. Since economic operation requires recovery of the seed material, this means that the 10% ash must be recovered as well, and recirculated. To keep the "seed" makeup at a minimum, scrubbers and electrostatic precipitators are required; but a more important problem is the large weight of ash that must be recirculated through the system in order to make use of the seed trapped in it. Way[34] has estimated that the ash recirculation is about one-third the weight of the coal being burned! Thus, the physical size of the scrubbers and precipitators becomes enormous. In addition, the molten ash will coat out on the inside of the generator and will quite likely short out the electrodes.

Also, ash will coat out on the regenerator. Thus, the problems of burning coal are quite difficult.

In addition to the problems caused by ash, there are two other important problems associated with continuously operated generators. First, the potassium attacks insulating materials and makes them conducting.[46] Second, the electrode materials - tungsten, carbon, or silicon carbide, are chemically eroded by combustion gases. This last problem might be solved by using consumable electrodes; that is, feed the electrodes continuously into the generator in a manner similar to that used in electric arc furnaces.[32]

The largest problem that is faced by large-scale, continuous generation of power by fossil fuel - MHD generators is economics. Although this system shows promise of increasing the overall thermal efficiency to as much as 56% as compared to 40% for conventional steam plants, the additional investment in the magnet, generator duct, compressors, regenerator, scrubbers, precipitators, dc to ac inverters if the ac is required, causes the plant cost of the generated electrical power to be essentially the same as that for present day steam plants.[30] For this reason, there is at present no major impetus to develop large fossil fuel MHD generator plants in the United States. However, in other countries such as Japan, England, and France, where the fuel cost is much higher, and capital cost is lower than the United States, there may be potential economic gain in the use of MHD power plants. For this reason, research on the development of fuel-burning MHD generators is being actively pursued in those countries.

If the cost of fossil fuel were to increase in the United States, then nuclear power would become economic rather than fossil fuel - MHD, primarily because of large successes in reducing the capital costs of nuclear plants in the United States.[30] On the other hand, the capital cost for nuclear plants in other countries has remained so high that even with higher fossil fuel costs, nuclear power is not economically competitive. This situation can of course be drastically altered by new innovations in technology.

14.8c Closed Nuclear - MHD Cycle for Space

A third possible application for MHD power generation is a closed cycle with a nuclear heat source. This appears to be especially attractive for the generation of electrical power in space, where the heat rejection must be by radiation, because the heat rejection per unit area varies as the fourth power of the surface temperature, and a high temperature cycle is required to minimize the radiator area. At present, high temperature nuclear reactors are under development; but the corresponding development of turbogenerators is difficult because of the combination of high operating temperatures, blade stresses in the turbine, and the corrosive properties of some high temperature working fluids, such as liquid metals. The advantage of the MHD generator is that the stress level is reduced drastically. On the other hand, it is not likely that the reactor temperature will be sufficiently high that thermal ionization of the working fluid in the MHD generator will be possible; thus, some form of non-thermal ionization will be required. Some other possibilities will be discussed later in this section.

(i) Optimum Heat Rejection Temperature

The radiator for a space nuclear closed cycle represents a major portion of the weight of such a generator system, and is also the largest component in terms of physical dimension, which is cumbersome for launch and also decreases the reliability of the system due to possible puncture by meteoritic dust. For this reason, it is desirable to minimize the radiator area. For a given output power and maximum cycle temperature T_o, the radiator area depends upon the reject temperature. If the reject temperature is set too close to the heat input temperature T_o, then the cycle overall thermal efficiency is too low, and the ratio of heat rejected to useful power is large. Since the radiator area is proportional to the total heat which must be rejected, the radiator area becomes large. On the other hand, if the reject temperature is set too low, then the cycle efficiency may be large, but since the heat rejection is proportional to the fourth power of the rejection temperature, the radiator area becomes

large again. Thus, there is an optimum rejection temperature for which the radiator area is a minimum. We will illustrate this optimum by considering a simplified Rankine (vapor) cycle.

Rankine Cycle

The Rankine cycle is extremely attractive for space applications because the heat rejection is at constant temperature, and the pumping power is small, see Figure 14.40. The top temperature in the cycle is T_o; the generator operates between 0 and 1; the working fluid is then condensed from 1 to 2 during which heat Q_{rej} per unit mass of working fluid is rejected from the space radiator. The liquid is then pumped from 2 to 3, and heat Q_{in} is added by the nuclear reactor from 3 to 0. It is assumed that there is no temperature drop through the walls of the radiator so that the radiator surface is also at temperature T_1. It is also assumed that there is no radiation interaction between parts of radiator, or with the spacecraft, and that the friction pressure drop is negligible.

Now the heat rejected is equal to the heat radiated, so that

$$\dot{m} Q_{rej} = \sigma \epsilon A T_1^4 \qquad \text{(a)}$$

where m is the mass flow rate of working fluid, σ is the Stefan-Boltzmann constant, ϵ is the total emissivity of the radiator surface (assumed constant), and A is the total radiator area. From the first law of thermodynamics, the total power P from the generator is given by:

$$P = \dot{m} (Q_{in} - Q_{rej}) \qquad \text{(b)}$$

and the overall thermal efficiency, η, is given by:

$$\eta = \frac{Q_{in} - Q_{rej}}{Q_{in}} \qquad \text{(c)}$$

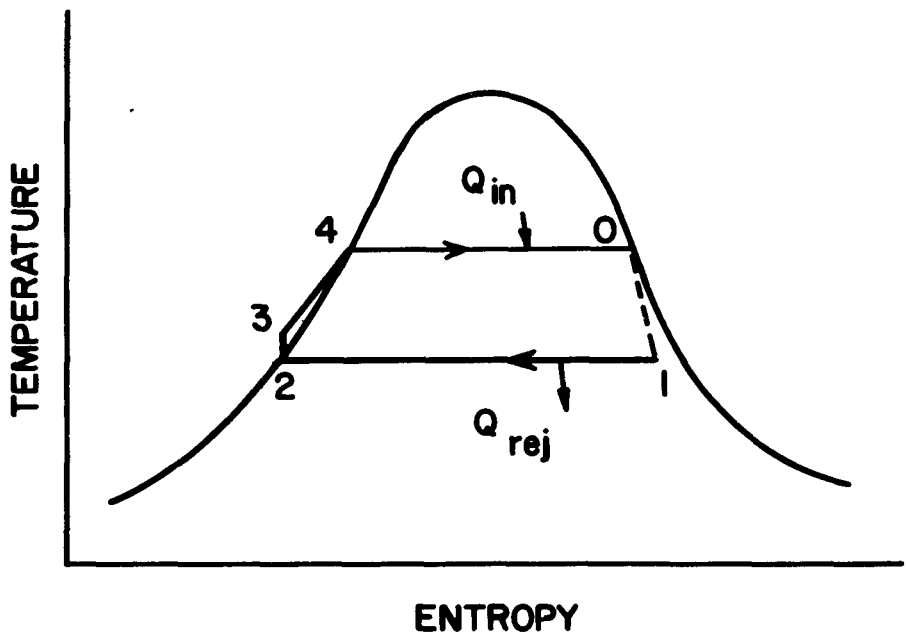

Figure 14.40. Rankine Cycle

From (b) and (c), $\dot{m}\, Q_{in}$ may be eliminated to yield:

$$\dot{m}\, Q_{rej} = \frac{P(1 - \eta)}{\eta} \tag{d}$$

Now the efficiency for a Rankine cycle may be expressed as a fraction η_c of the Carnot efficiency for a Carnot cycle operating between the same inlet and rejection temperatures, as follows:

$$\eta = \eta_c \left(\frac{T_o - T_1}{T_o} \right) \tag{e}$$

Substitution of (d, e) into (a) yields:

$$A^* = \frac{\sigma \epsilon T_o^{\,4} A}{P} = \frac{1 - \eta}{\eta} \left(1 - \frac{\eta}{\eta_c} \right)^{-4} \tag{14.233}$$

where A* is a non-dimensional area. For given values of ϵ, T_o, and the power level P, the radiator area is then proportional to A*, which is given by the right side of (14.233). It is seen that as the overall cycle efficiency becomes either zero or η_c, A* becomes infinitely large. To determine the minimum value of A*, (14.233) is differentiated and set equal to zero; the efficiency which then minimizes the radiator area is given by:

$$\eta = \frac{5 - \sqrt{25 - 16\,\eta_c}}{8} \tag{14.234}$$

and the optimum reject temperature is obtained from (e):

$$\frac{T_1}{T_o} = 1 - \frac{5 - \sqrt{25 - 16\,\eta_c}}{8\,\eta_c} \tag{14.235}$$

while the optimum value of A* is obtained from (14.233). These values are shown in Figure 14.41 as a function of the Carnot efficiency. The ratio (T_1/T_o) is a weak function of η_c, since it varies from 0.8 for η_c = 0 to 0.75 for $\eta_c = 1$. On the other hand, A* depends strongly on η_c. For typical Rankine cycles for space applications, $\eta_c \approx 0.65$, $\eta \approx 0.15$, and $(T_1/T_o) \approx 0.77$.

It is also possible to minimize the total weight of the entire space power system, by utilizing the specific weight of the radiator, nuclear reactor, and generator; such a study has also been made in reference 35. However, for large generator system, the optimum temperature is still between 0.75 and 0.8. At the present state of development of refractory materials, it appears that the upper temperature for Rankine cycles may be about 2500°R with a corresponding reject temperature of 1900°R. These temperatures require the use of a liquid metal, such as potassium or sodium for the working fluid, but are too low for thermal ionization even with the addition of cesium, so that some form of non-thermal ionization must be used. Calculations for magnetically induced ionization, however, indicate that this may be possible in potassium for relatively high field strengths, but low Mach numbers and total temperatures. A typical calculation is shown in Figure 14.42. Although this effect is not yet confirmed experimentally, the high power density makes magnetohydrodynamic generators with magnetically induced ionization extremely attractive for space power applications.

Brayton (Gas) Cycle

The Rankine cycle as described above has one main disadvantage: to operate at high temperatures, which is necessary to minimize the radiator size, liquid metals must be used as the working fluid which are quite corrosive. On the other hand, an inert gas such as helium, which could be used in a gas cycle, is not corrosive. Although the gas cycle has two disadvantages for space applications; namely, the heat rejection is at a continuously varying temperature, and a large compressor is required; nevertheless,

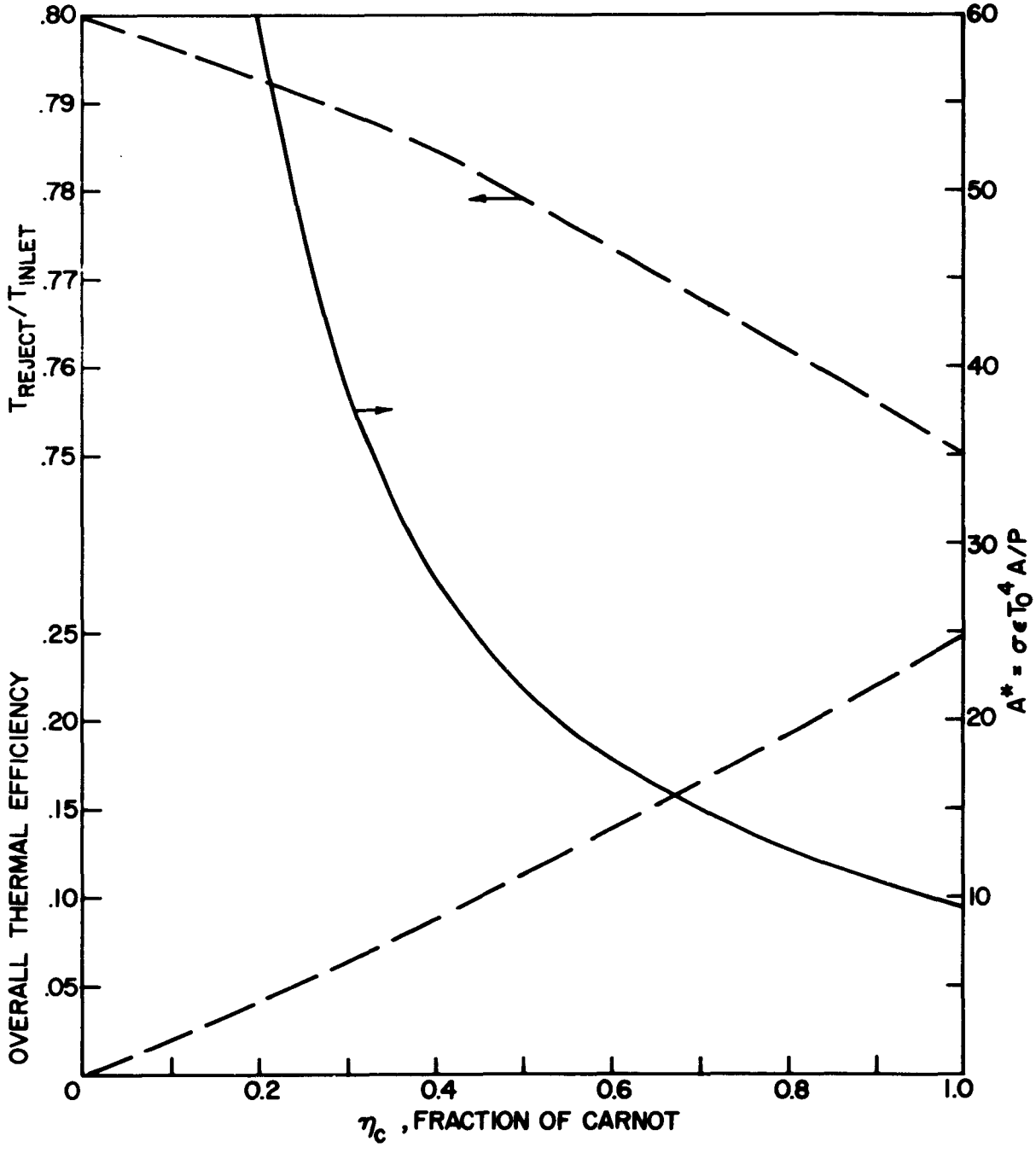

Figure 14.41. Optimum Temperature Ratio, Efficiency and Radiator Area For Rankine Cycles

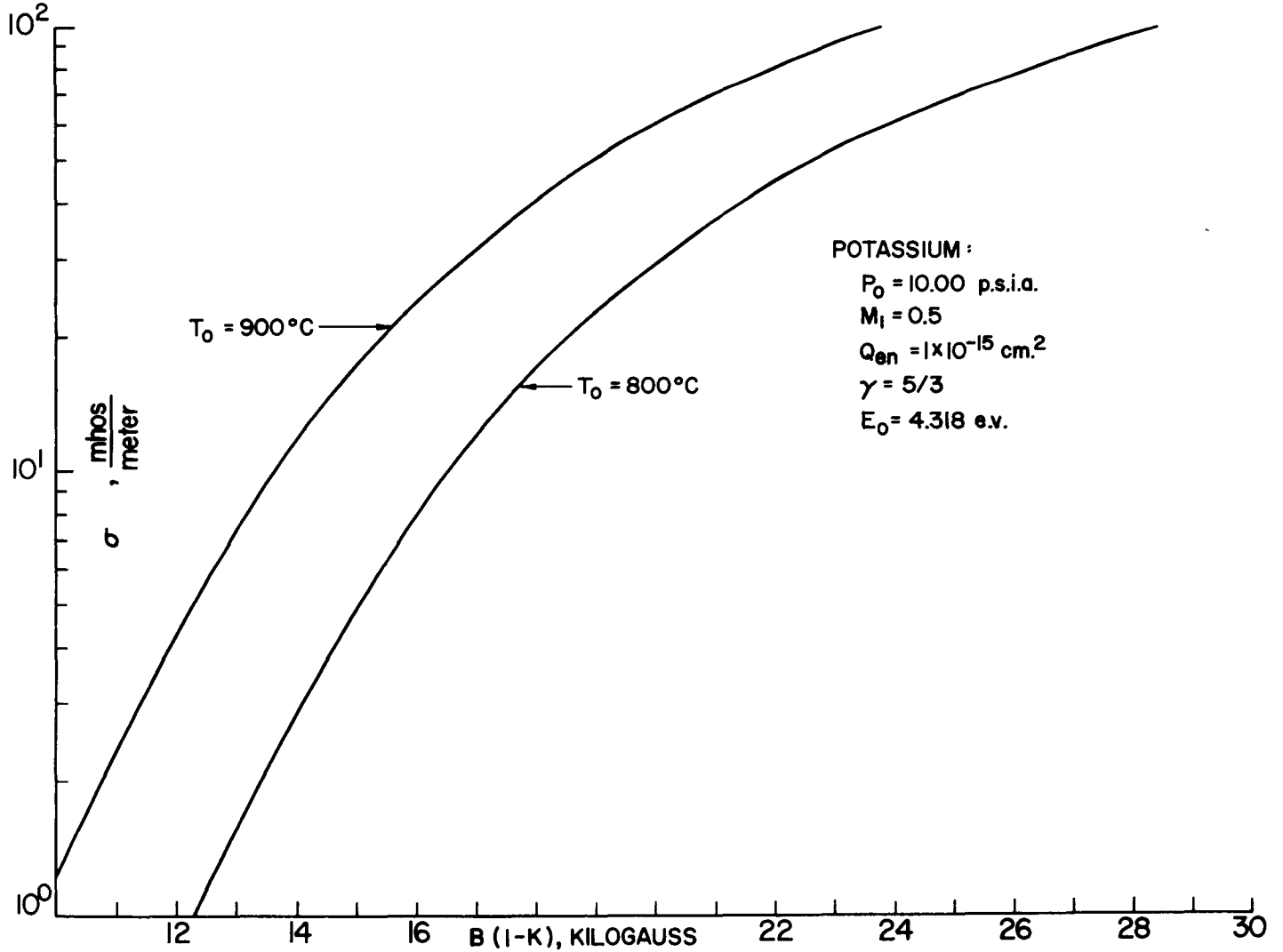

Figure 14.42. Theoretical Calculation of Conductivity for Magnetically Induced Ionization in Potassium Vapor (F. Shair, personal communication)

it is of interest to calculate the radiator area for such a cycle, and compare it to the Rankine cycle. The comparison can be made on two different bases: for the same top temperature T_o in the cycle, the radiator areas may be compared; or for the same radiator area, the top temperatures may be compared. For the gas cycles certain idealizations will be made, similar to those previously made in the Rankine cycle; namely zero temperature drop across the walls of the radiator, and zero friction pressure drop which is valid for high pressure operation. The cycle is shown in Figure 14.43; 0-3' - 4-5' is the ideal gas cycle, for isentropic compression (4-5') and generation (0-3'). More realistically, the compressor and generator are not isentropic and have an entropy increase, shown as 4-5 and 0-3, respectively.

Since the temperature of the working fluid in the radiator is constantly changing, we will write the radiator heat balance for a small amount of heat rejection dQ_{rej} which occurs between $T - \frac{1}{2}\Delta T$ and $T + \frac{1}{2}\Delta T$. The differential radiator area dA required is therefore given by:

$$\dot{m}\, dQ_{rej} = \sigma \epsilon T^4 dA \qquad (f)$$

At constant pressure, $dQ = C_p dT$; then integration of (f) yields:

$$\frac{\dot{m} C_p}{3} \left(\frac{1}{T_4^3} - \frac{1}{T_3^3} \right) = \sigma \epsilon A \qquad (g)$$

where the specific heat at constant pressure, C_p, has been taken constant. Now the total heat rejected per unit mass of gas is given by:

$$Q_{rej} = C_p (T_3 - T_4) \qquad (h)$$

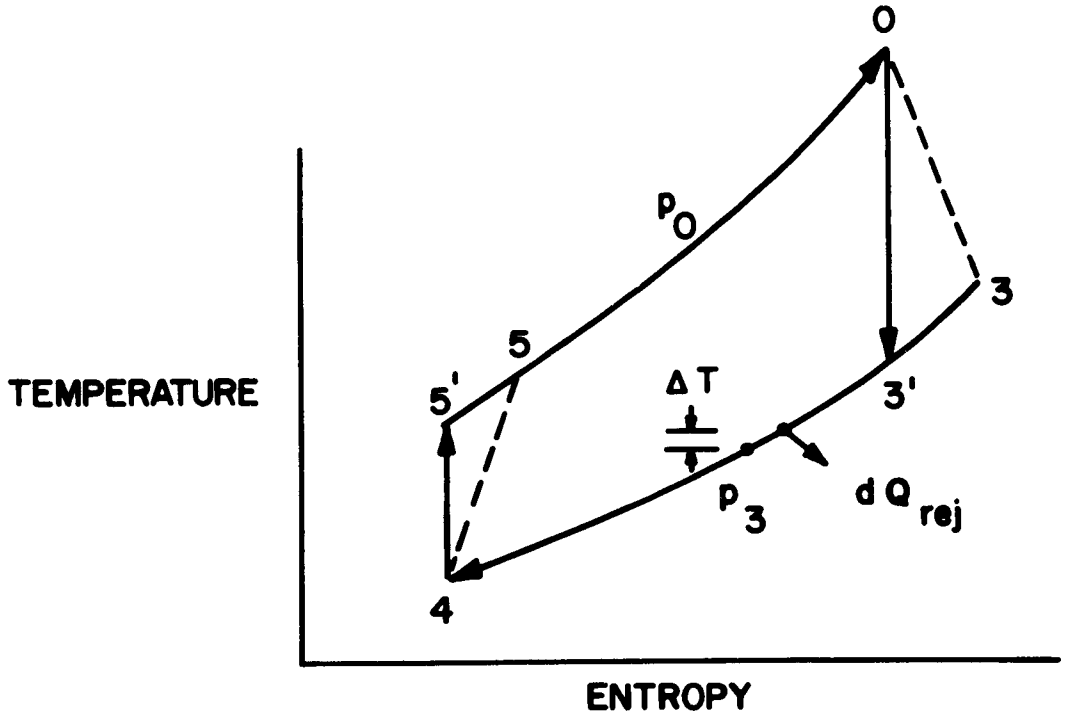

Figure 14.43. Gas Cycle

Use of (h, d) in (g) yields:

$$A^* \equiv \frac{\sigma \epsilon A T_o^4}{P} = \left(\frac{1-\eta}{\eta}\right)\left(\frac{T_o}{T_4}\right)^4 \frac{\left[1 - \left(\frac{T_4}{T_3}\right)^3\right]}{\left(\frac{T_3}{T_4} - 1\right)} \qquad (14.237)$$

where η is the overall thermal efficiency of the gas cycle, given by:

$$\eta = \frac{Q_{in} - Q_{rej}}{Q_{in}} = 1 - \frac{Q_{rej}}{Q_{in}} = 1 - \frac{T_3 - T_4}{T_o - T_5} \qquad (i)$$

If we let the compressor and generator adiabatic efficiencies be defined as:

$$\eta_c = \frac{T_5' - T_4}{T_5 - T_4} \qquad (j)$$

$$\eta_g = \frac{T_3 - T_o}{T_3' - T_o} \qquad (k)$$

where $T_o/T_3 = T_5/T_4$;
then it is easily shown that

$$\frac{T_5}{T_4} = 1 + \frac{1 - \frac{T_3}{T_o}}{\eta_c\left(\eta_g - 1 + \frac{T_3}{T_o}\right)} \qquad (l)$$

so that (14.237) becomes:

$$A^* = \frac{\left(\frac{T_o}{T_4}\right)^4 \left[1 - \left(\frac{T_4}{T_3}\right)^3\right]}{3\left\{\frac{T_3}{T_4} - \frac{T_o}{T_4} + \frac{1 - \frac{T_3}{T_4}}{\eta_c\left(\eta_g - 1 + \frac{T_3}{T_o}\right)}\right\}} \qquad (14.238)$$

From (14.238) it is seen that for a given value of T_o, the radiator area depends on two temperatures, T_3 and T_4, in contrast to the Rankine cycle, in which the area depended only on the condensor temperature. The determination of the minimum radiator area is therefore more complicated. The usual procedure used to determine the minimum radiator area is to simply compute the area for various values of (T_3/T_o) and (T_4/T_o) and locate the minimum in this manner.[36] The results of such a calculation are shown in Table 14.5, for two different compressor and generator efficiencies. Note that the non-dimensional radiator area, A*, is very sensitive to these efficiencies, and is much larger than the corresponding values for a Rankine cycle. Note also that the values of (T_3/T_o) are 0.75, which is similar to the result for an ideal Rankine cycle, while the heat rejection starts at T_3 and decreases to T_4. It is this large change in heat rejection temperature which is responsible for the large radiator area. The low values of T_4/T_o are required to obtain net power output; for an ideal gas cycle, then the minimization yields $T_4 \approx T_3$; but when the component efficiencies are less than unity, it is necessary that $T_4 < T_3$ in order to obtain net power.

TABLE 14.5. BRAYTON CYCLE FOR SPACE POWER

	(a) $\eta_c = \eta_g = 0.8$	(b) $\eta_c = \eta_g = 0.85$
A^*_4	145	84
η	0.15	0.15
T_3/T_o	0.75	0.75
T_4/T_o	0.3	0.375
T_4/T_3	0.4	0.5
T_5/T_4	1.57	1.50
T_3'/T_o	0.69	0.70
p_o/p_3	2.55	2.4

COMPARISON TO RANKINE CYCLE
($T_o = 2460^o$ R, $A^* = 16$) FOR SAME RADIATOR AREA

T_o	4260^o R	3730^o R
T_3	3190^o R	2790^o R
T_4	1280^o R	1395^o R
T_5	2000^o R	2090^o R

Column (a) was calculated by the minimization process; the values in column (b) were obtained by minimizing T_3/T_o while keeping the cycle efficiency the same. Note that for column (a), the overall cycle efficiency is 15%, which is close to the Rankine cycle, which implies that for a given power level, the thermal input to both cycles will be about the same.

Although the radiator area for the gas cycle is much larger than the Rankine cycle for the same cycle maximum temperature, because the gas cycle can use inert gases and avoid the corrosion problem, it may be possible to operate the gas cycle at a higher temperature. Now, for the same radiator area, (14.237) predicts that the top temperature T_o will vary as the one-fourth power of A*. Such a comparison is made at the bottom of Table 14.5, where it may be seen that for $\eta_c = \eta_g = 0.85$, the top temperature is 3730^o R. Although this temperature is quite high, it may be possible to develop nuclear reactors for use with inert gases in this range. This temperature is probably too high for the use of gas turbines, but not for MHD generators.

A major problem with the gas cycle is that a gas compressor is required. Since the gas pressure in the reactor is likely to be high in order to minimize the heat exchanger surfaces, it is unlikely that a magnetohydrodynamic compressor can be utilized, and an electrically driven rotating compressor is required. If, for the example in column (a), the electric motor for the compressor has an efficiency of 74%, then all of the electrical output would be used to drive the compressor, and there would be zero useful power output.

Of course, a magnetic field must be incorporated into a nuclear-MHD space power system, which raises two additional problems, namely, the weight of the magnet, and the rejection of heat from the magnet. Now, most space applications for use with electrical propulsion will require from one to twenty megawatts of power; from Section 14.81, the weight of a copper wound air core magnet is prohibitively large, and the weight of an iron core magnet is only slightly less. In addition, the heat

generated in the windings must be removed by an additional radiator. For example, if one allows 10% of the total power to energize the field coils, then the entire power plant including its radiator must be larger by 11%. The main radiator rejects 85% of the thermal energy (if the overall thermal efficiency is 15%), and if the windings are operated at the same temperature as the main radiator, then the additional radiator load is 15%. However, since the electrical resistivity of most metals increases with temperature, and the size of the windings increases with resistivity when the fraction of power consumed by the windings is held constant, it may be desired to maintain the windings at some lower temperature, and use a heat pump to increase the rejection temperature. This reduces the size of the radiator for the windings, but additional power is required for the heat pump.

The problems of the weight of the windings and the rejection of the ohmic heating in the windings may be solved by the use of high field superconducting materials. The high electric current densities of superconductors reduce the weight of the windings, while the only required heat rejection is that which is conducted into the magnet dewar, which tends to boil off the liquid helium in which superconductors are kept. The liquid helium can either be recooled by a cryostat which requires additional weight, power, and radiators; or sufficient liquid helium can be stored to allow boil-off of the helium during the required mission time.

14.8d Other Gas Cycles

Intercooled

Since the radiator area, per unit heat rejection, decreases with increasing heat rejection temperature, it appears advantageous to start compression when the working fluid reaches T_5, with the compression divided into many stages with intercooling by radiation between each compression stage. Ideally, this may be represented as an infinite number of infinitesimal compressions, and is a constant temperature line on the temperature entropy diagram, see

Figure 14.44. It is easily shown that if each compression stage has an adiabatic compression efficiency η_c, then the rejected heat from the intercooler radiator is given by:

$$\frac{Q''_{rej}}{\left(Q''_{rej}\right)_{ideal}} = \frac{1}{\eta_c} \tag{m}$$

where

$$\left(Q''_{rej}\right)_{ideal} = T(S_4 - S_5) = C_p T_4 \ell n \left(\frac{p_4}{p_5}\right)^{\frac{\gamma-1}{\gamma}} \tag{n}$$

From the definition of the generator adiabatic efficiency,

$$\eta_g = \frac{T_o - T_3}{T_o - T_3'} \tag{p}$$

the pressure ratio can be obtained:

$$\left(\frac{p_4}{p_5}\right)^{\frac{\gamma-1}{\gamma}} \cong \left(\frac{p_3}{p_o}\right)^{\frac{\gamma-1}{\gamma}} = \frac{\eta_g - 1 + \frac{T_3}{T_o}}{\eta_g} \tag{q}$$

where it has been assumed that the pressure drops are negligible. Also

$$Q_{in} = C_p(T_o - T_5); \text{ and } Q'_{rej} = C_p(T_3 - T_5).$$

The overall efficiency is

$$\eta = 1 - \frac{Q''_{rej} + Q'_{rej}}{Q_{in}}$$

or, with the use of (m, n, q):

$$\eta = \frac{1 - \frac{T_3}{T_o} + \frac{T_4}{T_o} \cdot \frac{1}{\eta_c} \ln \left(\frac{\eta_g - 1 + \frac{T_3}{T_o}}{\eta_g} \right)}{1 - \frac{T_4}{T_o}} \qquad (14.239)$$

In a similar manner, the radiator area can be expressed as:

$$A^* = \frac{\sigma \epsilon A T_o^4}{P} = \frac{1 - \eta}{\eta} \left(\frac{T_o}{T_4} \right)^4 \times$$

$$\left\{ \frac{\frac{1}{3} \left(1 - \frac{T_4^3}{T_3^3} \right) - \frac{1}{\eta_c} \ln \left(\frac{\eta_g - 1 + \frac{T_3}{T_o}}{\eta_g} \right)}{\frac{T_3}{T_4} - 1 - \frac{1}{\eta_c} \ln \left(\frac{\eta_g - 1 + \frac{T_3}{T_o}}{\eta_g} \right)} \right\} \qquad (14.240)$$

In order to effect a comparison with the Brayton cycle, calculations have been made with (14.239, 14.240), assuming that $\eta_c = \eta_g = 0.8$, and $\eta = 0.15$. Then (14.239) gives a relation between (T_3/T_2) and (T_4/T_o), and A* may be calculated for various values of T_3/T_o. The minimum radiator area, for these assumptions is A* = 220 as shown in Table 14.6, for which $(T_3/T_o) \approx 0.7$, and $(T_4/T_3) \approx 0.49$. Compared to the Brayton cycle (a), the radiator area has increased. This may be attributed to additional heat rejection due to intercooling which requires that T_3, and hence T_4, be decreased to obtain the same efficiency. This is the opposite effect of the usual effect of intercooling for ground based gas cycles, where the lowest temperature in the cycle corresponds to the available

cooling fluid; intercooling at the lowest temperature in the cycle decreases the net heat rejection.

To investigate whether complete intercooling, as shown in Figure 14.44, decreases the radiator area, a calculation was performed for $\eta_c = \eta_g = 0.90$. The optimum temperature ratio is $(T_3/T_o) = 0.5$, but the radiator area is still very large ($A^* = 144$) as shown in Table 14.6, as compared to a simple Brayton cycle for lower component efficiencies.

Another possible modification is the use of regeneration, see Figure 14.44. Again, the radiator area depends on η_c, η_g, (T_3/T_o), (T_4/T_o), and the temperature drop across the walls of the regenerator. Note that T_5 and T_6 are fixed by the other parameters. Calculations for minimizing the radiator area show that a value of $A^* = 48$ may be attainable,[37] which further reduces the required top temperature in order to achieve the same radiator area as the Rankine cycle, see Table 14.6. However, the pressure ratio is small, $p_3/p_o \approx 1.75$, which simplifies the compressor problem, but which then requires that the pressure drop in the regenerator be made very small. Now, the pressure drop in the regenerator is inversely proportional to the product of the absolute pressure in the regenerator, the number of tubes, and the tube cross-sectional area. Thus, to keep the regenerator small, high pressure operation of the cycle is required. On the other hand, in order to achieve non-thermal ionization in the MHD generator, low static pressures are required, which then requires supersonic flow in the generator with a supersonic diffusor downstream of the generator. Calculations of the losses associated with such a diffusor[37] indicate that there is an additional decrease of the generator adiabatic efficiency of about 10% which is undesirable since it is necessary in a gas cycle that the generator (and compressor) efficiency be as high as possible.

14.8e Two Phase Cycles

Of course, it is not necessary for the working fluid of a MHD generator to be an ionized gas; it could for example be a liquid metal, or a mixture of gas or vapor and liquid metal. Such a generator has the advantage of the very high

TABLE 14.6. RADIATOR AREA PARAMETER FOR VARIOUS CYCLES

Cycle	Component Efficiency	Overall Thermal Efficiency	Radiator Area Parameter $A^* = \frac{\sigma \epsilon T_o^4 A}{P}$	Working Fluid Max. Temperature For Same Area
Rankine	.66	15%	16	2460°R*
Brayton (a)	.80	15%	145	4260°R
Brayton (Intercooled)	.80	15%	220	4840°R
Tricycle	.90	10%	144	4230°R
Brayton (English & Stone)			~100	3900°R
Brayton (b)	.85	15%	84	3730°R
Regenerative	.85	25%	48	3230°R

*Assumed

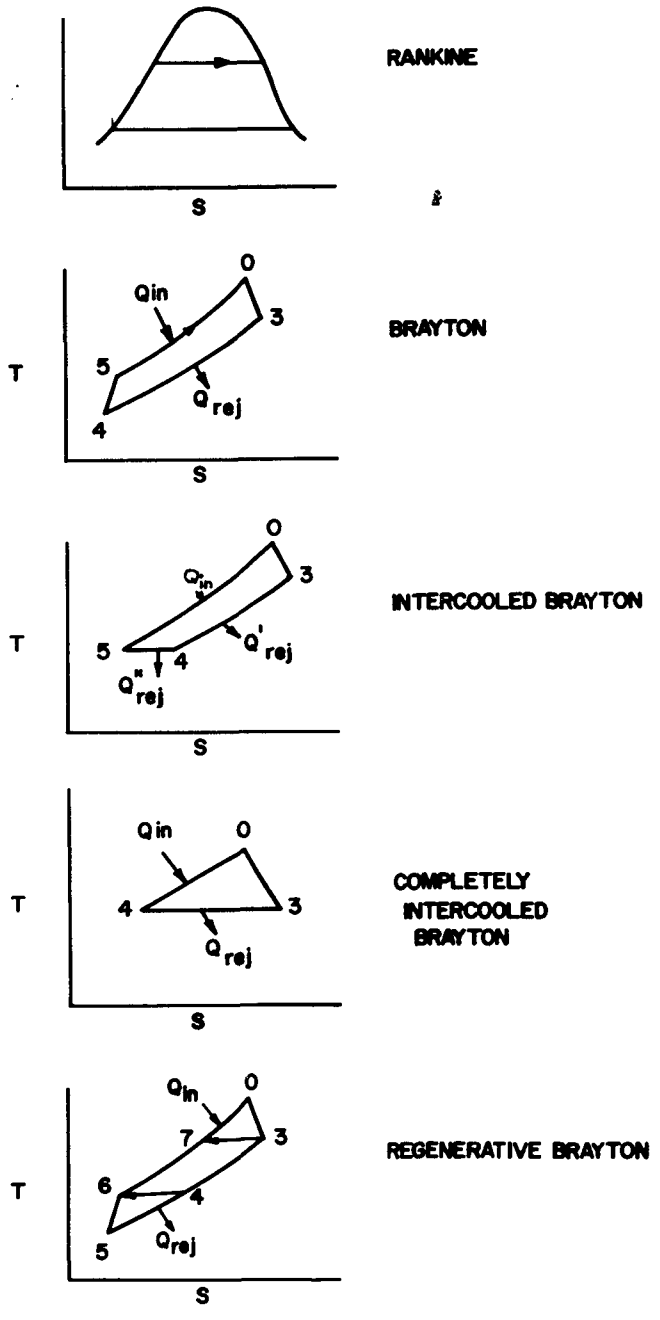

Figure 14.44. Simple Vapor and Gas Cycles for Space Applications

electrical conductivity of liquid metals at all temperatures. The main problem is the conversion of the thermal energy from the nuclear reactor into kinetic energy of motion of the liquid metal; normally a gas or vapor is used for this purpose. This can be accomplished by mixing a hot liquid metal of low vapor pressure with a cooler liquid metal of high vapor pressure. The hot liquid metal causes the lower temperature liquid metal to vaporize. The mixture is passed into a nozzle which allows the vapor to expand and accelerate the droplets of liquid metal. The mixture is then separated, without appreciable loss of kinetic energy or head of the liquid metal, and this head then forces the liquid metal through the generator against the Lorentz force. One such possible cycle[38] is shown in Figure 14.45. The lower loop is for the liquid metal while the upper loop is for the liquid metal vapor. The liquid metal enters the reactor at 9, leaves at 10, and is mixed with the high vapor-pressure liquid metal in the "mixer," in which some or all of the latter liquid metal is vaporized, and thermodynamic equilibrium between the two streams is reached at 1. The entire mixture then passes through the nozzle, where the vapor and liquid metal droplets are accelerated, and enters the separator at 2. The separated liquid metal uses the acquired kinetic energy to flow through the generator and reactor. The separated vapor passes through a regenerator (heat exchanger), radiator where it is condensed, a pump, and is then reheated by the regenerator before entering the mixer. Calculations of the efficiency of this cycle indicate about 11% is achievable if the mass flow rate through the lower loop is 100 times the mass flow rate through the upper loop;[38] this means that the increase in temperature in the reactor, $T_{10} - T_9$, will be small. The high mass flow ratio of liquid metal is required to keep the velocity of the mixture small in the separator since frictional losses increase approximately as the square of the velocity. The high mass flow ratio also precludes the use of a single fluid, since a single fluid if expanded from the saturated liquid line to a temperature equal to about 3/4 of the stagnation temperature will have a large mixture velocity, and hence, an excessive friction loss in the separator.

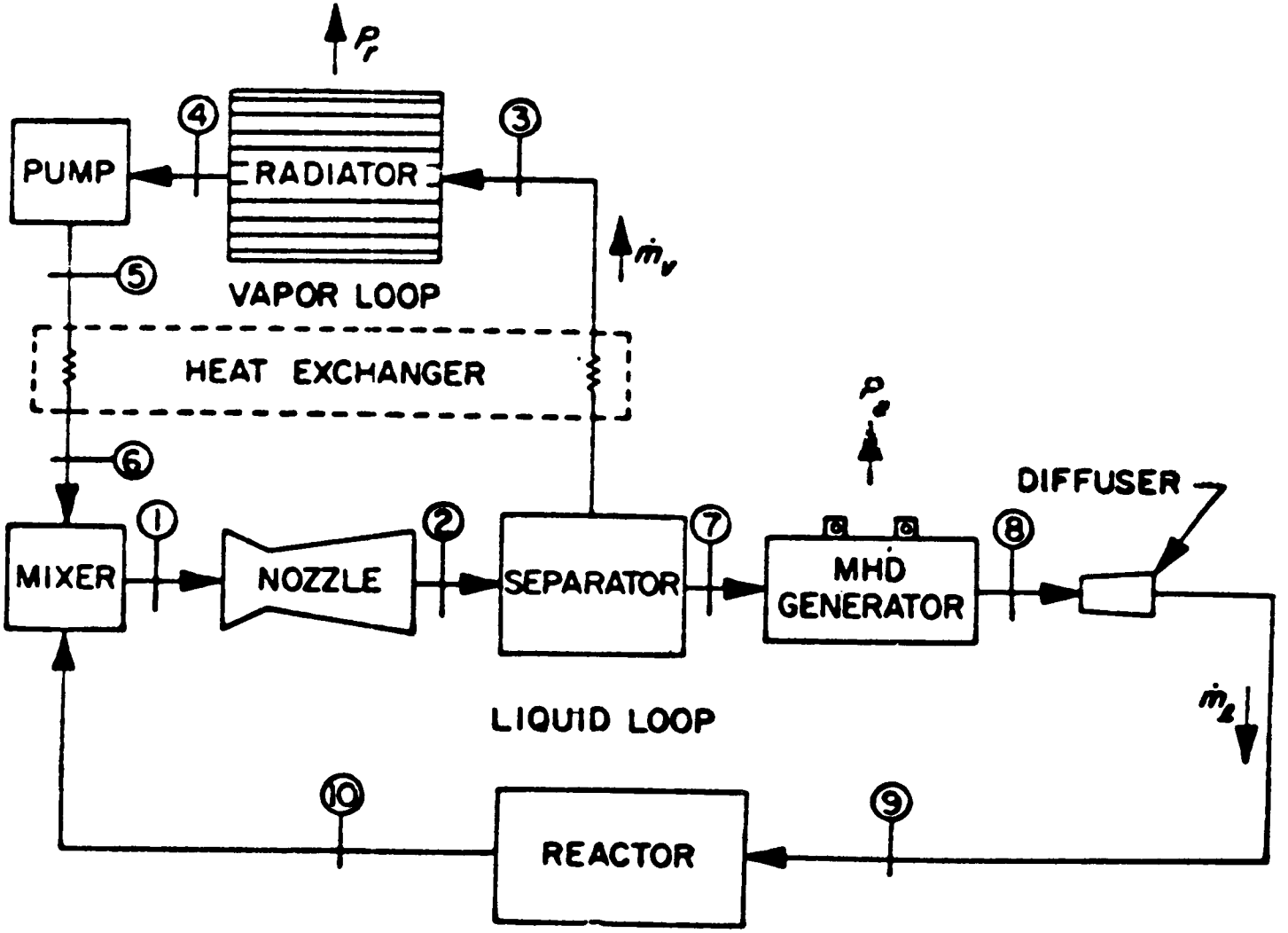

Figure 14.45. Two-Fluid MHD Power Conversion Cycle

Besides the problem of friction losses in the separator, because of the small temperature change in the reactor, the energy extraction per unit mass flow in the generator is quite small, which results in a generator of extremely small aspect ratio, see Figure 14.46, and hence large end losses in the absence of inlet and outlet vanes. But if inlet and outlet vanes are used, these will increase the friction pressure drop further. It is possible that there are other geometrical arrangements for the nozzle, separator, and generator which will have a smaller wetted surface area, and a more favorable generator aspect ratio.

14.8f Heat Rejection to Propellant

One possible use for space electrical power is electrical propulsion. This raises the possibility of using the reject heat from the space electrical power system to preheat the propellant, and thereby avoid the use of a radiator. For a regenerative cycle, the preheat heat balance is (see Figure 14.44):

$$\dot{m} Q_{rej} = P \left(\frac{1 - \eta}{\eta}\right) = \dot{m}_p C_{p_p} (T_6 - T_i) \qquad (r)$$

where T_i is the initial temperature of the propellant, and m_p and C_{p_p} is the mass flow rate and specific heat of the propellant, assumed constant. Also, it has been assumed for simplicity that there is a negligible temperature drop between the working fluid in the space power cycle and the propellant in the heat exchanger. Now, the electrical power from the cycle is used to heat the propellant further: this may be in a plasma jet, resistance heater or any other device; we assume that the efficiency for this process is 100%. Thus:

$$P = \dot{m}_p C_{p_p} (T_{o_p} - T_6) \qquad (s)$$

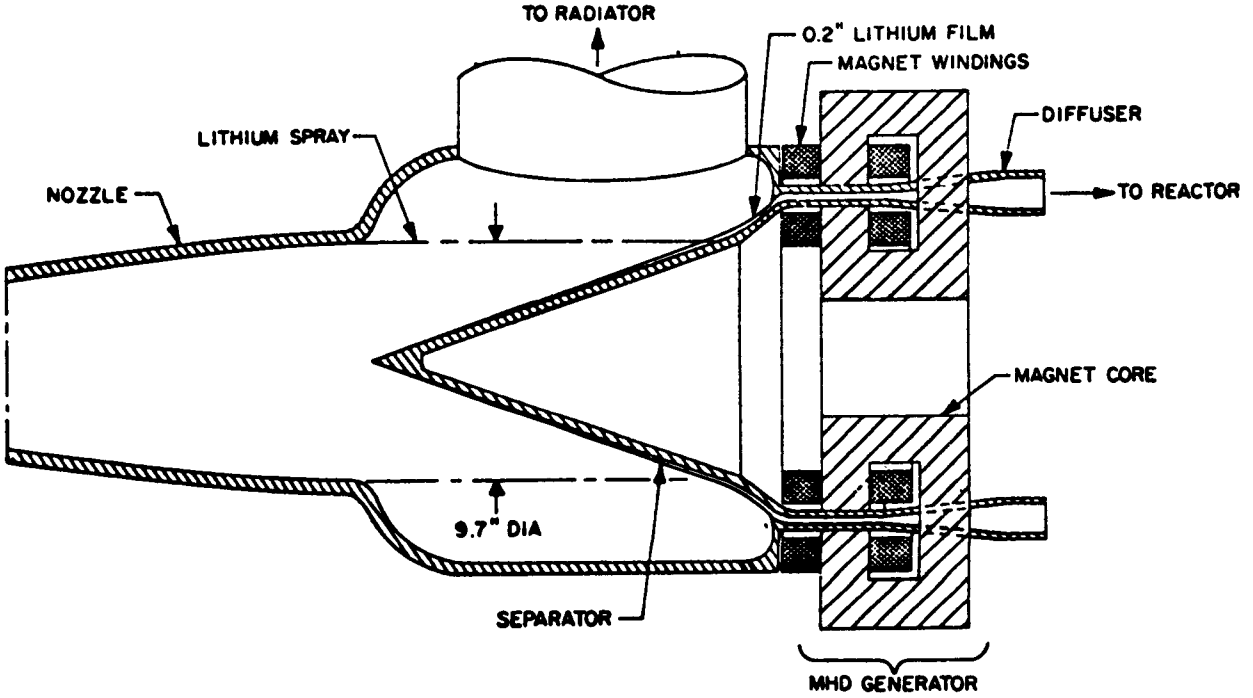

Figure 14.46. Nozzle, Separator, and Generator Configuration for 500-kwe Conversion System

where T_{o_p} is the final stagnation temperature of the propellant. Also, for a regenerative cycle,

$$\eta = 1 - \frac{Q_{rej}}{Q_{in}} = 1 - \frac{C_p (T_6 - T_5)}{C_p (T_o - T_3)} = 1 - \frac{T_5}{T_o} , \qquad (t)$$

since for a perfect gas cycle $(T_o/T_3) = (T_6/T_5)$. Division of (r) by (s), and use of (t) yields:

$$T_{o_p} - T_i = \left(\frac{T_o}{T_5}\right) \left(T_5 - T_i\right) \qquad (u)$$

Now, to maximize the propellant stagnation temperature, T_i must be made as small as possible, and (u) becomes $T_{o_p} \approx T_o$. Thus, the stagnation temperature of the propellant is no higher than if the propellant had been directly heated by the reactor! For fuel rod reactors, this cycle therefore has little advantage. However, if the reactor were a gaseous nuclear reactor, which virtually precludes mixing of the propellant with the nuclear fuel, then this cycle has the advantage that the fuel and propellant are kept separate, and also, much higher temperatures may be achievable in a gaseous nuclear reactor than in a reactor which uses solid or liquid nuclear fuel.

For fuel-rod cycles, this cycle may be improved by sending the propellant, after preheat but before electrical heating, through the reactor.[39] Then (s) is replaced by

$$P = \dot{m}_p C_{p_p} (T_{o_p} - T_o) \qquad (v)$$

Following the same procedure as in the previous case (with $T_i \approx 0$),

$$T_{o_p} = 2T_o - T_5 \approx 2T_o \qquad (w)$$

Thus, the stagnation temperature of the propellant is almost twice that which would have been obtained if the propellant were directly heated by the nuclear reactor.

As previously mentioned, gaseous nuclear reactors may be capable of higher temperatures than solid fuel rod reactors, but direct heating of the propellant is difficult, since the gaseous propellant must be separated from the gaseous nuclear fuel prior to expulsion. Although vortex separation has been suggested, it may also be possible to use an MHD generator for this purpose.[40] The working fluid consists of a mixture of propellant and gaseous nuclear fuel. The nuclear reaction heats the entire mixture to a sufficiently high temperature to ionize the gas, and the mixture flows through an MHD generator in which the nuclear reaction is stopped and enthalpy is extracted from the mixture. The temperature of the mixture is thereby reduced until the nuclear fuel condenses, which is then extracted from the flow and recirculated to the reactor. The electrical power which has been generated in the MHD generator is then added to the propellant, which is now free of nuclear fuel, and exhausted from the electrothermal engine. Such a system is interesting but highly speculative at present.

14.9 MHD GENERATOR EXPERIMENTS

The first MHD generator experiments were those of Halász and Karlovitz,[2] which were carried out at Westinghouse up to about 1946, using electron-beam ionization. Due to rapid recombination and formation of negative ions, the generated power density was far below theoretical. No further experiments were performed until about 1958, when experiments were initiated using thermal ionization of seeded gases, see Table 14.7. The earliest of these experiments utilized plasma jets as the method for thermal heating of the gas, since gas temperatures could easily be obtained which are much higher than those available from combustion flames.[3,41] In these experiments, the measured electrical conductivity and generated power agreed within a factor of two of the theoretically predicted performance, although the total power was small (less than 12KW) and the run times were less than 10 seconds. These experiments mainly verified the validity of the physical principle of MHD power generation. A typical voltage-current plot is shown in Figure 14.47.

The first combustion experiment was performed at Westinghouse Electric,[42] in which over 10 KW was generated; followed rapidly by a similar experiment at MHD Research,[43] and a much smaller experiment at the General Electric Research Laboratory.[44] These experiments also verified the theory closely; however, the magnetic interaction parameter for these experiments was quite small. The largest combustion experiment at the present time is the AVCO Mark II,[45] which generated 1300 kilowatts in October, 1962. A Hall generator has also been successfully operated on an air-hydrogen flame,[46] with also excellent agreement with theory. Combustion generation experiments have also been performed in Poland,[47] and have been reported in the Soviet Union,[48] but details of the latter are not yet available.

Power generation experiments have not yet been performed using non-thermal ionization as of October, 1962, but experimental equipment is under construction at C.A. Parsons Nuclear Research Centre[49] and the General Electric Space Sciences Laboratory.[50]

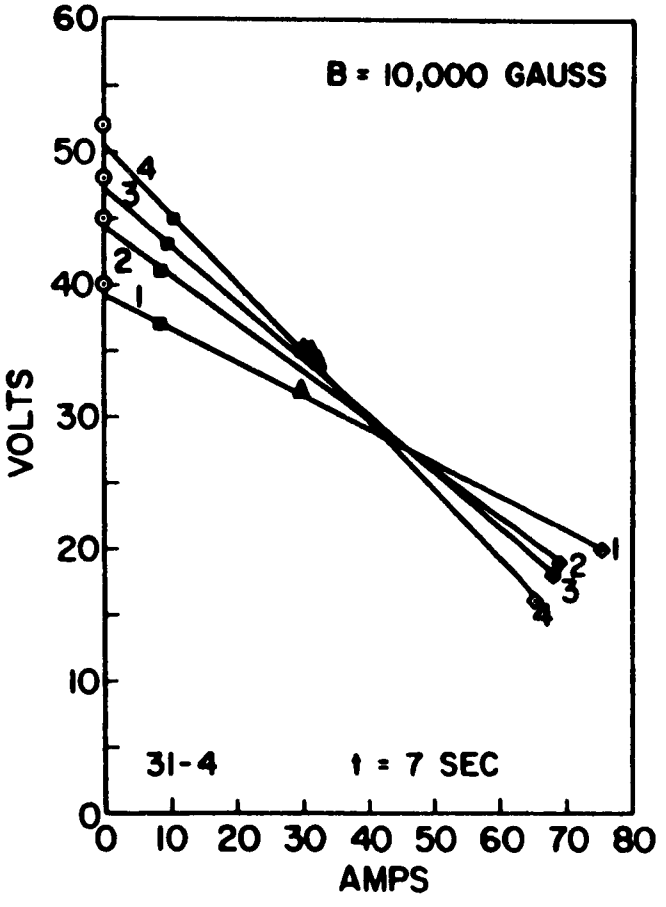

Figure 14.47. Voltage-Current Characteristics for a Four-Electrode Experimental MHD Generator[41]

TABLE 14.7 SUMMARY OF MHD EXPERIMENTS

	MHD Research	AVCO Mark I	AVCO Mark II	General Electric Space Sciences Laboratory	General Electric Research Laboratory	General Electric Research Laboratory	Westinghouse Model 1	Westinghouse Model 2
Working gas	Kerosene and ethanol (plus oxygen)	He and A with arc heater	Ethanol or Kerosene (plus oxygen)	Nitrogen with plasma jet heating	Propane (plus oxygen)	H_2 (plus air)	Diesel oil + octoate soap (plus $O_2 + x N_2$)	n-Heptane (plus $O_2 + 0.47$ Molar N_2)
Temperature, ^oK	3000^o	2800^o	3000^o	3200^oK	2300^oK	2550^oK	$2800-3000^o$	2570^o
Gas velocity	500-1000 M/sec	Mach 0.7	1000 M/s	700 M/s	56.8 M/sec	Mach 0.8	500-865 M/sec	757 M/sec
Seeding	1%	K_2CO_3	1% molar KOH powder	K_2CO_3	K_2CO_3	KOH	1.5% (molar K in gas) as soap in fuel	0.3% (molar K in gas) as K_2CO_3 slurry in fuel
Generator size, in.	1/2x2x16	1x3x20	60x (3x9) inlet (3x13) exit	1/2x4x29	1x2x2	2x4x12	1-5/8 x 4-5/7 x 16	3/4 x 3/4 x 16
Electrode material	Tungsten (Segmented, 5 electrodes 3" long)	---	graphite (Segmented)	graphite (4)	graphite	silicon carbide	C, ZrO_2, ZrB_2, W, etc.	ZrB_2
Insulator material	MgO	---	Non-ablating	Zirconia	MgO	MgO	MgO or cooled ZrO_2	MgO
Magnetic field, gauss	20,000	---	32,000	11,000	4,250	12,000	5000-14,000	10,000
EMF generated, DC volts	50-100	27	Up to 1400	75-90	0.7	90	30-100 open circuit	7.7 open circuit
Power generated, KW	1.03	11.6	600	6	.00002	1.9	1.5-10.4	3 watts per inch of length
Test duration	30 min.	10 sec.	10 sec.	5 sec.	5 min.	6 min.	3-50 min.	40 min.
Efficiency (heat to electricity)	0.1%	---	3%	0.1%	---	---	~0.3%	---
Reference	43	3	45	41	44	46	42	

14.9a MHD Generator Materials

For the plasma jet and combustion experiments, some initial experiments were performed using stabilized zirconia for the insulator; however, at high temperatures the zirconia generally becomes electrically conducting and most experimenters have changed to magnesia for the insulator. One unexpected effect is that the resistivity of the ceramic decreases during an experiment;[46] it is not yet known whether this is due to the presence of potassium which could change the chemical composition of the surface of the insulator. The presence of molten ash will probably intensify this problem.

For very large MHD generators, wall cooling may be possible without adversely affecting the performance, and experiments have been performed in which water-cooled tubes were used as the insulator. These same tubes can also serve as the electrodes if the tubes follow equipotential lines as in the series-segmented geometry, and if an insulation is placed in between the tubes.[51] Since the temperature of the tubes is low, presumably the temperature of the insulation between them will also be low and hence alumina may be satisfactory.

The most commonly used electrode material has been graphite,[3,41] although silicon carbide has also been utilized.[46] However, zircon compounds have also been utilized because of their relatively high electrical conductivity, both with and without embedded tungsten.[43] In general, if the electrodes are sufficiently hot to emit electrons thermionically, there has been almost zero cathode voltage drop;[41] otherwise voltage drops up to 100 volts have been observed. The graphite and carbide electrodes have been observed to erode very rapidly which is probably due to chemical reactions with water vapor in the products of combustion. For a continuously operating generator, these types of electrodes could be continuously fed into the generator, which may cause a leakage and seal problem if the gas inside the generator is above atmospheric pressure. The pressure of molten ash could interfere with proper operation of the electrodes as well as the insulator.

14.9b Seed Material

The seed has generally been injected as a salt, K_2CO_3, or as a hydroxide, KOH. The salt dissolves readily in water which provides a convenient method for injection, but powdered potassium carbonate has also been used. The hydroxide dissolves easily in alcohol, which then can be mixed directly with the fuel,[43] eliminating the necessity for a separate injection system and also allowing for more precise control of the seed injection rate.

For closed cycle operation, pure alkali metal is required for the seed. This can be provided by injection of the liquid metal; use of a side stream which is bubbled through the liquid metal;[9] a spray evaporator, or a direct boiler for the liquid metal.

REFERENCES

1. J. Faraday, "Experimental Researches in Electricity," Vol. 1, pp 81, 130, 188 (1838).

2. Bela Karlovitz, "History of the K&H Generator and Conclusions Drawn from the Experimental Results," Proc. Third Symposium on Engineering Aspects of Magnetohydrodynamics, Gordon and Breach, 1963, N.Y.

3. R. Rosa, "Physical Principles of Magnetohydrodynamic Power Generation," Physics of Fluids, 4, pp 182-194(1961).

4. L.S. Frost, "Conductivity of Seeded Atmospheric Pressure Plasmas," Journal of Applied Physics, 32, pp 2029-36(1961).

5. L. Steg and G.W. Sutton, "The Prospects of MHD Power Generation," Astronautics, Aug., 1960, pp 22-25, 82, 84-86.

6. H. Hurwitz, Jr., R. Kilb, and G.W. Sutton, "Influence of Tensor Conductivity on Current Distribution in a MHD Generator," Journal of Applied Physics, 32, pp 205-216 (1961).

7. L.P. Harris and J.D. Cobine, "The Significance of the Hall Effect for Three MHD Generator Configurations," Am. Soc. Mech. Engineers Paper 60-WA-329 (1960).

8. H. Hurwitz, Jr., G.W. Sutton, and S. Tomor, "Electron Heating in Magnetohydrodynamic Power Generators," ARS Journal, 32, pp 1237-1243 (1962).

9. J. Kerrebrock, "Conduction in Gases with Elevated Electron Temperatures," 2nd Symposium on Engineering Aspects of Magnetohydrodynamics, Columbia University Press, New York, 1962, pp 327-346.

10. G.W. Sutton and A. Carlson, "End Effects in Inviscid Flow in a Magnetohydrodynamic Channel," Journal of Fluid Mechanics, Vol. 11, part 1, pp 121-132, (1961).

11. G.W. Sutton, H. Hurwitz, Jr., and H. Poritsky, Jr., "Electrical and End Losses in a Magnetohydrodynamic Channel Due to End Current Loops," Communications and Electronics (AIEE Transactions) Jan., 1962.

12. F. Fishman, "End Effects in Magnetohydrodynamic Channel Flow," Research Report 78, AVCO-Everett Research Laboratory (June, 1959).

13. B. Podolsky and A. Sherman, "Some Aspects of the Hall Effect in Crossed Field MHD Accelerators," Am. Rocket Society Preprint 1531-60 (1960).

14. B. Podolsky and A. Sherman, "The Influence of Tensor Conductivity on End Currents in Crossed Field MHD Channels with Skewed Electrodes," Journal of Applied Physics, Vol. 33, pp 1414-1418 (1962).

15. H. Yeh and G.W. Sutton, "Velocity Profiles and Efficiency of MHD Generators with Segmented Electrodes," GE Report R61SD150, Sept., 1961.

16. J.C. Crown, :Analysis of Magnetohydrodynamic Generators Having Segmented Electrodes and Anistropic Conductivity," United Aircraft Research Laboratories Report R-1852-2, Feb., 1961.

17. G.W. Sutton, "End Losses in Magnetohydrodynamic Channels With Tensor Electrical Conductivity and Segmented Electrodes," GE Report R62SD135, 1962, Journal of Applied Physics.

18. L.S. Dzung, "Hall Effect and End Loop Losses of MHD Generators," Symposium on Magnetoplasmadynamic Electrical Power Generation," Newcastle upon Tyne, 6-8 Sept. 1962.

19. G.W. Sutton, "Quasi-One-Dimensional Flow of an Electrical Conducting Gas for the Generation of Electrical Power," GE Report R59SD307, Feb., 1959.

20. G.W. Sutton, "Magnetohydrodynamic Channel Flow of a Perfect Gas for the Generation of Electrical Power," GE Report R59SD473, Dec., 1959.

21. S. Blecher, "Theoretical Performance Analysis of a Constant Velocity MHD Generator for Combustion Products of Hydrocarbon and Air," ARS Journal, 32, 1394-6 (1962).

22. A. Sherman, "A High Performance Short Time Duration, MHD Generator System," American Rocket Society Space Power Conference, Sept., 1962. Preprint 2558-62.

23. J.E. McCune and W.R. Sears, "On Magnetohydrodynamic Channel Flow," Journal of Aero. Sciences, Vol. 27, 139-140 (1960).

24. E.F. Brocher, "The Constant Velocity MHD Generator with Variable Electrical Conductivity," Journal of Aero/Space Sciences, Vol. 29, pp 626-27 (1962).

25. F. LeBouc, "Conversion de la Chaleur en Electricite par Magnetohydrodynamique," Report No. 6647, Inst. Francais du Petrole, Rueil-Malmaison (S. et-O.), August, 1961.

26. Joseph L. Neuringer, "Optimum Power Generation from a Moving Plasma," Journal of Fluid Mechanics, Vol. 7, Part 2, pp 287-301. (Feb., 1960).

27. Mostafa E. Talaat, "Magnetohydrodynamic Electric Power Generators," Advanced Energy Conversion, Vol. 1, pp 19-35 (1961).

28. Bernstein, I.B., Fanucci, J.B., Fischbeck, K.H., Jarem, J., Korman, N.I., Kulsrud, R.M., Lessen, M., and Ness, N., "An Electrodeless MHD Generator," Engineering Aspects of Magnetohydrodynamics, Edited by Clifford Mannal and Norman W. Mather, Columbia University Press, pp 255-276.

"Magnetohydrodynamics - future power process?"

29. P. Sporn and A. Kantrowitz, Power, Vol. 103, No. 11, pp 62-65 (Nov., 1959).

30. J.W.W. Brown, "Some Aspects of MHD Power Plant Economics," Proc. 3rd Symposium on Engineering Aspects at Magnetohydrodynamics, Gordon & Breach Science Publishers, N.Y., 1963.

31. T.R. Brogan, et al, "A Review of Recent MHD Generator Work at the AVCO-Everett Research Laboratory," ibid.

32. R.C. Allen, "Feasibility of 300 Mwe MHD Power Plant," American Power Conference, Chicago, March, 1962.

33. Stewart Way, "Reduction of Operating Temperature in MHD Power Plants," Pacific Energy Conversion Conference, sponsored by AIEE, Aug. 13-16, 1962.

34. S. Way, Round Table on MHD Power Generation held at M.I.T., June 28, 1961.

35. E.T. Pitkin, "Optimum Radiator Temperature for Space Power Systems, ARS Journal, Vol. 29, pp. 596-7.

36. Robert E. English and Henry O. Slone, "Comparison of Gas Turbine Cycles for Space Applications, ARS Journal Vol. 30, No. 11, pp. 1097-1098 (Nov., 1960).

37. Steven Freedman, "Thermodynamic Considerations for MHD Space Power Systems," G.E. Report R62SD83, Sept., 1962.

38. D.G. Elliot, "Two-Fluid Magnetohydrodynamic Cycle for Nuclear-Electric Power Conversion," ARS Journal 32, 924-928 (1962).

39. E.L. Resler, Jr., and N. Rott," Rocket Propulsion with Nuclear Power," ARS Journal 30, pp. 1099-1100 (1960).

40. R.J. Rosa, "Magnetohydrodynamic Generators and Nuclear Propulsion," ARS Journal, 32, pp. 1221-1230.

41. G.W. Sutton and F. Robben, "Preliminary Experiments on MHD Channel Flow with Slightly Ionized Gases," Proc. Symp. on Electromagnetics and Fluid Dynamics of Gaseous Plasma, Polytechnic Press, Brooklyn, 1962, pp. 307-321.

42. S. Way, S.M. De Corso, R. L. Hundstad, G.A. Kemeney, W. Stewart and W.E. Young, "Experiments with MHD Power Generation," Trans. A.S.M.E. 83, A (J. Eng. for Power), p. 397, (1961).

43. V.H. Blackman, M.S. Jones, Jr., and A. Demetriades, "MHD Power Generation Studies in Rectangular Channels," Proc. 2nd Symp. Eng. Aspects of Magnetohydrodynamics, Columbia U. Press, N.Y. 1962, pp. 180-210.

44. G.J. Mullaney and N.R. Dibelius, "Small MHD Power Generator Using Combustion Gases as an Energy Source," ARS Journal, 31, pp. 555-557 (1961).

45. T.R. Brogan, J.F. Louis, R.J. Rosa, Z.J.J. Stekly, "A Review of Recent MHD Generator Work at the AVCO-Everett Research Laboratory," Proc. 3rd Symp. Eng. Aspects of Magnetohydrodynamics, Gordon and Breach, N.Y., 1963.

46. L.P. Harris and G.E. Moore, "Some Electrical Measurements on MHD Channels," Proc. 3rd MHD Symposium, Gordon and Breach, N.Y., 1963.

47. W.S. Brzozowski, Unscheduled paper, Symposium on Magnetoplasmadynamic Electrical Power Generation, Newcastle-upon-Tyne, Sept., 1962.

48. New York Times, July 17, 1962.

49. B.C. Lindley, "A Closed Cycle MPD Experiment," Symp. on Magnetoplasmadynamic Electrical Power Generation, Newcastle-upon-Tyne, Sept., 1962.

50. G.W. Sutton and A. Sherman, "Research on Methods of Increasing the Electrical Conductivity in MHD Generators at the Space Sciences Laboratory of General Electric Company," ibid.

51. J. Maycock, D.T. Swift-Hook, J.K. Wright, "Permanent Insulating Duct Walls for Magnetohydrodynamic Power Generation," Nature, 196, pp. 260-261 (Oct. 20, 1962).

GENERAL ELECTRIC

SPACE SCIENCES LABORATORY
MISSILE AND SPACE DIVISION

TECHNICAL INFORMATION SERIES

AUTHOR	SUBJECT CLASSIFICATION	NO.
G. W. Sutton	Magnetohydrodynamics	R62SD990
		DATE: Dec. 1962
TITLE: The Theory of Magnetohydrodyaamic Power Generators		G. E. CLASS: I
		GOV. CLASS: None
REPRODUCIBLE COPY FILED AT MSD LIBRARY, DOCUMENTS LIBRARY UNIT, VALLEY FORGE SPACE TECHNOLOGY CENTER, KING OF PRUSSIA, PA.		NO. PAGES: 205

SUMMARY

Magnetohydrodyaamic power generation has now been under active development for over four years, but there has not yet appeared any complete description of the theory. This report is intended to close this obvious gap. Most of the theory presented herein was developed by the author and personnel at the General Electric Company. Some of this material has not been published previously; those results which have been published are referenced.

The topics covered are: electrical conductivity in MHD generators, optimum "seed" ratio, local analyses of the continuous and segmented electrode geometries; Hall geometry, helical flow geometry; magnetically induced ionization; polytropic efficiencies; compressible analyses of the constant velocity, temperature, Mach number, pressure and cross-sectional area flows; end losses; AC generation; cycle efficiencies; and a summary of generating experiments at the General Electric Company and other places. Geometries other than linear are not considered herein; the most important of those omitted is the vortex generator.

By cutting out this rectangle and folding on the center line, the above information can be fitted into a standard card file.

AUTHOR George W Sutton

COUNTERSIGNED Joseph Fabri